Tesi di Dottorato di DANILO CUCCATO
Matricola 753302

POLITECNICO DI MILANO

**DIPARTIMENTO
DI
CHIMICA,
MATERIALI
E
INGEGNERIA CHIMICA
"Giulio Natta"**

QUANTUM CHEMISTRY INVESTIGATION OF FREE RADICAL POLYMERIZATION KINETICS: POWER AND LIMITS OF THE TOOL

**Dottorato di Ricerca in
Chimica Industriale e
Ingegneria Chimica (CII)**

XXV ciclo
2010 - 2012

Coordinatore: prof. Tiziano Faravelli
Tutore: prof. Carlo Cavallotti
Relatore: prof. Davide Moscatelli

IV

List of Publications

1.   D. Cuccato, M. Dossi, D. Moscatelli, G. Storti, "A Density Functional Theory Study of Poly (vinyl chloride) (PVC) Free Radical Polymerization", *Macromolecular Symposia*, **2011**, *302*, 100-109.

2.   D. Cuccato, M. Dossi, D. Moscatelli, G. Storti, "Quantum Chemical Investigation of Secondary Reactions in Poly(vinyl chloride) Free-Radical Polymerization", *Macromolecular Reaction Engineering*, **2012**, *6*, 330-345

3.   D. Cuccato, M. Dossi, D. Polino, C. Cavallotti, D. Moscatelli, "Is Quantum Tunneling Relevant in Free-Radical Polymerization?", *Macromolecular Reaction Engineering*, **2012**, *6*, 496-506.

4.   D. Cuccato, E. Mavroudakis, M. Dossi, D. Moscatelli, "A Density Functional Theory Study of Secondary Reactions in n-Butyl Acrylate Free Radical Polymerization", *Macromolecular Theory and Simulations*, **2013**, *22*, 127-135.

5.   D. Cuccato, E. Mavroudakis, D. Moscatelli, "A Quantum Chemistry Investigation of Secondary Reaction Kinetics in Acrylate-Based Copolymers", submitted to *The Journal of Physical Chemistry, Part A* (jp-2013-02025p).

_____ _____ _____ _____ ____ __ __

_____ _____ _____ _____ ____ __ __

Abstract
_____ _____ _____ _____ ____ __ __

Among the large number of elementary steps involved in free radical polymerization, secondary reactions running beside the conventional kinetic scheme are as effective on the process features as they are hard to be experimentally characterized. Otherwise, computational chemistry based on quantum mechanics is emerging as a useful resource in the investigation of polymerization reaction kinetics. In this study, a theoretical approach is adopted to determine kinetic parameters of secondary reactions active in radical polymerization. Particularly, an improved density functional theory method is applied to the investigation of polymer systems with increasing complexity, with the final aim being acrylate polymers and copolymers. The relevance of backbiting in well-known free radical polymerization systems is highlighted, determining the effect of quantum tunneling on hydrogen transfer reactions. The role of mid-chain radicals in the origination of short branches is established by the characterization of their reactivity in the context of internal backbiting, propagation, β-scission, and chain transfer to agent reactions. Quantum chemistry is found to be a powerful tool in the estimation of kinetic parameters of less accessible reactions as well as in the understanding of intriguing radical polymerization mechanisms. Eventually, the cost-effectiveness of density functional theory methods in providing accurate rate coefficients is critically evaluated with respect to the study of borderline conditions, such as solvent and molecular conformation effects on reaction kinetics.

_____ _____ _____ _____ ____ ___ __

_____ _____ _____ _____ ____ ___ __

Contents
_____ _____ _____ _____ ____ ___ __

Part I - BACKGROUND

Part II – RESULTS AND DISCUSSION

List of Figures

Figure 13. *Reaction schemes of backbiting reactions involving polyethylene chains. Reaction symbolism referred to: 1:3 (bb13), 1:5, (bb15), and 1:7 (bb17) backbiting on linear chain; 1:3 (bb13^B), 1:5 (bb15^B), and 1:7 (bb17^B) backbiting on branched chain; 1:5 backbiting of short-branch radical (bb15^{SBR}).*

Figure 14. *Optimized geometries of reactant (top) and transition state (bottom) structures relative to the 1:5 backbiting reaction involving 1-octyl radical. Detail of the torsion motions around the dihedral angles at issue, according to the HR model adopted.*

Figure 15. *Reaction schemes of backbiting reactions involving polystyrene chains with atactic configuration m-m-r-m-r (left) and r-r-m-r-r (right), with the order of the diads starting from the radical end of the chain. From top to bottom: 1:3, 1:5, 1:7, and 7:3 backbiting.*

Figure 16. *Reaction schemes of backbiting reactions involving syndiotactic poly (vinyl chloride) chains. From top to bottom: 1:3 (left) and 1:7 (right) backbiting; 1:5 (left) and 7:3 (right) backbiting;5:9 backbiting.*

Figure 17. *Temperature dependence of 1:5 backbiting rate constant (k_{bb}) and ratio of 1:5 backbiting to chain-end propagation rate coefficients (k_{bb}/k_p) with and without considering the tunneling correction, referred to backbiting of 1-hexadecyl radical.*

Figure 18. *Reaction schemes of 1:3, 1:5, 1:7, and 7:3 backbiting reactions involving poly (butyl acrylate) chains investigated according to the simplified molecular model.*

Figure 19. *Reaction schemes of 5:9, 1:9, 1:11, and 1:13 backbiting reactions involving poly (butyl acrylate) chains investigated according to the simplified molecular model.*

Figure 20. *Optimized geometries of the transition state structures relative to the secondary reactions involving poly (butyl acrylate) chains investigated with the complete molecular model. Reactions of: a) propagation of mid-chain radical; b) propagation of short-branch radical; c) 1:5 backbiting of short-branch radical; d) β-scission.*

Chapter 5. *Pushing toward Prediction*

Figure 21. *Reaction schemes of the investigated backbiting steps, and detail of the replacement units.*

Figure 22. *Reaction schemes of the investigated propagation steps, and detail of the replacement units.*

Figure 23. *Reaction scheme of the investigated β-scission steps, and detail of the replacement units.*

List of Tables

Table 10. *Calculated values of activation energy, imaginary frequency associated to the transition state structure, tunneling factor, and rate coefficient for the forward (fw) and backward (bw) backbiting reactions involving poly (vinyl chloride) radicals. Rate coefficients are calculated at 330 K and comprehensive of the tunneling correction.*

Table 11. *Temperature dependence of the tunneling factors evaluated for 1:3, 1:5, and 1:7 backbiting reactions involving polyethylene, polystyrene, and poly (vinyl chloride) radicals. Backbiting along the main-chain of linear radicals is considered for polyethylene, while atactic polymer configuration r-r-m-r-r is adopted for polystyrene.*

Table 12. *Calculated values of reaction enthalpy, activation energy, pre-exponential factor, and rate coefficient for propagation involving poly (butyl acrylate) radicals at increasing chain length. Rate parameters are calculated at 298 K.*

Table 13. *Calculated values of tunneling factor, reaction enthalpy, activation energy, pre-exponential factor, and rate coefficient for forward and backward 1:3, 1:5, 1:7, 1:9, 1:11, and 1:13 as well as reversible 7:3 and 5:9 backbiting reactions involving poly (butyl acrylate) radicals according to the simplified molecular model. Rate constants and kinetic parameters are calculated at 298 K.*

Table 14. *Calculated values of activation energy, rate coefficient, size of the C-H-C angle in the transition state, and ring strain of the cycloalkane corresponding to the transition state ring for 1:3, 1:5, 5:9, 1:7, 1:9, 1:11, and 1:13 backbiting reactions involving poly (butyl acrylate) radicals according to the simplified molecular model. Rate constants are calculated at 298 K.*

Table 15. *Calculated values of reaction enthalpy, activation energy, pre-exponential factor, and rate coefficient for propagation of mid-chain radical, propagation and 1:5 backbiting of short-branch radical, and β-scission reactions involving poly (butyl acrylate) radicals according to the complete molecular model. Rate constants and kinetic parameters are calculated at 298 K.*

Chapter 5. *Pushing toward Prediction*

Table 16. *Calculated values of activation energy, rate coefficient, radical equilibrium parameter, and forward (fw)-to-backward (bw) backbiting rate constant ratio for the investigated backbiting reactions. In the reaction formulas, the characters A, S, and M correspond to methyl acrylate, styrene, and methyl methacrylate units, respectively. Rate constants and parameters are evaluated at 323 K.*

Table 17. *Sequence of the calculated radical equilibrium parameters for the most relevant backbiting reactions investigated, referred to a specific radical unit. The subscript bw denotes the backward backbiting step and indicates that the corresponding ΔE* value from Table 16 must be considered with the opposite sign.*

Chapter 6. *Exploring the Limits*

_____ _____ _____ _____ ____ __ __

_____ _____ _____ _____ ____ __ __

Summary
_____ _____ _____ _____ ____ __ __

F ree radical polymerization is a common and versatile way to synthesize macromolecular materials. However, a proper regulation of chain length distribution and morphology of the resulting polymer is often not easily achievable. Concerning the latter aspect, the presence of side reactions makes radical polymerization a complex network of kinetic steps: they involve a large number of species, which can be characterized by remarkably different physicochemical behavior. Moreover, they originate a huge variety of chemical pathways running beside the conventional scheme of radical polymerization. The kinetics of such "secondary" reactions may have a strong impact on the final polymer features, from chain microstructure to the macroscopic properties, depending on their relevance in the selected polymerization conditions.

The most important secondary steps are those involving the formation of mid-chain radicals, which exhibit quite different reactivity in comparison with conventional chain-end radicals. Backbiting reactions are the primary source of mid-chain radicals, which can undergo monomolecular β-scission or propagate, thus producing branches. Regarding copolymer systems, chain composition is an additional source of complexity in the entire kinetic mechanism, while cross-propagation reactions represent another relevant class of secondary steps. A common feature to all of the secondary reactions is the difficulty in determining their kinetics, due to the very small concentration and high reactivity of the active species involved as well as the large number of reactions that are in competition.

Nowadays, the development of pulsed-laser polymerization based techniques of analysis has led to a large investigation of reaction kinetics, mostly focused on acrylates. However, the experimental advances are still not sufficient to provide a detailed characterization of the kinetics of some interesting secondary steps. On the other hand, computational chemistry based on quantum mechanics allows the investigation of less accessible reaction pathways by a relatively easy procedure and using cost-effective methods.

Based on these issues, the PhD research summarized hereinafter has been focused on the quantum chemistry investigation of secondary reaction kinetics in free radical polymerization. Specifically, the first aim of the work was an attempt to improve the latest theoretical studies on the topic through an enhancement of the computational procedure. Afterwards, the investigation has been extended toward more complex and challenging systems, in order to test the predictive capability of the tool to examine quite inaccessible reactions. Finally, the limits of applicability of the method have been studied, considering borderline systems. A consolidated quantum chemistry approach based on the density functional theory has been adopted for the purpose, therefore kinetic and energy parameters could be estimated combining reasonable accuracy and computational effort. Reaction rate coefficients have been determined through the conventional transition state theory.

The quantum chemistry investigation of free radical polymerization kinetics has been focused primarily on homopolymer systems. Specifically, rate coefficients of reactions active in the polymerization of vinyl chloride have been determined using an improved density functional theory method, starting from a well-known reaction scheme and extending the kinetic study to a wide range of secondary reactions. Moreover, an efficacious modeling of the polymerization process based on a detailed reaction scheme including mid-chain radicals has been carried out. Particular attention has been given to backbiting kinetics, where the relevance of the quantum tunneling effect on hydrogen transpositions has been highlighted. Investigations have been then moved to acrylates, and secondary reactions active in butyl acrylate polymerization have been studied with respect to a set of interesting side steps. The relevance of consecutive internal hydrogen shifts has been determined, and a novel route to form short branches through backbiting of short-branch radicals has been proposed.

Afterwards, the attention has been turned toward the kinetic study of secondary reactions in acrylate copolymers. In particular, a terpolymer system composed by methyl acrylate, methyl methacrylate, and styrene monomer units has been adopted in order to examine the effect of copolymer composition on the kinetics of backbiting, propagation, and β-scission steps. The physicochemical behavior of different radical species with respect to the investigated reactions has been determined, providing the estimation of a large number of kinetic parameters. Furthermore, reactions of atom transfer from poly (butyl acrylate) active chains to various chain transfer agents have been investigated, with the aim of shedding light on their kinetic behavior when radicals of different nature and size are involved. The results have led to a deeper understanding of the mechanism of mid-chain radical patching by the action of chain transfer agents in the context of branching.

With the aim of exploring the limits of application of the adopted computational approach, the capability of the method in predicting solvent effect as well as the kinetics of copolymer systems characterized by functional monomers has been tested. The quantum chemistry tool improved with the implementation of an implicit solvent model has proven to be useful in determining the qualitative behavior of copolymerization involving functional acrylic monomers in the presence of polar solvents. Eventually, the research of optimized geometries of reactants, products, and transition states has been addressed, with a focus on the discrimination between global and local minimum energy structures. Torsion motions of side-chain groups have been performed on monomers and radicals involved in the propagation of methyl methacrylate, in order to elucidate the impact of the different possible conformers on the rate coefficient estimation.

In conclusion, quantum chemistry has proven to be suitable to the kinetic study of secondary reactions, especially when the attention is focused on the most challenging and inaccessible steps. Moreover, this approach represents a valid support to the experimental investigation as well as a useful tool for the comprehension of complex polymerization mechanisms.
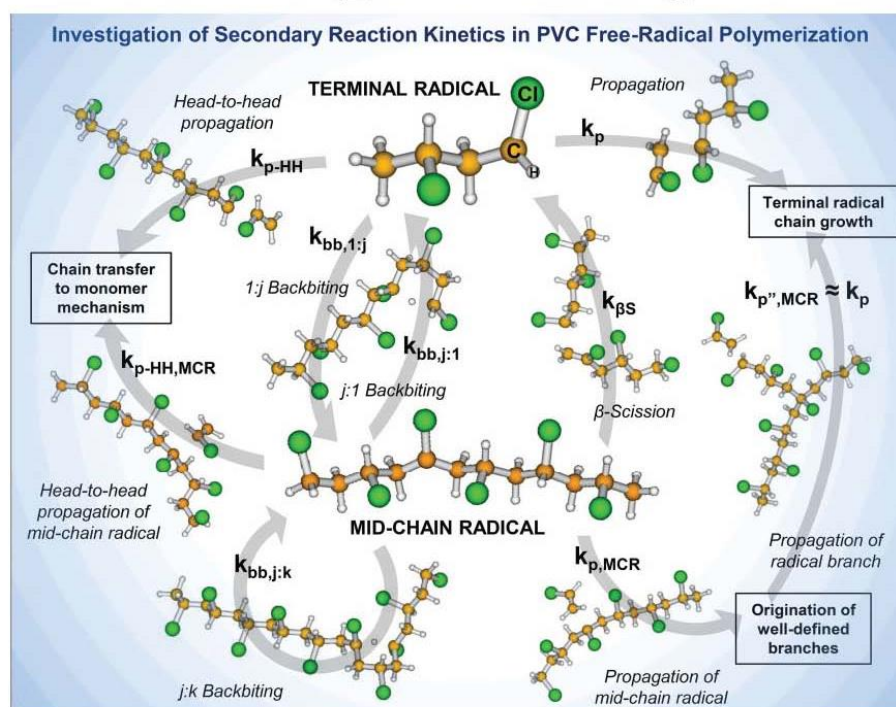
In the figure above, a scheme of relevant secondary reactions active in the free radical polymerization of vinyl chloride investigated through quantum chemistry is reported. Picture from the front cover of Macromolecular Reaction Engineering, Issue 8, 2012.

_____ _____ _____ ____ ___ __ __

CHAPTER 1

_____ _____ _____ ____ ___ __ __

Free Radical Polymerization
_____ _____ _____ ____ ___ __ __

1.1. Introduction

Free radical polymerization (FRP) is a common way to synthesize macromolecular materials through a radical chain process and avails itself of a large variety of vinyl compounds that are exploitable for the purpose. Moreover, high molecular weight polymer can be easily produced even under mild polymerization conditions and with the only need of monomer and a radical initiator. These features make FRP a very versatile process to obtain several polymer and copolymer compounds with peculiar properties.

Besides the advantages, the major issue with FRP is that it is often unsuited for a proper regulation of the chain length distribution as well as the morphology of the resulting polymer. The former aspect is primarily referable to the peculiarity of radical termination mechanisms, which have great relevance in determining the molecular weight distribution (MWD) of the final product. On the other hand, undesired or unpredicted polymer microstructure and morphology may come from the fact that FRP is, basically, a network of reaction steps that involve a large number of different species, including very reactive radicals. An indefinite variety of possible reaction pathways is therefore originated: their kinetics actually regulates the polymerization process and determines the final polymer features from the level of chain microstructure up to the macroscopic properties.

For this reasons, an accurate modeling of the FRP process may be a difficult task. However, the obstacle can be overcome in principle by the individuation of a set of fundamental reactions and parameters that regulate the most important polymer

properties in the most common polymerization conditions. Indeed, the polymerization behavior of many world-widely produced polymers is well known in many aspects, while it is possible to identify some fundamental reactions characterizing the polymerization process and get accurate estimations of the corresponding kinetic parameters.

1.1.1. Fundamental Reaction Scheme

Before going into a discussion of the challenging aspects of FRP as well as an analysis of the critical reaction pathways that may influence the polymerization process, a general overview of the classical scheme of reactions is given in this subsection. Focusing on the fundamental kinetics lying at the basis of radical chain polymerization, conventional steps of radical initiation, chain growth, bimolecular termination, and chain transfer belong in this context, as shown in **Figure 1**.

The initiation step produces active species able to start the polymerization process. In radical chain polymerization, the activation of an initiating molecule (i.e., an initiator or the monomer itself) forms radicals, and it occurs through a homolytic bond scission induced by heat, light, or another source of radiation. Once generated, the active molecule adds to a monomer unit by opening the π-bond of the vinyl compound: the first fragment of a propagating radical chain is thus produced.
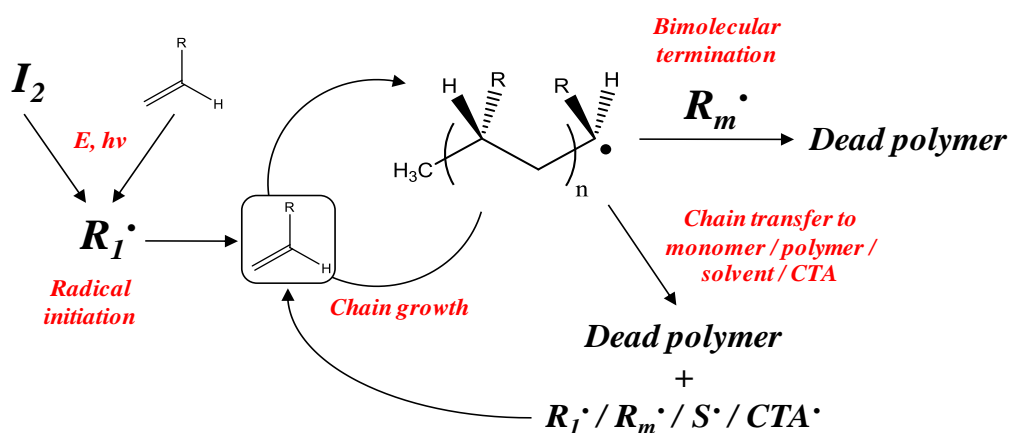
Figure 1. *Scheme of the fundamental reactions active in radical chain polymerization. I_2 is the initiator, $R_1^•$ and $R_m^•$ are radical chains composed of one and m units, $S^•$ and $CTA^•$ are radical fragments from solvent and CTA molecules, respectively.*

The radical chain propagates through consecutive additions of the active moiety to monomer molecules. The degree of polymerization reached by a growing chain is determined by the relative extent of propagation and termination events as well as by the mechanism of radical deactivation. Bimolecular termination implies the simultaneous death of two active chains, which can happen by coupling of the radical moieties, or by disproportionation (i.e., forming two non-radical products).

Chain transfer of an atom with unpaired electrons may cause the simultaneous termination of a radical chain and the activation of another molecule. The most common chain transfer events imply a shift of the radical toward a polymer chain, a monomer or solvent molecule, or a chain transfer agent (CTA). Chain transfer reaction acts as a regulator of the molecular weight in the circumstances in which it is in competition with the other termination mechanisms. While chain transfer does not modify the total amount of radicals, it may change the nature of the radical species, thus the reactivity of the system can be substantially affected if this reaction gains relevance.[1]

1.1.2. Challenges in Free Radical Polymerization

In the last decades, interest in the investigation of FRP kinetics has been growing. With the aim of getting a deeper understanding of the polymerization mechanisms of relevant monomers, the attention has been focused on those steps lying beyond the fundamental reactions mentioned above as well as beneath them. The former category is referred to the side reactions that run in parallel with the conventional ones, and may compete with them under certain polymerization conditions; the latter indicates those specific steps that can be at the basis of the fundamental mechanisms, though their detection may not be very easy.

Specifically, the interest in FRP was primarily driven by the fact that several side steps, usually referred to as secondary reactions, are responsible for undesired effects on the produced polymer, like the origination of microstructural defects, branches, and short-chain products. In this context, acrylates are to be mentioned, due to their large industrial application for the synthesis of polymer and copolymer materials. Moreover, these compounds are known to be subject to intermolecular and

intramolecular side reactions that quickly gain relevance as the process temperature is increased. The determination of the kinetics of secondary reactions for acrylate and other polymer systems of industrial relevance is a challenge at present, while its knowledge is valuable information for sophisticated modeling of FRP.

Another topic of relevant interest in the FRP field is represented by copolymerization. The additional parameter of monomer and copolymer composition increases the number of conventional reactions for which kinetic parameters need to be determined to describe properly the behavior of the system. The investigation of copolymerization is even more complicated if side reactions are also considered, as in the case of processes for the production of acrylate-based copolymers.

Finally, the attention is also moving toward functional monomers and polymers, with emphasis on acrylic compounds. The presence of particularly interactive side-chain moieties (e.g., carboxyl, ester, and hydroxyalkyl groups) may give rise to strong interactions between monomer or polymer molecules and the reaction medium, with significant effects on the polymerization kinetics. Functional monomers are under wide investigation at present, especially in the areas of acrylate copolymerization and the influence of polar solvents on reaction kinetics.

1.2. Secondary Reactions

In the complex reaction network of FRP, secondary reactions are those steps lying beyond the scheme of fundamental pathways described in the previous section and may regulate part of the features of the polymerization process. These secondary steps are in general responsible for the definition of a peculiar polymer microstructure, which can be ascribed to the formation of defects of various natures in the polymer chains. Nevertheless, secondary reactions may acquire relevance under process conditions far from the ideal, particularly at high temperature, when their effects can be observed clearly even in the macroscopic properties (e.g., MWD and polymerization rate).

All of these features come from the fact that secondary steps are the primary source of formation of mid-chain radicals (MCRs) and determine their reacting

behavior with respect to further reactions. An MCR exhibits a reactivity that can be remarkably different from that of a chain-end radical, due to the higher stability of the radical carbon in the former species. Moreover, MCRs can be involved in a wide range of other secondary steps, thus determining deviations from polymer chain linearity as well as from a regular sequence of monomer units (i.e., branches and microstructural defects can be originated).[2, 3]

While the effects of secondary pathways are in many cases directly observable in the final polymer, their kinetics at the molecular level is not easily detectable. Features and mechanisms of the most relevant secondary reactions are given in the following subsections, with emphasis on their correlation to MCRs and their direct consequences on the polymerization process. Furthermore, issues in the study of secondary reaction kinetics are highlighted, in order to point out the challenging aspects in the investigation of FRP.

1.2.1. Hydrogen Transfer and Backbiting

An MCR is originated by hydrogen transfer to polymer reaction, which determines the radical shift from the chain-end of an active macromolecule to a generic mid-chain position. This radical shift may involve different chains, as in the case of intermolecular chain transfer to polymer, or it may occur within the same chain itself. The latter reaction is intramolecular chain transfer, and it is commonly referred to as backbiting, especially when the radical is shifted in a well-defined mid-chain position close to the original chain-end. Backbiting is considered the primary event that originates MCRs, followed by chain transfer to polymer.[2]

The relevance of intramolecular transfer to polymer reaction in FRP processes has been described in the first half of the twentieth century.[4, 5] Hydrogen shift from a mid-chain position to the chain-end of an active macromolecule determines the formation of an MCR starting from a chain-end radical, as shown in **Figure 2** along with the detail of the commonly adopted nomenclature for backbiting. The different stability of the two radicals, which is usually in favor of the MCR, makes backbiting from a chain-end radical thermodynamically favorable.
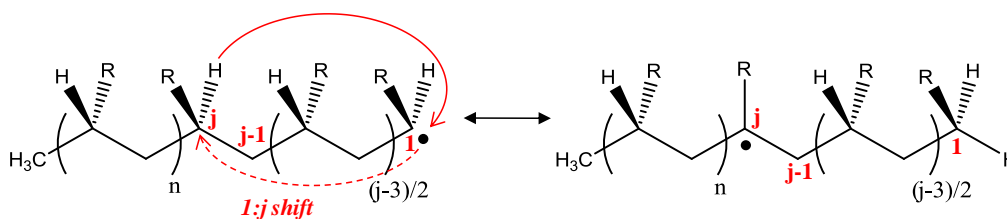
Figure 2. *Scheme of 1:j radical shift reaction, with detail of the notation adopted for backbiting nomenclature in relation to the carbon atom numeration.*

Backbiting is a monomolecular reaction, usually characterized by substantially high activation energy. More precisely, the configuration of the transition state ring associated to a backbiting step is a relevant parameter determining a reduction of the energy barrier from the average range of high values. In particular, the very stable six-member ring transition state typical of 1:5 backbiting can place this reaction in direct competition with other relevant steps in FRP, making its contribution on the overall polymerization kinetics far from negligible.[6, 7]

Besides well-defined hydrogen shift reactions, a chain-end radical can be transferred to an indefinite mid-chain position, due to the random-coil shape of polymer chains. However, the kinetics of this reaction is better comparable to that of intermolecular chain transfer. Moreover, a radical shift to a random mid-chain position is not likely to be affected by the transition state configuration, as it can be assumed for backbiting reactions involving very large transition state rings.

The probability of a backbiting event occurring from an MCR is in principles smaller than that of 1:*j* backbiting from a chain-end radical. The backward *j*:1 step usually agrees with this condition, given that the 1:*j* backbiting equilibrium is usually shifted to the MCR due to the different stability of the two carbon radicals. This is not the case of backbiting between MCRs, often referred to as *j*:*k* internal backbiting. There, hydrogen transfer is in principles equally favorable in both directions, and the corresponding equilibrium may shift the radical indefinitely along the chain, as shown in **Figure 3** for *j*:*j*±4 backbiting.
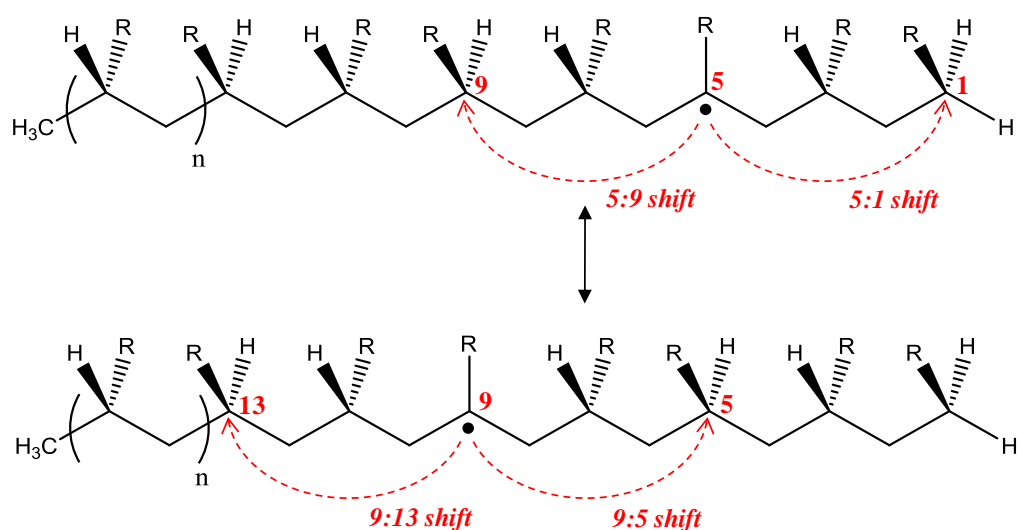
Figure 3. *Scheme of j:j±4 internal radical shift reactions following 1:5 backbiting.*

Recently, the interest in understanding backbiting mechanisms and determining their kinetics has been growing. In particular, the studies are being focused on backbiting in acrylate polymerization, where this reaction is known to be remarkably effective. The consequences of the radical nature and other features affecting the stability of the radical carbon with respect to backbiting reaction (e.g., backbiting involving different radical units, as in the case of intramolecular chain transfer occurring in copolymer chains) are challenging aspects in the investigation of FRP kinetics.

1.2.2. Branching Propagation

Once an MCR is formed, it can be subject to the conventional step of propagation, as shown in **Figure 4**. Propagation of MCR is an intriguing reaction, due to both its kinetics and consequences. The reactivity of a tertiary carbon radical with respect to the monomer addition is expected to be smaller than that of a less stabilized secondary radical. This feature leads to a slower propagation rate of MCRs if compared to chain-end radicals.
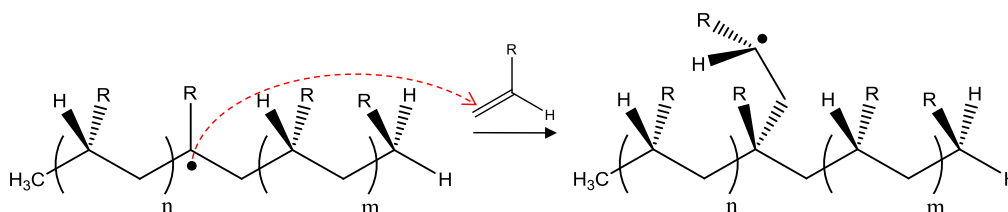
Figure 4. *Scheme of propagation reaction of mid-chain radical originating a short-branch radical.*

This kinetic aspect places propagation of MCR in competition with other secondary reactions whose kinetics is not equally scaled down when moving from chain-end to mid-chain radical, as in the case of backbiting. On the other hand, the smaller reactivity of MCRs often makes the contribution of their propagation on the overall polymerization rate negligible, especially under mild temperature conditions. It should be noted that this parameter is also correlated to the relative quantity of MCRs with respect to chain-end radicals in the system, which is in principle a function of the global secondary reaction kinetics.

The most relevant consequence of MCR propagation is the formation of branching points. While the relative extent of propagation of mid-chain versus chain-end radicals is a key parameter in the determination of the branching density produced by this mechanism, the size of the formed branches is related to the nature of chain transfer events.[8, 9] Specifically, MCRs produced after intermolecular transfer to polymer or random intramolecular chain transfer reactions are likely to originate long-chain branches (LCBs), while backbiting forms mostly short-chain branches (SCBs) with well-defined length. Regarding the latter case, the extent of the radical shift, in addition to the competition between MCR propagation and internal backbiting, may affect the side-branch length distribution, as detailed in **Figure 5**.
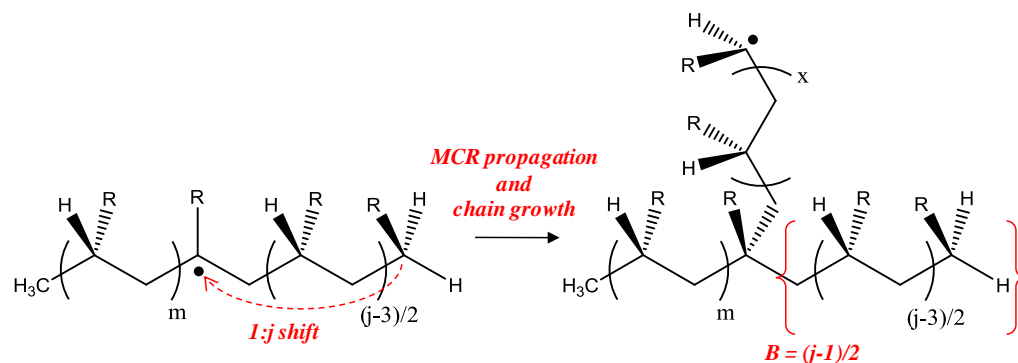
Figure 5. *Correlation between 1:j backbiting extent and size of the branch (B) formed after mid-chain radical propagation.*

After the monomer addition on an MCR, the product can be considered approximately a chain-end radical, as shown in **Figure 4**. More precisely, the proximity of the branching point characterizes the formed short-branch radical (SBR) with a peculiar reactivity, which is in principle intermediate between those of chain-end and mid-chain radicals. Moreover, the reactivity of SBR is likely to approach that of chain-end radical as long as few additional monomer units are attached. However, a detailed evaluation of MCR and SBR propagation kinetics in relation to that of chain-end radicals is not easy to be achieved and requires an accurate definition of the total radical distribution with respect to the different radical species.

1.2.3. β-Scission

MCRs can undergo monomolecular chain scission reaction through the break of a σ carbon-carbon bond in β position with respect to the radical carbon, which can happen in two symmetric directions. The so-called β-scission reaction is particularly active in high temperature processes, and it is characterized by very high activation energy values, comparable to those of depolymerization. This reaction leads to the formation of lower molecular weight products and originates a portion of dead chains with terminal double bonds, as shown in **Figure 6**.[2] Such olefin products can be considered as macromonomers, and in some cases their propagation can give a relevant contribution in the definition of the MWD of the final polymer.[10]
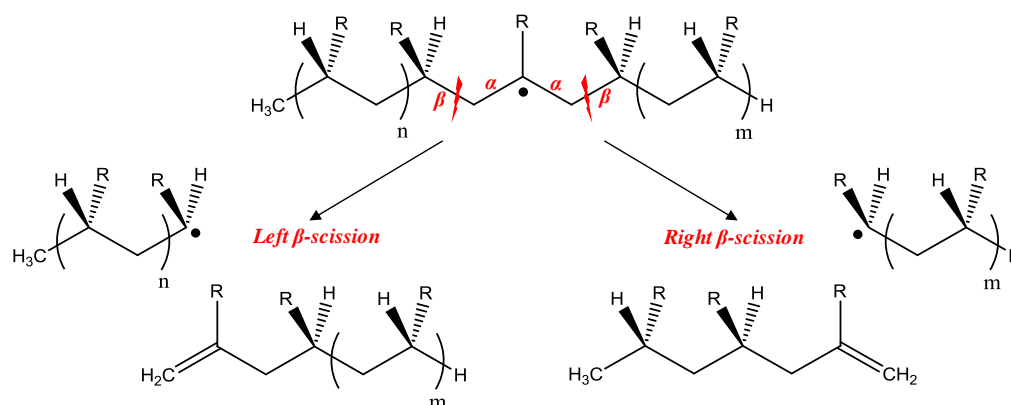
Figure 6. *Scheme of right and left β-scission reactions, with formation of low molecular weight products and terminal double bonds.*

In the case of β-scission following backbiting events, the break of the chain from a tertiary carbon radical relatively close to the chain-end produces radicals and polymers characterized by remarkably short chain length. For instance, the formation of dimers and trimers is a consequence of 1:5 backbiting followed by right or left β-scission. Such production of low molecular weight species is particularly observed in processes for the production of oligomers, such as what happens in the pyrolysis of hydrocarbons.[7, 11, 12]

1.2.4. Termination of Mid-Chain Radicals

Bimolecular termination involving MCRs is expected to be hindered by the less accessible radical site in an intra-chain position. Despite this steric effect, the intrinsic reactivity of an MCR with respect to bimolecular termination is commonly assumed to be close to that of a chain-end radical, given that such reaction is driven by diffusion limitations rather than a chemically activated process.[13, 14] In general, bimolecular termination involving MCRs is responsible for the production of LCBs, particularly in the case of termination by coupling.

In this regard, the combination of two MCRs or branched radical chains may give rise to crosslinking phenomena and is critical for the origination of gel polymer fractions. Gel formation is an undesired effect in many polymerization processes, not only determined by termination of MCRs but also by the presence of LCBs and the

extent hydrogen transfer reactions in general.[15] An accurate determination of these reactions kinetics can be relevant in understanding and preventing, or regulating, the crosslinking between polymer chains.

1.2.5. Other Secondary Reactions

Focusing on conventional reactions of chain transfer to small molecules (e.g., monomer, solvent, and CTA), it is reasonable to assume that the corresponding kinetics in presence of MCRs may be different from that of chain-end radicals. However, the kinetics of these reactions is hard to predict in principle as well as to determine. This issue is particularly relevant when dealing with polymer systems where such reactions cannot be neglected (i.e., where chain transfer to monomer is the dominant termination mechanism, or when a CTA is intentionally added).

Moving to SBRs, their peculiar reactivity opens the way for a wide range of other specific secondary steps, besides their propagation that has been mentioned previously. The unusual kinetic behavior of SBRs compared with chain-end and mid-chain radicals makes their reactivity hard to predict in the context of the other secondary reactions described in the previous chapters. In particular, it is interesting to understand how the backbiting probability can be affected by the different geometry configuration and stability of an SBR with respect to the corresponding chain-end radical.

1.3. Functional Monomers

Functional monomers are those showing particularly reactive side-chain groups that can be exploited in order to synthesize more complex vinyl compounds, such as macromonomers, or to improve the functionality of preformed polymer chains. Moreover, these monomers and polymers can be used to trim some polymerization features and properties of the final product, taking the advantage of a solvent or a polymerization medium able to interact specifically with the functional groups.

Acrylamides, vinyl ethers, and vinyl esters are the most important classes of functional monomers suitable for radical polymerization. Cyclic amides and esters are well-known functional groups, in addition to the carboxyl, hydroxyalkyl, and glycidyl moieties characterizing acrylates. The class of vinyl esters includes very common functional monomers that are widely used in FRP processes. Besides acrylic acid (AA) and its methacrylic equivalent (MAA), monomers characterized by the hydroxyalkyl moiety are to be mentioned, such as 2-hydroxyethyl acrylate (HEA) and the corresponding methacrylate (HEMA).

Functional polymers are widely used in the making up of biochemistry applications, due to their established biocompatibility and, in many cases, biodegradability feature. Specifically, copolymer formulations involving the monomers cited above (e.g., AA-co-acrylamide, MAA-co-HEMA) are employed in the production of nanoparticles for drug delivery systems, as well as thermo- and pH-sensitive stimuli-responsive coatings.[16] Moreover, functional monomers HEA and glycidyl methacrylate (GMA) can be used in the preparation of acrylic resins in order to enhance the crosslinking reactions.

1.3.1. Solvent Effect on Reaction Kinetics

Functional monomers and polymers are likely to interact with a polar solvent or reaction medium due to the effect of intermolecular forces, which can vary from polarization and dipole interactions up to stronger hydrogen bonding. As anticipated before, the nature and extent of these interactions can modify the standard polymerization behavior of monomers and radical species. In principle, all of the reactions in FRP can be influenced, from the conventional propagation up to the secondary steps, through modification in the standard reactivity of the radical moieties.

Starting from the fact that propagation kinetics can be affected by the choice of the polymerization medium in the presence of functional monomers, this aspect for copolymers is reflected in the overall copolymerization rate and copolymer composition. Even in the absence of a specifically selected solvent for the reaction, a bulk copolymerization medium including functional monomers can be a critical

solvent by itself, with properties that, in principle, are changing alongside the monomer composition. In this regard, acrylic copolymers are often produced combining greater and lesser functionalized monomers, and the solvent effect is thus likely to be observed as much in bulk as in presence of an interactive reaction medium.[17] However, a considerably large experimental investigation is required in order to examine the combined parameters of monomer composition and solvent choice; therefore, it is interesting to investigate the problem from another perspective (i.e., by using alternative tools).

Focusing on backbiting, recent studies have examined the kinetic effect of various solvents on those reactions determining the polymer microstructure in the context of the formation of branches. An enhancement of hydrogen bonding has been found to reduce the extent of intramolecular chain transfer in polymer systems where backbiting is effective, as in the case of the polymerization of butyl acrylate (BA) in presence of *n*-butanol (BuOH). This feature is also observable in the bulk polymerization of HEA, where the monomer acts as a hydrogen bond hosting reaction medium. On the other hand, solvents disrupting the hydrogen bond interactions enhance the backbiting probability, as in the case of radical polymerization of HEA in dimethylformamide (DMF).[18, 19]

This specific case of intramolecular chain transfer, together with the knowledge that all individual reaction kinetics can also be modified with respect to a proper choice of the solvent, gives relevance to the investigation of solvent effect on FRP kinetics. The challenging aspect of this study is represented by the possible introduction of the reaction medium as an additional parameter to trim the effects, whether desired or not, of secondary reactions and pathways determining the polymer morphology.

CHAPTER 2

Investigation of Reaction Kinetics

2.1. Background

With reference to the topics discussed in the previous chapter, the kinetic study of FRP conducted in the past decades has been made possible due to a rapid and decisive development of methods and tools for the investigation of reaction kinetics. On the one hand, the experimental analysis has received a strong incentive by the introduction of pulsed-laser polymerization (PLP) techniques, which are now adopted as benchmarking methods for accurate determination of reaction rate parameters. One the other hand, the computational approach based on quantum chemistry has reached a good level of reliability through a series of studies and applications on FRP that have been carried out in the past recent years, in parallel with the necessary development of the computing power.

The two approaches focus on the issue of evaluating reaction kinetics starting from opposite foundations. Eventually, their results are supposed to converge within a range of uncertainty, providing that the sources of inaccuracy intrinsic of both methods are removed or at least minimized. Up to now, quantum chemistry has been applied to macromolecular systems mostly in an incessant attempt to validate the obtained computational results through a comparison with better reliable experimental data. However, the increasing urge to deepen the investigation of FRP on reactions and pathways not easily accessible by the current experimental procedure is emphasizing the predictive potentiality of the quantum chemistry tool.

From a general perspective, the experimental and computational approaches can be considered as complementary, while the better suitability of one method rather than the other is strongly dependent upon the nature of the reactions that are to be studied in relation with the level of development reached by the experimental techniques. Although in principles the quantum chemistry approach goes beyond the physicochemical limitations that a certain reaction may exhibit from an experimental point of view, it should be noted that the accuracy of the computational results is in many cases hard to be enhanced. The issue of maintaining a reasonable level of calculation feasibility is often a priority (i.e., very accurate calculations requiring prohibitive computing time are poor support to the experimental analysis), thus a necessary level of approximation needs often to be considered.

Given these remarks, the most recent developments in the analysis of reaction kinetics are discussed in the following sections with reference to the literature. The focus is particularly stressed on the potentiality and limits of both experimental and computational approaches, in the context of the estimation of rate coefficients concerning the reactions and systems of interest described in the previous chapter.

2.2. Experimental Advances

A particular attention has been recently focused on the FRP of acrylic monomers. Owing to the large variety of functional groups available, numerous monomers belong to this category, and they are characterized by peculiar kinetic behavior and final polymer properties. Acrylate polymers find a wide range of applications, including surface treatments, biomedical applications, and their use as additives for material processing, all of these features determining their great industrial and commercial relevance.

Focusing on the kinetic aspects, a close correlation is present between secondary reactions kinetics in acrylate polymerization and some features observed in the resulting polymer, such as the degree of branching and the formation of gel fractions.[8, 20-22] Particularly critical cases are high temperature polymerization processes, as like as those carried out to obtain low molecular weight polymer resins

and oligomers in general.[11, 23] Moreover, the peculiar functionalities of acrylic compounds and their consequent attitude to interact with polar molecules or moieties broaden the variability of kinetic behaviors, especially in the case of copolymerization.[17]

The great interest towards acrylates has motivated the performing of large experimental investigations on FRP of acrylic monomers in the past decades, supported by the development of advanced techniques for the analysis of reaction kinetics based on PLP. This method has improved significantly the quality of measurement of individual reaction rate coefficients in radical polymerization.

2.2.1. Pulsed-Laser Polymerization

PLP consists in an instantaneous production of small radicals by the irradiation of a photoinitiator through laser pulses with a given frequency. Within the time lapse between two consecutive laser pulses (t_0), the formed radicals are able to propagate up to reaching a chain length (L_0) which is inversely proportional to the pulse repetition rate characteristic of the laser, as long as chain transfer reactions do not play a significant role. In this case, the correlation between the polymerization parameters is shown in **Equation 2.1**, where M is the monomer concentration and k_p is the propagation rate coefficient. PLP combined with analytical chemistry techniques allows the determination of fundamental kinetic parameters.[24, 25]

$$L_0 = k_p \, M \, t_0 \tag{2.1}$$

PLP is usually combined with chromatography, spectroscopy, or nuclear magnetic resonance (NMR) methods of analysis, in order to determine the fundamental features of the produced polymer as well as the relative concentration of the different radical species that populate the system. Specifically, PLP coupled with size-exclusion chromatography (SEC), electron paramagnetic resonance (EPR), and near infrared spectroscopy (NIR) allows the investigation of a relatively large set of reactions in FRP.[14, 24] Details and features of the most common PLP-based techniques are given in the following paragraphs, focusing on the relevant reactions whose investigation has been made possible by these experimental approaches.

2.2.2. Propagation Kinetics

Accurate propagation rate coefficients of various monomers, specifically acrylates, have been determined so far by PLP-SEC at low temperature and high pulse repetition rates.[26-28] Besides AA and MAA esters, styrene (St) and its substituted derived compounds, vinyl esters, and other olefins have been extensively studied through this approach. The propagation rate coefficient is determined through the analysis of the peculiarly structured MWD of the polymer obtained by PLP. This operation is usually carried out by SEC sampling.

Although PLP-SEC has been selected as the IUPAC-recommended method to yield propagation rate coefficients, its performances are called into question when intramolecular chain transfer acquires relevance, as in the case of acrylate polymerization. Studies in the last decade have shown that secondary reactions, particularly 1:5 backbiting, can be a source of significant interference in the determination of propagation kinetics through PLP over room temperature and applying pulse repetition rates below 100 Hz. Unstructured MWD are likely to be obtained, thus propagation rate coefficients cannot be determined properly in these conditions.[26, 28, 29]

Such partial failure of PLP-SEC in determining accurate rate parameters for acrylates has been overcome by operating at a higher laser frequency.[26] Moreover, a recent publication provided the definition of a feasibility region in the temperature versus pulse frequency map, that is aimed to help obtaining accurate propagation rate coefficient values even if high temperature reaction is carried out.[30]

2.2.3. Secondary Reactions and Termination

Experimental studies of secondary reaction kinetics have been focused almost exclusively on acrylic monomers, particularly on BA. The investigation of backbiting kinetics has been performed by frequency-tuned (ft)-PLP-SEC.[13] Moreover, carbon (^{13}C)-NMR has been adopted for the analysis of the branching density.[8]

Propagation of MCRs has been also studied by ft-PLP-SEC experiments.[13] Alternatively, EPR has been adopted to measure the ratio of chain-end to mid-chain radical concentrations, which is directly correlated to the ratio of MCR propagation to

backbiting rate coefficients.[31] The investigation of MCR propagation kinetics is made feasible under the assumption of an equilibrium between chain-end and mid-chain radical concentrations, determined by the corresponding equilibrium between the two mechanisms of radical interconversion (i.e., backbiting and MCR propagation).[13] This assumption is valid as long as the contribution of bimolecular termination on the death of MCRs is negligible.

Focusing on bimolecular termination, rate coefficients have been determined through PLP techniques initiated by a single pulse (SP). Specifically, the SP-PLP-NIR has been adopted first, and mean values of the termination rate coefficient have been obtained.[27] The performing of SP-PLP-EPR experiments has allowed monitoring the concentration of the two types of radical under non-stationary reaction conditions, in order to estimate directly the chain length dependent termination rate coefficients for chain-end radicals and MCRs.[14]

2.3. Computational Chemistry

Through the computational investigations of FRP that have been performed so far, the theoretical approach based on quantum chemistry has proven to be a useful tool in the qualitative prediction of the polymerization reaction behavior. Moreover, in many cases the accuracy of the obtained kinetic data has shown to be satisfactory compared with the experimental uncertainties, though better results have been obtained in the determination of reactivity ratios rather than the estimation of absolute rate coefficients. At last, the computational investigation keeps free from some issues related to managing a real system, such as restricted ranges of temperature operability and toxicity of the materials, thus this approach can be applied to different contexts through a common and relatively simple procedure.

Computational chemistry methods based on quantum mechanics have been applied to the investigation of polymerization kinetics for a couple of decades. Starting from the first approaches to the study of radical propagation of short molecules, the attention has been progressively moved toward larger systems. The development of density functional theory (DFT) methods has allowed the treatment of

longer and more complex polymer chains and paved the way for the investigation of secondary reactions involving MCRs.[32]

Given that a detailed description of the quantum chemistry approach is produced afterwards in a dedicated chapter, with particular focus on the DFT, an overview of the computational studies on the FRP topics previously discussed is shown in the following paragraphs. The attention is driven on the most relevant achievements, organized in the chronological sequence of reactions and systems that have been subject of investigation in the past fifteen years.

2.3.1. Radical Addition to Alkenes

The early studies have been focused on the addition reaction of carbon-centered radicals to alkenes and other unsaturated molecules.[33, 34] Reaction barriers and enthalpies are determined explicitly and directly by the quantum chemistry approach. Therefore, estimates of such parameters at different levels of theory could be compared with experimental data obtained for the addition of a methyl radical to ethene and various other alkenes with generic formula CH_2CXY.[33] The study of reactions involved in the thermal cracking of hydrocarbons, particularly the addition of ethylbenzene radical to ethene, was one of the first attempts to test the DFT in the investigation of reaction kinetics belonging to the radical polymerization field.[34] Latest computational works on these radical initiation-like reactions have been performed involving typical vinyl monomers of FRP, such as methyl acrylate (MA) and methacrylate (MMA), acrylonitrile, and St.[35, 36]

As anticipated above, the development of DFT methods has allowed the treatment of relatively large polymer systems, thus the studies were subsequently moved from the reactivity of monomer radicals to that of radical chains with definite length. In this regard, the investigation of propagation reaction was made feasible taking into consideration the chain length effect on the reaction rate coefficient. The first studies approached the radical propagation of ethene,[37, 38] vinyl chloride,[39, 40] and acrylonitrile,[39, 41] which are alkenes characterized by very simple molecular structure. The attention was then moved toward monomers that are more complex and

exhibit larger substituent groups. Specifically, the homopolymerization of St has been studied in addition to that of acrylic and methacrylic esters.[35, 42]

2.3.2. Copolymerization Kinetics

The development of the computational investigation of propagation kinetics and chain length effect turned the attention on copolymer systems. Particularly, the interest was driven by the need of determining cross-propagation rate coefficients, which are those involving the addition of a terminal radical unit to an alkene of a different monomer nature. Since this reaction kinetics is not directly accessible by the experimental approach, quantum chemistry has placed itself as a useful tool for a detailed investigation of copolymerization.

Computational studies have been carried out extensively on acrylate-based copolymer systems. In many cases, the validity of the obtained results has been supported by experimental investigations with PLP-SEC combined with proton (^{1}H)-NMR analysis, thus measuring copolymerization rate and polymer composition as a function of the comonomer fractions. The copolymerization of common acrylic monomers MMA and MA was studied first, and then the attention has been focused on systems involving other acrylates and vinyl esters as well as functional acrylates and methacrylates.[43-48] In these works, monomer reactivity ratios have been predicted *a priori*, while on the basis of terminal and penultimate unit models of copolymerization the results could be compared with the experimental data, obtaining appreciable agreements between the two approaches.

2.3.3. Reactivity of Mid-Chain Radicals

The potentiality of the quantum chemistry approach has driven the investigation toward MCRs and secondary reactions for a bit less than a decade. Intramolecular hydrogen transfer reaction was firstly studied on poly (vinyl chloride) (PVC),[49] focusing on the 1:2 radical shift, as well as on peroxy radicals undergoing 1:5 backbiting in the context of low temperature processes of hydrocarbon oxidation.[50]

21

The importance of the transition state ring size on backbiting kinetics has been confirmed by subsequent investigations of St polymerization at high temperature, where the 1:5 shift was found to be the most favored step as well as 3:7 backbiting. Moreover, β-scission reaction was studied, and its impact in the production of low molecular weight oligomers in combination with the 1:5 radical shift producing MCRs confirmed the experimental observations.[7] Further studies on the combined effect of backbiting and β-scission reactions kinetics under high temperature conditions were conducted on vinyl chloride and acrylonitrile.[51]

The latest computational studies on the topic have extended the computational approach to other secondary reaction, in order to shed light on the role of MCRs in a wider perspective. Detailed works on PVC belong in this context, where various reactions responsible for the formation of structural defects (e.g., branches and internal double bonds) have been investigated.[52, 53] Finally, intermolecular chain transfer in acrylate polymers has been approached by quantum chemistry investigation.[54]

2.3.4. Modeling of Solvent Effect

The majority of the quantum chemistry calculations have been performed in a vacuum environment, thus considering polymerization reactions as if they are proceeding in the gas phase. However, most of the polymerization processes are carried out in solution, with the interactions between reacting moieties and solvent molecules often non-negligible. This issue is particularly relevant when the reaction medium exhibits a strong polarity, and in presence of monomer and side-chain groups with particularly interactive functionalities, as discussed before. From the computational point of view, the solvent effect can be modeled considering explicit solvent molecules and characterizing the specific interactions, or using continuum models.[32] The former approach is clearly more effective, while it is often coupled with a prohibitive computational cost. Few recent works are reported in the literature in the attempt of investigating the influence of water on the propagation of acrylamide,[55] and the solvent effect on the tacticity of a propagating MMA chain.[56] One of the major issues of this approach is represented by the restricted number of

solvent molecules that can be treated, not to mention the choice of their displacement around the reaction site that must retain a degree of arbitrariness.

Continuum models for treating the solvent effect consider the solvent molecules as implicitly embedded in cavities surrounded by a dielectric continuum. Typical models belonging to this category are COSMO (conductor-like screening model) and PCM (polarizable continuum model), particularly suitable for treating large systems.[57, 58] Continuum models are considered adequate for radical thermochemistry, and have been used in the determination of the solvent effect and its relevance for various FRP systems.[39, 42, 59, 60]

2.4. Status Quo of the Approaches

The relevance of secondary reactions along with other challenging aspects of FRP has been discussed in the previous chapter, with specific focus on the most interesting steps as well as on the importance of understanding their kinetic behavior. The analysis of the existing methods for the investigation of reactions kinetics in FRP has revealed that computational chemistry and the experimental analysis can be considered as complementary approaches, each one showing its own advantages. However, they both exhibit limitations as well as points to be improved, which are summarized in this section.

2.4.1. Limitations and Room for Improvement

Despite the remarkable improvements in the experimental analysis that have been achieved in the recent past, the complexity of FRP kinetic schemes makes some areas and topics still difficult to be examined. Focusing on backbiting, the determination of single reaction rate coefficients related to well-defined hydrogen shift steps is still hardly affordable at the experimental level, therefore average values of the rate coefficient or pseudo-kinetic constants are usually estimated rather than the evaluation of the contributions of specific steps. Moreover, while backbiting and MCR propagation rate coefficients have been determined so far, there is no information about the kinetic behavior of SBRs and other peculiar radical chain configurations.

Finally, the most relevant studies have been focused on few acrylates, while the behavior of other interesting polymer systems is still undetermined at the PLP level. In this regard, the focus on copolymerization increases the interest as well as the difficulties of a comprehensive experimental investigation of the numerous reaction pathways that may be involved.

On the other hand, the computational tool has helped to overcome some of the experimental obstacles, and it is well suited to the investigation of the less accessible reaction pathways. However, an improvement of the accuracy of the predicted energy and rate coefficient values is still a primary issue. The major limits and sources of inaccuracy of the computational approach are related to the restricted size of the polymer system that can be studied at this level of detail, despite the application of the DFT. This way, part of the molecular interactions determining the physicochemical behavior of the real systems is not considered properly, if not neglected. Moreover, dynamic motions of the reacting moieties, especially those related to side-chain groups, cannot be described properly with the only contribution of quantum chemistry.

2.4.2. PhD Thesis Project

Based on these issues, the PhD research has been focused on the quantum chemistry investigation of secondary reaction kinetics in FRP, as well as on the improvement of the computational methodology. Specifically, the work has been carried out answering three specific purposes, which are described below. In accordance with these objectives, the results of the computational research that are showed in the dedicated part of the Thesis (Part II) are subdivided in three corresponding chapters.

1)   *Widening and Improvement*. The first aim of the work was an effort to improve the latest quantum chemistry studies on FRP through the enhancement of the computational procedure. Moreover, the previous investigations were extended towards more interesting reactions and polymer systems, besides the development of a simple but fundamental modeling of FRP including MCRs in the kinetic scheme.

2)   *Pushing toward Prediction*. The potentiality of the tool has thereafter motivated the direction of the study to more challenging systems characterized by higher complexity and intrinsic limitations from the experimental point of view. This way, the predictive feature of the method has been tested. In this regard, secondary reactions in copolymer systems and chain transfer to agent kinetics have been studied, comparing the reactivity of MCRs, chain-end, and other sort of radicals.

3)   *Exploring the Limits*. The last purpose of this work was an attempt to get a better understanding of the limits of applicability of the computational tool at the quantum chemistry scale, focusing on solvent effect in the presence of functional copolymers as well as on the relationship between reactant geometries and corresponding kinetic rate coefficients.

The aim of this research is pursued through a computational approach, and in particular using a well-established procedure for kinetic calculations based on quantum chemistry. A description of the computational method adopted is provided in the following chapter, along with the theoretical fundamentals lying at its basis.

—————————— —————————— ———— ——— ——— ——

CHAPTER 3

—————————— —————————— ———— ——— ——— ——

Computational Method

—————————— —————————— ———— ——— ——— ——

3.1. Quantum Chemistry

Theoretical quantum chemistry is a branch of the general field of computational chemistry, which is focused on the investigation of chemical phenomena using computers and their essential power in performing calculations. Specifically, the solution of a chemical problem involving polyatomic species, the so-called many-body problem, is obtained applying the principles of quantum mechanics. Quantum chemistry takes advantage of various methods derived from the theoretical chemistry in order to determine the energy of multi-atom, multi-electron systems starting from the basic Schrödinger equation.[61]

3.1.1. Fundamentals of Quantum Mechanics

Quantum mechanics provides a mathematical description of the physical properties of particles through the introduction of a wavefunction (Ψ), which characterizes their quantum state and behavior. Regarding a quantum system, the Schrödinger equation describes its physical evolution over time, as like as Newton's law works for a classical mechanics system. A compact form of the time-independent Schrödinger equation, at the basis of quantum chemistry, is given by **Equation 3.1**, where H is the Hamiltonian operator, and E is the total energy.

$$H\Psi = E\,\Psi \tag{3.1}$$

The Hamiltonian operator can be written as a function of kinetic energy (T) and potential energy (V) of the system of interest. For a multi-atom system, the kinetic energy accounts for the motions of nuclei (n) and electrons (e), while the potential energy contribution due to electrostatic interactions between the charges must include nucleus-nucleus (n-n), electron-electron (e-e), and nucleus-electron (n-e) interaction terms. Accordingly, a compact form for the Hamiltonian is given by **Equation 3.2**.

$$H = T_n + T_e + V_{n-n} + V_{e-e} + V_{n-e} \tag{3.2}$$

In general, the solution of the Schrödinger equation depends on spin and position coordinates of all the electrons ($\bar{y}$) and nuclei ($\bar{Y}$) of the system, as shown in **Equation 3.3**.

$$[(T_n + V_{n-n}) + (T_e + V_{e-e} + V_{n-e})]\Psi(\bar{Y}, \bar{y}) = E\,\Psi(\bar{Y}, \bar{y}) \tag{3.3}$$

However, the two contributions of nuclei and electrons can be separated with the introduction of the Born-Oppenheimer approximation.[62-64] The physical principle that electrons may reach an equilibrium position faster than nuclei (i.e., nuclei can be considered stationary in comparison with the motion of the electrons) allows neglecting the coupling between nuclear and electronic velocities. Hence, the Schrödinger equation can be solved as the product between two wave function contributions, referred respectively to the nuclei *(Ψ_n)* and to the electrons *(Ψ_e)*, with the former depending on the nuclear position only, as shown in **Equation 3.4**.

$$\Psi(\bar{Y}, \bar{y}) = \Psi_n(\bar{Y})\,\Psi_e(\bar{Y}, \bar{y}) \tag{3.4}$$

Introducing the obtained functional form in **Equation 3.3**, the Schrödinger equation can be written for the electrons only, while the nuclei are treated separately as classical particles giving rise to an electrostatic field in which the electrons move. Finally, the total energy can be determined as a function of the electronic energy (E_e) and the contribution of nuclei, according to **Equation 3.5**.

$$E = \frac{(T_n + V_{n-n})\Psi_n(\bar{Y})}{\Psi_n(\bar{Y})} + E_e \tag{3.5}$$

The main issue of quantum chemistry is represented by how to calculate the electronic energy, since an accurate determination of the electronic wave function is required (a procedure that is known to be very demanding). Methods that are aimed at solving the electronic Schrödinger equation are referred to as electronic structure methods and are discussed in the following paragraph.[61]

3.1.2. Electronic Structure Methods

A detailed description of the electron distribution is achievable by means of quantum chemistry through a solution of the time-independent Schrödinger equation. Electronic structure methods treat the dynamic of multi-electron systems under the simplification of the independent-particle model, which means that the interaction between particles is approximated. In this context, the Hartree-Fock (HF) method considers all interactions but in an average fashion, therefore its accuracy is considered acceptable in comparison with other electronic structure methods.[65-70]

In the HF model, each *i*-th electron is described by a molecular orbital wave function (ϕ_i), and the total wave function is approximated by a product of orbitals, which are rearranged in the Slater determinant shown in **Equation 3.6** in order to satisfy the asymmetric condition for the overall wave function.

$$\Phi(\bar{y}) = \frac{1}{\sqrt{N!}} \begin{vmatrix} \phi_1(\bar{y}_1) & \phi_2(\bar{y}_1) & ... & \phi_N(\bar{y}_1) \\ \phi_1(\bar{y}_2) & \phi_2(\bar{y}_2) & ... & \phi_N(\bar{y}_2) \\ \vdots & \vdots & \ddots & \vdots \\ \phi_1(\bar{y}_N) & \phi_2(\bar{y}_N) & ... & \phi_N(\bar{y}_N) \end{vmatrix} \qquad (3.6)$$

Starting from the definition of the HF equations, additional approximations can lead to the development of semi-empirical methods, in the case of a direct reference to experimental data. On the other hand, where no parameter is fitted to experimental data in order to generate the solution, the method is referred to as *ab initio*. Finally, the addition of more determinants generates models that can be made to converge toward the exact solution of the electronic Schrödinger equation. The definition of a multi-determinant wave function is necessary for electron correlation methods, which are discussed hereinafter.[61]

3.1.3. Electron Correlation Methods

The HF method takes into account an average contribution of the electron-electron interaction. This feature allows the HF wave function to be able to account for approximately 99% of the total energy, providing that a sufficient basis set is adopted (with reference to the next paragraph for a discussion of basis sets). However, the remaining 1% is often very important for describing chemical phenomena. The difference between HF energy and the lowest possible energy in the given basis set is the electron correlation energy, which accounts for the correlated feature of relative motions between the electrons. Electronic structure methods take into account also the electron correlation energy and provide its calculation, and they are usually referred to as electron correlation or post-HF methods.[65-68, 70, 71]

As anticipated before, increasing the number of Slater determinants is a condition that makes accessible the calculation of the electron correlation energy, and the HF solution can be adopted as a starting point for an improvement of the method. A generic multi-determinant wave function can be written as in **Equation 3.7**, in the shape of a linear combination of the single Slater determinant used in the HF model, with a_0 determined by normalization condition.

$$\Psi = a_0 \, \Phi_{HF} + \sum_{i}^{N_d} a_i \, \Phi_i \tag{3.7}$$

The total number of determinants (N_d) that can be generated depends upon the basis set dimension. Electron correlation methods differ in the way they calculate the coefficients in front of the other determinants (a_i). The main post-HF methods for calculating the electron correlation energy are the multi-reference configuration interaction (CI), the many-body perturbation theory (MBPT), the Møller-Plesset (MP), and the coupled cluster (CC).[61, 72-74]

3.1.4. Basis Sets

Although *ab initio* methods do not use directly experimental data to obtain the solution of the wave function, they can make indirect reference to them as an expedient to guide the selection of the proper computational model with respect to the corresponding level of approximation. In this context, an essential approximation inherent in all *ab initio* methods is the introduction of the basis set, which consists of the expansion of the molecular orbital wave function in a finite number (N_b) of known basis functions (χ_i), as shown in **Equation 3.8**.[70, 75]

$$\phi_k(\bar{y}) = \sum_{i}^{N_b} c_{ik}\ \chi_i(\bar{y}) \tag{3.8}$$

The basis set approximation makes feasible the calculation of the wave function for multi-atom systems, through the selection of type and number of functions to be used. There are two types of basis functions: the Slater-type orbitals (STO) and the Gaussian-type orbitals (GTO), which differ in the functional dependence upon the radial coordinate and in the description of the behavior near the nucleus.[76, 77] With regard to N_b, the smallest number of functions possible is referred to as the minimum basis set (e.g., two *s*-functions and one set of *p*-functions for the first row in the periodic system). Improved double-zeta (DZ) and triple-zeta (TZ) basis sets contain respectively twice and three times as many functions as the minimum basis set, and so on. In the case of a multiplication of the number of valence orbitals only, basis sets are referred to as split-valence.

Contracted basis sets are combinations of full sets of primitive basis functions into smaller sets of functions by forming linear combinations, in order to focus on describing also the chemically important (but energetically less relevant) electrons far from the nuclei, which depend on the wave function tail rather than its core.[78] In this category, Pople basis sets are very popular for the investigation of macromolecular systems. Moreover, they can be improved with the addition of diffuse functions (to heavy atoms only or also hydrogen), and/or a number of polarization functions with a separated designation for heavy atoms and hydrogen.[79, 80]

Another important class of basis functionals is represented by complete basis set (CBS), which is a composite procedure that is aimed to extrapolate the calculations with systematically larger basis sets up to the basis set limit. CBS methods combine calculations at different levels of theory, in order to produce very accurate energy estimates with an uncertainty comparable to that of experimental results (i.e., within 4 kJ mol^{-1}). For instance, the CBS-Q procedure combines geometry optimization at the HF level, re-optimization and energy calculations at the MP2 level, and an empirical expression for correction to correlation effects.[61, 81]

3.1.5. Density Functional Theory

The HF method takes into account an average contribution of the electron-electron interaction. One of the major problems of HF and post-HF methods is the high computational effort that is required for the treatment of relatively large molecular systems (e.g., macromolecules). An alternative quantum chemistry method for the calculation of the electronic energy is rooted in the DFT, which has allowed a decisive improvement in the computing feasibility of kinetics estimation in polymer and other chemical systems. Indeed, the number of degrees of freedom is reduced from $3N$ to 3 with the use of the DFT, with N corresponding to the number of electrons in the system under investigation.[82]

The DFT was first developed in the early twentieth century on the basis of the Thomas-Fermi model,[83, 84] and later formalized by the Hohenberg-Kohn theorems.[85] Particularly, the Kohn-Sham theory has put the foundations for the use of the DFT in computational chemistry.[86] On the basis of this theory, the ground state electronic energy can be completely determined by the electron density. The goal of the DFT is thus to design functionals which correlate the electron energy to the electron density function.

An approximation of the electron density (ρ) as a set of one-electron molecular orbitals, each for one of the N_{el} electrons considered, is given by **Equation 3.9**.

$$\rho = \sum_{i}^{N_{el}} |\phi_i|^2 \tag{3.9}$$

The DFT energy (E_{DFT}) can be expressed as a function of the electron density as reported in **Equation 3.10**. In the formula: T_S is the exact kinetic energy; E_{ne} is the electron-nucleus interaction energy; J is the potential energy of the electrostatic interaction between electrons; E_{xc} is the exchange-correlation energy (square brackets denote that the energy is a functional of the electron density function).

$$\mathrm{E}_{\mathrm{DFT}}[\rho] = T_S[\rho] + E_{ne}[\rho] + J[\rho] + E_{xc}[\rho] \tag{3.10}$$

The various DFT methods differ in the way the exchange-correlation term is calculated, or alternatively in the choice of the functional form for this energy contribution. Although exact functionals for exchange and correlation energies are not known, the use of local density approximation (LDA) or its straightforward generalization, the local spin density approximation (LSDA), allow a relatively accurate calculation of certain physical quantities. Particularly, under the LSDA the exchange-correlation energy can be expressed as a function of the electron density at the coordinate where the functional is evaluated.[87]

As a further improvement, gradient-corrected methods consider the exchange and correlation energy dependent not only on the electron density, but also on the derivatives of the density. For instance, in generalized gradient approximation (GGA) methods the first derivative of the density is included as a variable, and GGA functionals have been proposed for the definition of both exchange and correlation energies (e.g., Becke functionals for the exchange energy, Lee-Yang-Parr functionals for the correlation energy, Perdew-Wang functionals for the exchange-correlation energy).[88-92] Eventually, hybrid DFT methods are to be mentioned, which are those including an exact HF derivation for the exchange energy contribution.[61, 93, 94]

3.2. Transition State Theory

Transition state theory (TST) allows the determination of absolute rate coefficients for reactions characterized by the presence of a transition state (i.e., a configuration of the reacting system intermediate between reactants and products and characterized by the highest energy along a reaction coordinate) that is assumed to be in thermal equilibrium with the reactants. TST was introduced in 1935, and incorporates dynamical postulations which make the theory a model based essentially on classical mechanics.[95-97] A number of assumptions are made in order to derive the temperature-dependent expression of the rate constant, and they are hereinafter summarized:

- electronic and nuclear motions are separated in agreement with the Born-Oppenheimer approximation;
- reactant molecules are distributed among their states in accordance with the Maxwell-Boltzmann distribution;
- molecular systems cannot reform reactants once the transition state is crossed in the direction of the products;
- motion along the reaction coordinate in the transition state may be treated as translational and separated from the other motions;
- transition states that are becoming products are distributed along their states according to the Maxwell-Boltzmann laws.

Following these assumptions, the absolute rate constant for a bimolecular reaction in the form "$A + B \rightarrow$ products" is given by **Equation 3.11**. In the formula: Q_A and Q_B are partition functions of the reactants; $Q^{\neq}$ is the partition function of the transition state which has been separated from the translational contribution of the reaction coordinate motion, in agreement with the hypothesis written above; k_b and h are respectively Boltzmann and Planck constants; T is the temperature; E_a is the activation energy of the process.

$$k(T) = \frac{k_b\,T}{h}\frac{Q^{\neq}}{Q_A\,Q_B}e^{-\frac{E_a}{k_b\,T}} \tag{3.11}$$

Calculating the rate constant for a reaction requires that one knows how to evaluate the partition functions that arise out of the TST derivation. A standard expression for the total partition function associated with the internal motion for each molecule is given by the product of independent rotational, vibrational, electronic, and translational terms, as shown in **Equation 3.12**.

$$Q = Q_{rot} \, Q_{vib} \, Q_{elec} \, Q_{trans} \tag{3.12}$$

Besides the terms mentioned above, additional partition functions may be considered, specifically those related to the treatment of internal rotors. An overview of common expressions for the partition functions in relation with kinetic and thermodynamic parameters is given in the following paragraphs.[98]

3.2.1. Partition Functions

For a polyatomic molecule with moments of inertia I_x, I_y, and I_z about its principal axes and rotational symmetry number σ_R, the rotational partition function of the whole molecule is given by **Equation 3.13**, which is derived from the expression of the energy level for a generic linear rigid rotor.

$$Q_{rot} = \frac{\sqrt{\pi}}{\sigma_R} \left(\frac{8\,\pi^2 I_x\, k_b\, T}{h^2} \right)^{\frac{1}{2}} \left(\frac{8\,\pi^2 I_y\, k_b\, T}{h^2} \right)^{\frac{1}{2}} \left(\frac{8\,\pi^2 I_z\, k_b\, T}{h^2} \right)^{\frac{1}{2}} \tag{3.13}$$

The vibrational partition function accounts for the contribution of each vibrational mode of the molecule. Under the assumption of a simple harmonic oscillator (HO), the vibrational partition function for a polyatomic molecule is given by **Equation 3.14**, where v_i is the i-th harmonic frequency corresponding to one of the N_{vib} vibrational modes.

$$Q_{vib} = \prod_{i=1}^{N_{vib}} \frac{1}{1 - e^{\left(-\frac{h\, v_i}{k_b\, T} \right)}} \tag{3.14}$$

The electronic partition function is given by **Equation 3.15**, where g_i is the degeneracy number and E_i is the energy above the lowest state of the system.

$$Q_{elec} = \sum_i g_i \, e^{-\frac{E_i}{k_b T}} \tag{3.15}$$

The one-dimensional (1D) translational partition function is determined from the corresponding energy derived from the Schrödinger equation written for a particle that is moving in a 1D box of length *l*. The total translational partition function for a molecule with mass *m* moving in a volume $V = l^3$ is a product of the three 1D contributions, and it is shown in **Equation 3.16**.

$$Q_{trans} = \frac{(2\pi \, m \, k_b \, T)^{\frac{3}{2}}}{h^3} V \tag{3.16}$$

In order to calculate the individual partition functions, the knowledge of parameters such as moments of inertia, vibrational frequencies, and electronic states is required. Such information for reactants can be obtained from spectroscopic data in many cases. However, computational chemistry calculations need to be carried out for the transition state. On the whole, the quantum chemistry tool is an indispensable support to the effort of estimating reaction rate coefficients on the basis of the TST, especially in the context of polymerization kinetics.[98]

3.2.2. Hindered Rotor Model

The HO model for treating the vibrational modes of a given molecule can be considered in many cases a reasonable approximation for the characterization of the internal motions of a molecule. However, if a number of vibrational frequencies that are smaller than a threshold value are present, these motions must be treated as internal rotations rather than harmonic rotors. The so-called hindered rotor (HR) approximation provides a more reliable description of a polyatomic system through the definition of a specific contribution on the partition functions, which aims to replace the vibrational functions corresponding to the lower frequencies. Particularly, internal rotations that are subject to hindrance due to the presence of a torsion energy barrier are treated by the HR model.

The HR approximation is accounted for by the definition of an internal rotation partition function (Q_{IR}) which in its simplest form accounts for hindered torsions that are 1D and uncoupled with the other rotors and motions. With focus on a specific internal rotation, the parameters required to the evaluation of this partition functions are the rotational hindrance potential as a function of the dihedral angle torsion (i.e., a set of energy values obtained performing a rotational energy scan) and the reduced internal moment of inertia (I_r). The latter parameter can be approximated as shown in **Equation 3.17**, as a function of the two inertia moments computed about the axis containing the twisting bond and with respect to the moieties at both ends of that bond (i.e., left and right inertia moments).[99]

$$I_r = \frac{I_{right}\, I_{left}}{I_{right} + I_{left}} \tag{3.17}$$

Once the rotational hindrance potential and I_r are known, the 1D Schrödinger equation can be solved in order to determine the eigenvalues (ε_k) defining the rotational energy levels. The partition function corresponding to a specific internal rotation ($q_{IR,i}$) can be expressed as a function of the rotational energy levels, as shown in **Equation 3.18**, while the overall partition function corresponding to the internal rotors is defined by **Equation 3.19**.[100]

$$q_{IR,i} = \frac{1}{\sigma_R} \sum_k g_k\, e^{-\frac{\varepsilon_k}{k_b T}} \tag{3.18}$$

$$Q_{IR} = \prod_i q_{IR,i} \tag{3.19}$$

The HR model improves the quality of the reaction rate calculations through TST. Particularly, the importance of considering the HR model for polymerization reactions, such as the radical addition to olefins, is well documented in the literature.[34, 39, 42, 101, 102] However, it has also been shown that this correction to the standard partition functions is much less critical where kinetic calculations are performed at low temperatures and when a relatively small number of atoms is involved.[102-104]

Focusing on FRP again, these remarks let one suppose that the hindered rotor issue is likely to be more relevant as the complexity of the polymer chain (i.e., of the monomer units involved) is increased, or if reactions are investigated in the context of high temperature processes. In the result chapters, the application of the HR model is proposed with reference to a simple FRP system involving polyethylene (PE), and the relevance of treating internal rotations is highlighted. Moreover, the choice of considering uncoupled hindered rotors is discussed.[105]

3.3. Quantum Tunneling

Quantum tunneling is a common feature of all reactions involving hydrogen atom transfer. When active, the hydrogen atom is able to tunnel through the energetic barrier, given that its small mass is associated to a wavelength comparable with the barrier width typical of such transfer reactions. Since hydrogen transfer reactions (in general hydrogen abstractions, hydrogen shifts, or isomerizations) play a relevant role in a large variety of chemical and biochemical processes (e.g., combustion chemistry, peptide rearrangements, and radical polymerization), it is often necessary to accurately evaluate their rate constants, thus introducing a coefficient to properly account for the quantum tunneling effect.

3.3.1. Overview of the Methods

Various methods have been developed to account for the tunneling effect in reaction rate constant estimation. They can be classified in two categories, depending on the approach adopted to solve the Schrödinger equation. The first class includes the early methods proposed in literature. They are based on the solution of the 1D Schrödinger equation introducing a parabolic function to approximate the potential energy barrier. The quantum mechanical transmission coefficient through this barrier is obtained with both approximated and analytical solutions.[106-108]

Another similar approach has been formulated by Eckart. In detail, Eckart proposed a new functional form to approximate the shape of the potential energy barrier and its asymptotic properties. Notably, he also provided the analytical solution of the associated Schrödinger equation, leading to the formulation of a relatively

simple expression for the microcanonical transmission probability. A detailed description of the Eckart model, which has been used in this work, is given in the following paragraph.[109]

In the following decades, a new class of methods has been introduced in order to account for tunneling in reacting systems with improved accuracy. It had in fact been shown that the integration of the 1D Schrödinger equation over the standard TST tunneling path, which is the minimum energy path (MEP), leads to significant underestimations of the tunneling coefficient. To explain this effect Marcus and Coltrin proposed an alternative tunneling path, removed from the MEP by an orthogonal displacement equal to the maximum vibrational amplitude.[110]

Successively, Truhlar and co-workers extended the Marcus and Coltrin path to a multi-atomic system using the harmonic vibrational frequencies of the Hessian defined by the reaction path Hamiltonian proposed in a seminal paper by Miller, Handy, and Adams.[111] Truhlar theory was named Small Curvature Tunneling (SCT) and it is currently probably the most effective approach for the calculation of accurate quantum tunneling effects.[112] More accurate theories based on quantum dynamics simulations have been proposed in the literature,[113] but they require high level *ab initio* data as input and are thus unfeasible for relatively large reacting systems.[105]

3.3.2. Eckart Model

The quantum tunneling effect can be introduced multiplying the canonical rate coefficient by the tunneling factor (Q_{tun}), as shown in **Equation 3.20**. This parameter is defined as the ratio between quantum and classical fluxes across the energy barrier, as shown in **Equation 3.21**, where $P(E)$ is the transmission probability.

$$k(T)_{tun} = Q_{tun}\, k(T) \tag{3.20}$$

$$Q_{tun} = \frac{\int_0^\infty P(E)\, e^{\left(\frac{-E}{k_b T}\right)} dE}{\int_{E_1}^\infty e^{\left(\frac{-E}{k_b T}\right)} dE} \tag{3.21}$$

⠀⠀⠀⠀⠀The tunneling probability, or transmission coefficient, has been calculated using the analytical solution of the 1D translational Schrödinger equation for the asymmetrical Eckart potential barrier, as shown in **Equation 3.22**. In the expression, μ is the reduced mass of the moving moiety, x is the reaction coordinate, and $V(x)$ is the Eckart potential energy surface (PES), which is defined by **Equation 3.23** as a function of parameters A, B, and l.[109]

$$-\frac{h}{4\,\pi\,\mu}\frac{d^2\Psi}{dx^2} + V(x)\,\Psi = E\,\Psi \tag{3.22}$$

$$V(x) = A\,\frac{e^{\left(\frac{2\,\pi\,x}{l}\right)}}{1 + e^{\left(\frac{2\,\pi\,x}{l}\right)}} + B\,\frac{e^{\left(\frac{2\,\pi\,x}{l}\right)}}{\left(1 + e^{\left(\frac{2\,\pi\,x}{l}\right)}\right)^2} \tag{3.23}$$

⠀⠀⠀⠀⠀**Equation 3.22** can be integrated using hypergeometric series. The wave function so determined is the sum of an incident and a reflected wave function contribution. The ratio between their amplitudes gives the reflection probability, from which the transmission probability can be computed as shown in **Equation 3.24**, with parameters α, β, and δ given by **Equations 3.25-3.27**.

$$P(E) = 1 - \frac{\cosh\big(2\pi\,(\alpha - \beta)\big) + \cosh(2\,\pi\,\delta)}{\cosh\big(2\pi\,(\alpha + \beta)\big) + \cosh(2\,\pi\,\delta)} \tag{3.24}$$

$$\alpha = \frac{1}{2}\left(\frac{E}{C}\right)^{\frac{1}{2}} \tag{3.25}$$

$$\beta = \frac{1}{2}\left(\frac{E - A}{C}\right)^{\frac{1}{2}} \tag{3.26}$$

$$\delta = \frac{1}{2}\left(\frac{B - C}{C}\right)^{\frac{1}{2}} \tag{3.27}$$

⠀⠀⠀⠀⠀The parameter C is defined by **Equation 3.28**, while parameters A, B, and l mentioned above can be computed as shown in **Equations 3.29-3.31** applying three conditions to the Eckart PES.

$$C = \frac{h^2}{8\,\mu\,l^2} \tag{3.28}$$

$$A = E_1 - E_{-1} \tag{3.29}$$

$$B = \left(\sqrt{E_1} - \sqrt{E_{-1}}\right)^2 \tag{3.30}$$

$$l = \frac{1}{|v|}\sqrt{\frac{2\,E_1\,E_{-1}}{\mu}}\frac{1}{\sqrt{E_1} + \sqrt{E_{-1}}} \tag{3.31}$$

The first condition equals the asymptotic limit of the PES to the reaction energy and allows for the calculation of *A*; the second one equals the maximum on the PES to the forward activation energy and gives *B*; the third one equals the imaginary frequency to the value of the second derivative of the PES with respect to the reaction coordinate and gives *l*, where E_1 and E_{-1} are the activation energy barriers for the forward and backward reactions, and v is the TS imaginary frequency.[105]

3.4. Evaluation of Reaction Rate Coefficients

With reference to the TST and the equations derived in the previous paragraphs, a general expression for the rate constant is given by **Equation 3.32**, with the temperature-dependent pre-exponential factor *A(T)* defined as shown in **Equation 3.33** for a reaction involving N_r reactants.

$$k(T) = A(T)\, e^{-\frac{E_a}{k_b T}} \tag{3.32}$$

$$A(T) = Q_{tun}\, \frac{k_b\, T}{h}\, \frac{Q_{trans}^{\neq}\, Q_{rot}^{\neq}\, Q_{vib}^{\neq}\, Q_{el}^{\neq}\, Q_{IR}^{\neq}}{\prod_{i}^{N_r} Q_{trans}^{i}\, Q_{rot}^{i}\, Q_{vib}^{i}\, Q_{el}^{i}\, Q_{IR}^{i}} \tag{3.33}$$

The quantum chemistry tool allows estimating a very large set of energy and kinetic data. Among them, those necessary for the calculation of the reaction rate coefficient based on the TST are the kinetic parameters involved in the expressions of the partition functions as well as the energy values required for the evaluation of the activation energy. Specifically, this parameter is defined as the difference between the

electronic energy of the transition state and that of the reactants, including the zero-point energy (E_{ZP}), as shown in **Equation 3.34**.

$$E_a = (E_e + E_{ZP})_{\neq} - \prod_i^{N_r} (E_e + E_{ZP})_i \qquad (3.34)$$

The procedure that allows evaluating the reaction rate coefficient based on quantum chemistry calculations is described hereinafter. Firstly, a geometry optimization of the reactants and products taking part in the examined reaction is performed. Subsequently, the transition state structure is located through a discrete scan of the breaking/forming bond distance along the selected reaction coordinate, in order to detect the first-order saddle point in the PES. Finally, single point calculations are performed about the optimized structures (i.e., reactants, products, and transition state) at the chosen level of theory, in order to estimate the required kinetic parameters. The thermodynamic and kinetic data are calculated at the quantum chemistry level with the use of Gaussian 09 program suite.[114]

3.4.1. Selected Levels of Theory

With the aim of calculating reaction rate coefficients for a wide range of reactions in FRP, two quantum chemistry methods have been adopted in this work. The hybrid DFT method B3LYP, which combines the Becke 3 parameters exchange functional (B3) with the Lee-Yang-Parr correlation functional (LYP), has been used mostly to perform geometry optimizations and frequency calculations.[93, 94] Single point calculations have been carried out mainly with the hybrid meta DFT method MPWB1K developed by Zhao and Truhlar, based on modified Perdew and Wang exchange functional (MPW) and Becke 1995 correlation functional (B95).[115] In some cases, the performances of the two methods in estimating energy parameters have been compared.

The molecular orbitals have been described with the use of the Pople basis sets, primarily 6-31G and 6-311G, with the addition of polarization and diffuse functions.[116-119] Moreover, a CBS method has been used to obtain very accurate kinetic data for specific reactions of interest. Particularly, the CBS-QB3 developed by

Petersson and co-workers has been adopted, which performs optimization and frequency calculations altogether at the B3LYP level.[120] Specific details about the methods and basis sets adopted in the calculations are given in the result chapters.

In particular, a combined B3LYP/6-31G(d,p)//MPWB1K/6-31G(d,p) method has been tested and extensively used in this work. In this approach, calculations at two levels of theory are combined. This way, the first step of geometry optimization could be performed with a limited cost of computing time, while more demanding simulations with the MPWB1K were carried out starting from predefined molecular structures. This approach was found to be well suited to treat acrylate polymers and copolymers.

_____ _____ _____ _____ ____ ___ __

CHAPTER 4

_____ _____ _____ _____ ____ ___ __

Widening and Improvement

_____ _____ _____ _____ ____ ___ __

4.1. Summary

The computational procedure that has been applied to the study of FRP in the latest works of Moscatelli and co-workers has been improved, and the results are reported in this chapter. Specifically, the first investigation has been focused on the homopolymerization of vinyl chloride, with the aim of extending the kinetic study toward a wide range of secondary reactions as well as of providing an efficacious modeling of the FRP process based on a detailed reaction scheme including MCRs. In addition to the examination of novel reaction pathways, an improved computational method has been applied, in order to check its performances in comparison with the approaches that were adopted in the previous studies.[121, 122]

In the second part, the attention has been centered on backbiting reaction, with focus on the quantum tunneling effect on hydrogen transfer kinetics in the context of FRP. Starting from backbiting on PE, the study has been extended to PVC and polystyrene (PS), which are common FRP systems that have been subject to previous computational investigations in the topic of secondary reactions, therefore they were suitable for an improved inspection of reaction kinetics.[105]

Eventually, the quantum chemistry investigation has been moved to the polymerization of BA, in order to extend the approach toward acrylates. As like as what has been done in the first part, secondary reaction kinetics has been studied with respect to a set of interesting side steps. In addition to the conventional ones, reactions of $1{:}j$ and $j{:}j{\pm}4$ radical migration along the chain as well as backbiting involving SBRs have been examined. A simplified molecular model has been adopted for the

description of poly (butyl acrylate) (PBA) chains, in order to make feasible treating longer polymer chains.[123]

4.2. Secondary Reactions in Poly (Vinyl Chloride)

The FRP process of vinyl chloride is computationally investigated with special attention to the secondary reactions involving MCRs. Namely, rate constants of backbiting, β-scission, chain transfer, and propagation reactions are evaluated using a DFT method. The rate coefficients of such reactions are estimated taking into account the position of the radical along the chain as well as its distance from the chain-end. In particular, 1:5, 5:1, and 5:9 backbiting show to be the most relevant secondary reactions, followed by the slower propagation of MCRs. Finally, a kinetic model of suspension polymerization including the investigated reactions is developed, in order to determine the impact of such radicals on the quality of the final polymer.[122]

4.2.1. Introduction

PVC is one of the most widely produced thermoplastic materials. Due to its cheapness as well as the remarkable chemical and mechanical resistance, it finds application in many fields such as construction, piping, clothing, electric insulation, and packaging.[124] PVC processing is usually carried out at operating conditions as well as involving additives for plasticization and stabilization that may cause the degradation of the material. Accordingly, a detailed understanding of the degradation mechanisms and their relation with the chain architecture is of paramount importance to design and produce high quality materials.

In the last two decades, many studies focused on PVC have shown that its thermal stability is negatively affected by the presence of structural defects in the polymer chains. Acting as breaking-labile points during thermal- or photo-treatments, these irregularities in the backbone are directly responsible for the polymer degradation. This process usually begins with HCl elimination from the defects and ends up with the formation of conjugated polyene sequences. The foremost irregularity precursors of degradation are both tertiary chlorine atoms, usually located

at the root of branches, and allylic chlorine atoms. The former originate after propagation of tertiary carbon radicals, the latter are produced by transfer reactions involving chlorine abstraction.[125, 126]

The mechanisms leading to the formation of branches and allylic chlorines have been widely studied and reviewed in recent publications.[52, 126] The corresponding reaction scheme involves multiple reactions whose sequences are connected to the production of such defects. As shown in **Figure 7**, an LCB of indefinite length is originated by transfer to polymer reaction followed by propagation of the newly formed MCR.
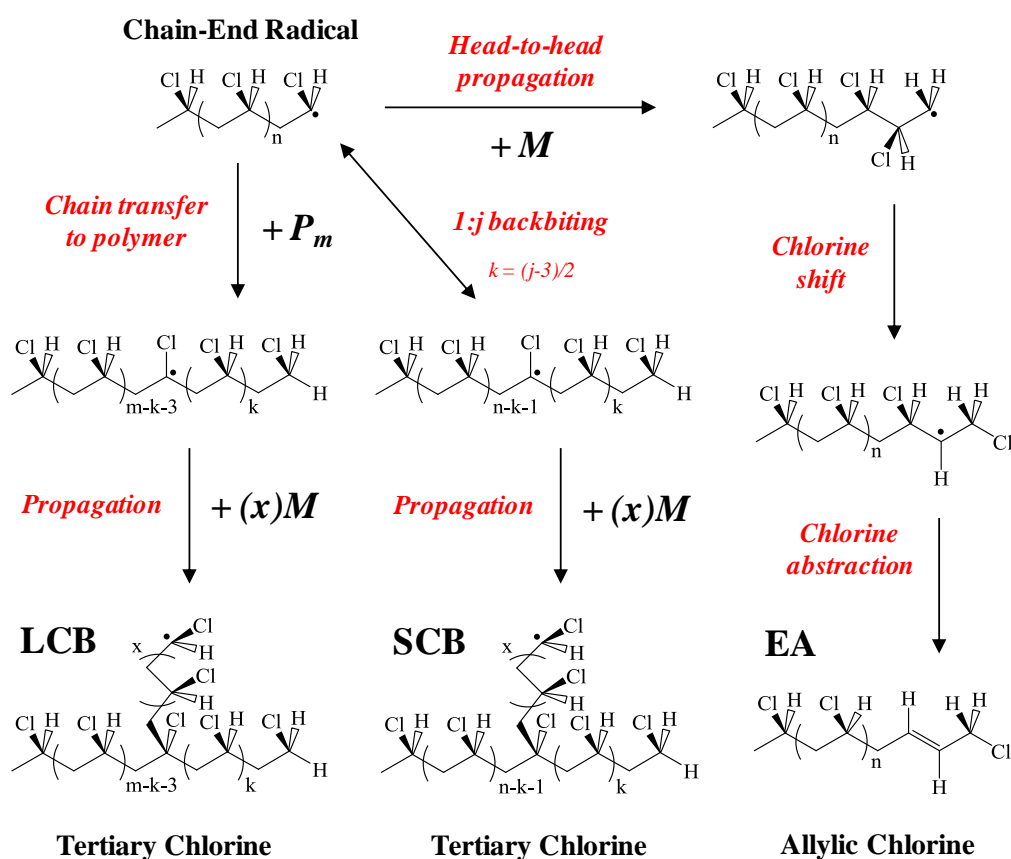
Figure 7. *Scheme of reactions leading to the formation of short-chain branches, long-chain branches, and chloro-allylic end groups in vinyl chloride polymerization.*

On the other hand, a well-defined SCB, also carrying tertiary chlorine, is formed primarily through intramolecular transfer reaction. Among the different mechanisms producing allylic chlorines, the formation of allylic end groups (EA) takes place through head-to-head (HH) propagation of chain-end radicals. The originated MCR, bringing a secondary carbon radical, rearranges quantitatively through 1:2 chlorine shift, followed by chlorine abstraction.

Summarizing, the formation of relevant defects in PVC polymer chains is strongly connected to secondary reactions involving MCRs.[2] These active species can be quite stable due to the presence of tertiary carbon radicals, thus showing significant difference in reactivity with respect to chain-end radicals. As explained above, MCRs are primarily originated by intermolecular and intramolecular transfer to polymer reactions. Among them, backbiting seems to be the most favorite, especially when the internal hydrogen shift reaction is characterized by a transition state involving a stable six-member ring.[6, 7] Further reactions involving MCRs may produce branches and double bonds inside the chains, thus affecting the chain architecture as discussed above. Finally, chain scission reactions can also occur as unimolecular termination of MCRs, usually referred to as β-scissions, and they affect the molecular weight distribution producing lower molecular weight species.[2, 12]

The extent of these side effects is determined by the MCR concentration and reactivity, and thus by the role of secondary reactions in the kinetic scheme: this is why the evaluation of the corresponding rates is highly valuable. In the context of FRP, some direct experimental measurements of the rate constants of secondary reactions have been recently reported applying pulsed-laser polymerization.[13, 14, 24, 28] The largely different results of such measurements reflect the difficulties associated with the direct experimental evaluation of such reaction kinetics, usually complicated by the simultaneous presence of many parallel reactions that make almost impossible to isolate their specific contributions. Much easier is the evaluation of the corresponding effects (i.e., the formation of microstructural defects, usually detected by NMR). Even if such experimental results are not providing discriminating information about specific reactions, they are very helpful in checking the reliability of the proposed mechanisms.

Many efforts have been reported in the literature about the theoretical estimation of such rate constants. By using quantum mechanics, and in particular DFT methods, the kinetics of secondary reactions has been investigated concerning PVC and other FRP systems of industrial relevance.[7, 51, 52, 121] In particular, the polymerization of vinyl chloride has been studied quite recently, in order to elucidate the mechanisms leading to the formation of structural defects such as branches and internal double bonds.[52, 53] Among these reactions, propagation of MCR and backbiting seem to be the most relevant secondary steps, which are involved in the production of internal double bonds as well as methyl, ethyl, and butyl branches.[52] With reference to the secondary pathways shown in **Figure 7**, the main computational results can be summarized as follows:

- the rate constant of HH propagation has been estimated as $3.82 \ 10^{-2} \ \text{L mol}^{-1} \ \text{s}^{-1}$ at 330 K, using the B3LYP/6-31+G(d) computational method and considering a polymer chain made of seven repeating units;[40]

- on the other hand, a quite different value of the same constant ($0.18 \ \text{L mol}^{-1} \ \text{s}^{-1}$) has been evaluated at 330 K with the BMK/6-311+G(3df,2p)//B3LYP/6-31+G(d) combined method and considering trimer chains.[52] In the same work, the rate constants of 1:5 and 1:6 intramolecular transfer reactions at 330 K have been also estimated as $0.809 \ \text{s}^{-1}$ and $2.80 \ 10^{-5} \ \text{s}^{-1}$, respectively.[52] Accordingly, these reactions are much slower than propagation, for which a pseudo-first order rate constant (i.e., rate constant times the monomer concentration within the polymer-rich phase) equal to $127 \ \text{s}^{-1}$ has been calculated in the same reference;

- in a previous work,[121] computational investigations of other backbiting pathways (1:3, 1:5, and 1:7) as well as β-scission reactions have been carried out. In both cases, the B3LYP/6-31G(d,p) method has been used, and a good agreement with the literature data mentioned above has been found for the 1:5 backbiting rate constant;

- in a more recent publication the reversibility of some backbiting reactions has been discussed, showing that 1:5 and 1:6 shifts can be considered irreversible;[127]

-   with regard to propagation reactions, MCRs add monomer units more slowly than chain-end radicals. In fact, the corresponding rate constant value at 330 K has been computationally estimated as 3.73 10^{-2} L mol^{-1} s^{-1}.[52] In a previous work,[121] the rate constant of the same reaction as well as those of the subsequent propagation steps have been evaluated. Such values are larger than those reported in the previous reference by two-three orders of magnitude.

Given the results as well as the inconsistencies summarized above, this work is aimed at evaluating the rate constants of the main secondary reactions typical of vinyl chloride polymerization by using quantum chemistry. Since some of those reactions have been already analyzed in our previous work,[121] our purpose here is to refine such evaluations but also to examine other interesting kinetic steps not included before, thus widening the set of the studied reactions. Moreover, all calculations are carried out using an improved basis set as well as a novel DFT functional. Specifically, calculation are performed using the B3LYP/6-311+G(d,p) as well as the MPWB1K/6-31G(d,p) methods, with reference to the details about functionals and basis sets reported in Chapter 3.

A comparison between the estimated rate constants of secondary reactions and the corresponding ones involving chain-end radicals is reported in the end of the first part of this work. In the second part, the estimated rate coefficient values are embedded in a kinetic model of the polymerization process simulating the reactivity inside the polymer-rich phase at constant monomer concentration. This way, the actual impact of MCRs and their reactions is made clear, with emphasis on the final architecture of the polymer chains.

4.2.2. Computational Results

PVC polymer chains have been modeled using a number of monomer units large enough to render properly the chain-length effect, and small enough to reduce the computational effort. Namely, chains made of six monomer units and with the configuration shown in **Figure 8** have been considered. Accordingly, the reactivity of MCRs located up to the seventh carbon atom from the chain end could be carried out, as needed for 1:7 backbiting reactions. In particular, the syndiotactic configuration has

been simulated, since it corresponds to the global minimum energy for PVC.[39] This molecular model has been used in all calculations with the exception of those focused on 5:9 backbiting reactions, where chains made of ten repeating units have been considered to investigate intramolecular chain transfer of the radical up to the ninth carbon atom from the chain-end.
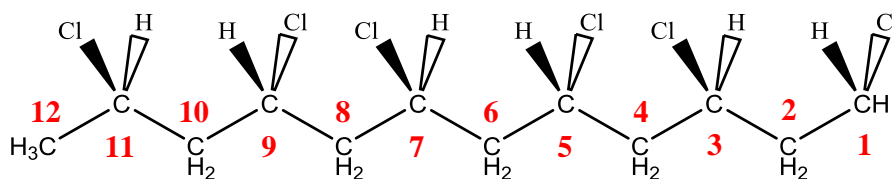
Figure 8. *Representative model of a poly (vinyl chloride) chain made of six repeating monomer units. Carbon atom numeration in evidence*.

First, the rate constant of a reaction step well studied experimentally has been evaluated in order to assess the reliability of the computational approach. Namely, the propagation rate constant has been calculated for the monomer addition to chain-end radicals at increasing chain length. The results obtained with the two computational methods detailed above (i.e., B3LYP and MPWB1K) are reported in **Table 1** and **Table 2**, respectively, while the configuration of the transition state relative to the propagation of a dimer radical is shown in **Figure 9a**. The predicted values are comparable with the experimental ones reported in the literature, ranging from 1.06 10^3 to 1.20 10^4 L mol^{-1} s^{-1} at 330 K.[49, 128] Moreover, it is worth noting that the MPWB1K functional is also able to predict the chain-length effect with better accuracy.

After the method validation, the computational investigation has been turned to secondary reactions of backbiting, β-scission, HH propagation, and monomer addition to MCR. The 1:3, 1:5, 1:7 forward and backward backbiting reactions have been examined in order to quantify the probability of the radical shift from the chain-end to intramolecular carbon atoms in well-defined positions and vice versa. With the aim of comparing the obtained results with those previously reported in the literature, the tunneling effect correction has been initially neglected. The rate constant values obtained with the B3LYP functional, and shown in **Table 1**, are in reasonable

agreement with those reported in the literature.[52, 121] These results suggest that quantum chemistry evaluations for backbiting reactions are quite independent upon the specifically selected basis set. On the contrary, the use of the MPWB1K functional provides rate constant values that are smaller for 1:3 backbiting and larger for 1:7 in comparison with the corresponding values estimated at the B3LYP level of theory, as shown in **Table 2**. However, in both cases 1:5 backbiting is the most favored intramolecular transfer reaction, as expected.
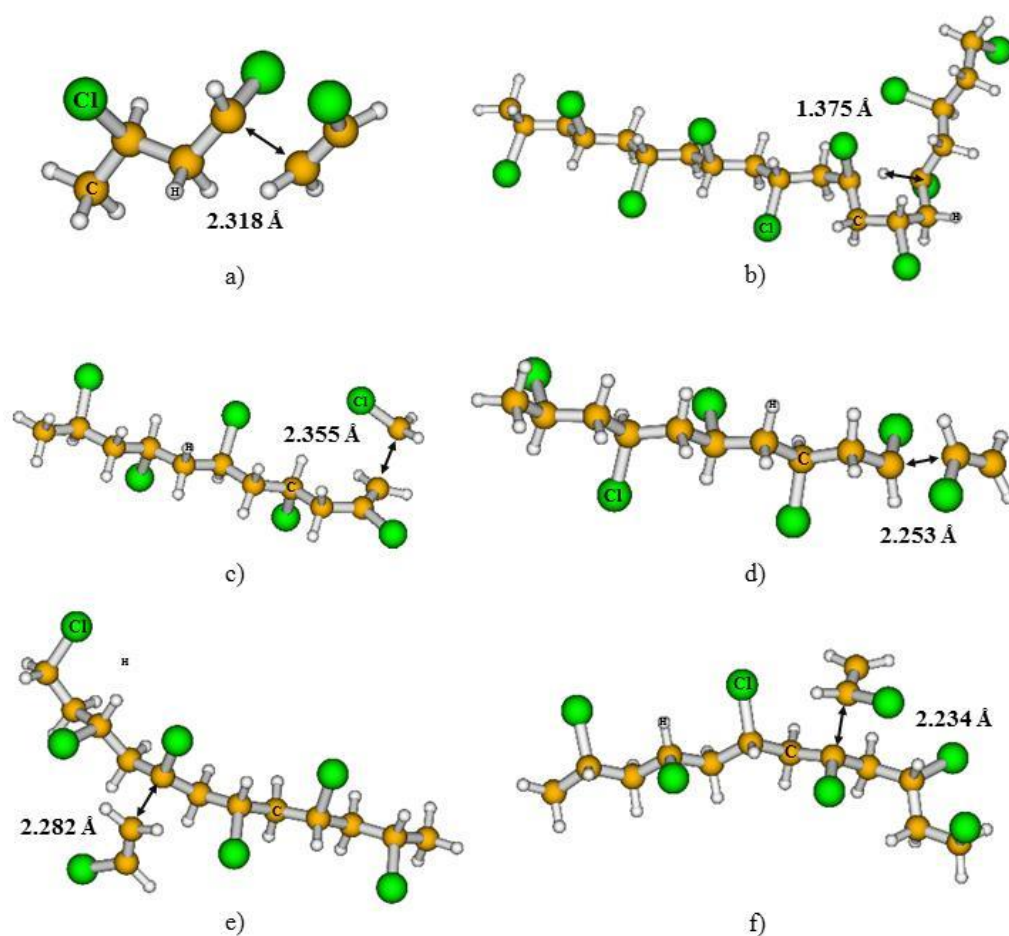
Figure 9. *Optimized geometries of the transition state structures relative to the investigated reactions: a) head-to-tail propagation of chain-end radical, b) 5:9 backbiting, c) 3-right β-scission, d) head-to-head propagation of chain-end radical, e) head-to-tail propagation of mid-chain radical, f) head-to-head propagation of mid-chain radical.*

Table 1. *Calculated values of activation energy and rate coefficient for reactions involving chain-end and mid-chain radicals theoretically determined with the B3LYP/6-311+G(d,p) functional and basis set. Rate constants are calculated at 330 K and do not include the tunneling correction.*

Reaction		E_a	k
		$kJ\ mol^{-1}$	$L\ mol^{-1}\ s^{-1}\ or\ s^{-1}$
Chain-end HT propagation	$R_1 + M \rightarrow R_2$	30.9	$6.74\ 10^3$
Chain-end HT propagation	$R_2 + M \rightarrow R_3$	30.7	$5.84\ 10^3$
Chain-end HT propagation	$R_3 + M \rightarrow R_4$	30.6	$7.30\ 10^3$
Chain-end HT propagation	$R_4 + M \rightarrow R_5$	30.4	$7.56\ 10^3$
Chain-end HT propagation	$R_5 + M \rightarrow R_6$	30.7	$5.66\ 10^3$
Chain-end HT propagation	$R_6 + M \rightarrow R_7$	31.0	$4.16\ 10^3$
1:3 backbiting	$R_{6,1} \rightarrow R_{6,3}$	161.8	$1.48\ 10^{-13}$
3:1 backbiting	$R_{6,3} \rightarrow R_{6,1}$	168.4	$1.12\ 10^{-14}$
1:5 backbiting	$R_{6,1} \rightarrow R_{6,5}$	73.9	1.16
5:1 backbiting	$R_{6,5} \rightarrow R_{6,1}$	77.3	$2.20\ 10^{-1}$
1:7 backbiting	$R_{6,1} \rightarrow R_{6,7}$	103.0	$6.48\ 10^{-6}$
7:1 backbiting	$R_{6,7} \rightarrow R_{6,1}$	106.5	$1.20\ 10^{-6}$
5:9 backbiting	$R_{10,5} \rightarrow R_{10,9}$	72.7	$7.98\ 10^{-1}$
9:5 backbiting	$R_{10,9} \rightarrow R_{10,5}$	72.5	1.09
3-right β-scission	$R_{6,3} \rightarrow R_{1*} + P_{5*}$	117.8	$4.51\ 10^{-6}$
3-left β-scission	$R_{6,3} \rightarrow R_4 + P_2$	107.2	$2.57\ 10^{-4}$
5-right β-scission	$R_{6,5} \rightarrow R_{2*} + P_{4*}$	100.0	$1.39\ 10^{-3}$
5-left β-scission	$R_{6,5} \rightarrow R_3 + P_3$	98.1	$1.96\ 10^{-3}$
7-right β-scission	$R_{6,7} \rightarrow R_{3*} + P_{3*}$	97.9	$2.12\ 10^{-3}$
7-left β-scission	$R_{6,7} \rightarrow R_2 + P_4$	99.7	$1.04\ 10^{-3}$
Depolymerization	$R_6 \rightarrow R_5 + M$	107.5	$1.80\ 10^{-4}$
Chain-end HH propagation	$R_5 + M \rightarrow R_{6h}$	44.8	$1.77\ 10^1$
HH propagation of MCR	$R_{6,5} + M \rightarrow R_{7h}^{2,3}$	79.7	$5.42\ 10^{-6}$
HT propagation^I of MCR	$R_{6,5} + M \rightarrow R_7^{2,3}$	56.0	$4.44\ 10^{-2}$
HT propagation^{II} of MCR	$R_7^{2,3} + M \rightarrow R_8^{2,5}$	37.7	$1.96\ 10^2$
HT propagation^{III} of MCR	$R_8^{2,5} + M \rightarrow R_9^{2,7}$	30.1	$1.03\ 10^4$

Table 2. *Calculated values of activation energy and rate coefficient for reactions involving chain-end and mid-chain radicals theoretically determined with the MPWB1K/6-31G(d,p) functional and basis set. Rate constants are calculated at 330 K and do not include the tunneling correction.*

Reaction		E_a	k
		kJ mol^{-1}	*L mol^{-1} s^{-1} or s^{-1}*
Chain-end HT propagation	$R_1 + M \rightarrow R_2$	24.0	3.19 10^4
Chain-end HT propagation	$R_2 + M \rightarrow R_3$	23.1	2.61 10^4
Chain-end HT propagation	$R_3 + M \rightarrow R_4$	23.0	2.55 10^4
Chain-end HT propagation	$R_4 + M \rightarrow R_5$	23.0	2.51 10^4
Chain-end HT propagation	$R_5 + M \rightarrow R_6$	23.5	1.89 10^4
Chain-end HT propagation	$R_6 + M \rightarrow R_7$	23.5	1.73 10^4
1:3 backbiting	$R_{6,1} \rightarrow R_{6,3}$	164.0	5.34 10^{-14}
3:1 backbiting	$R_{6,3} \rightarrow R_{6,1}$	173.1	1.80 10^{-15}
1:5 backbiting	$R_{6,1} \rightarrow R_{6,5}$	74.9	2.05
5:1 backbiting	$R_{6,5} \rightarrow R_{6,1}$	78.3	2.95 10^{-1}
1:7 backbiting	$R_{6,1} \rightarrow R_{6,7}$	97.1	3.61 10^{-4}
7:1 backbiting	$R_{6,7} \rightarrow R_{6,1}$	100.8	4.25 10^{-5}
5:9 backbiting	$R_{10,5} \rightarrow R_{10,9}$	66.8	2.66 10^1
9:5 backbiting	$R_{10,9} \rightarrow R_{10,5}$	66.9	3.33 10^1
3-right β-scission	$R_{6,3} \rightarrow R_{1*} + P_{5*}$	146.3	1.03 10^{-10}
3-left β-scission	$R_{6,3} \rightarrow R_4 + P_2$	140.0	1.83 10^{-9}
5-right β-scission	$R_{6,5} \rightarrow R_{2*} + P_{4*}$	124.7	6.43 10^{-7}
5-left β-scission	$R_{6,5} \rightarrow R_3 + P_3$	122.8	3.71 10^{-7}
7-right β-scission	$R_{6,7} \rightarrow R_{3*} + P_{3*}$	124.6	1.15 10^{-7}
7-left β-scission	$R_{6,7} \rightarrow R_2 + P_4$	123.9	3.58 10^{-7}
Depolymerization	$R_6 \rightarrow R_5 + M$	137.9	2.62 10^{-9}
Chain-end HH propagation	$R_5 + M \rightarrow R_{6h}$	35.9	1.05 10^2
HH propagation of MCR	$R_{6,5} + M \rightarrow R_{7h}^{2,3}$	62.8	1.36 10^{-3}
HT propagation^I of MCR	$R_{6,5} + M \rightarrow R_7^{2,3}$	37.9	1.43 10^1
HT propagation^{II} of MCR	$R_7^{2,3} + M \rightarrow R_8^{2,5}$	28.1	4.45 10^3
HT propagation^{III} of MCR	$R_8^{2,5} + M \rightarrow R_9^{2,7}$	23.6	1.57 10^4

With the aim of understanding better the mechanism of this preferential intramolecular chain transfer reaction, and particularly its dependence upon the distance from the chain-end, also the 5:9 backbiting reaction has been investigated. The computational results obtained using the B3LYP functional show that this radical shift reaction exhibits a rate constant close to that of 1:5 backbiting. On the other hand, calculations carried out with the MPWB1K functional have provided a value of the same rate constant that is one order of magnitude larger than that of 1:5 backbiting. Hence, the two methods differ in the evaluation of MCRs reactivity toward this specific reaction, though there is no direct experimental evidence that allows discriminating the reliability of the two approaches.

The reversibility of backbiting reactions has been also studied, comparing activation energy and rate constant values between forward and backward steps. The 1:j backbiting reaction, where j is a generic intramolecular location of the hydrogen to be abstracted as shown in **Figure 8**, can be considered irreversible according to De Vleeschouwer et al.,[127] due to the smaller value of activation energy and the higher value of pre-exponential factor of the 1:j forward reaction with respect to the backward step. The results in this work support this expectation, confirming that chain transfer of the radical from the chain-end to an intra-chain position is favorable compared to the opposite radical shift. On the other hand, focusing on 5:9 and 9:5 backbiting reactions very similar activation energies of the forward and backward reactions have been calculated with both the functionals, as reported in **Table 1** and **Table 2**. Accordingly, this step can be considered almost fully reversible. This seems reasonable, since forward and backward reactions involve radicals with similar stability, being both reagents and products tertiary radicals. The transition state configuration of 5:9 backbiting is shown in **Figure 9b**.

Being backbiting characterized by a hydrogen atom transfer, the tunneling effect has been investigated for such reactions. Tunneling factors have been calculated as a function of the activation energies as well as of the imaginary frequencies associated with the transition state structures, both evaluated with the two selected DFT functionals. The tunneling factors evaluated at 330 K are reported in **Table 3**, along with the updated values of the rate constants of the investigated backbiting reactions. Quantum tunneling increases backbiting pre-exponential factors by ten to

ten thousand times. In particular, the enhancing effect is stronger on 1:3 backbiting, which is characterized by larger values of imaginary frequency and activation energy. However, neither 1:3 nor 1:7 backbiting reactions increase their relevance due to the tunneling effect to become as important as the other intramolecular transfer reactions (i.e., 1:5 and 5:9 backbiting). The MPWB1K functional predicts larger values of imaginary frequency, and thus higher tunneling factors, than the B3LYP. The estimated tunneling corrections are in agreement with similar calculations performed by Purmova et al. on 1:3 and 1:5 backbiting reactions in PVC. Such parameters were determined using the Eckart model and are based on kinetic parameters evaluated at the G3(MP2)-RAD//MPW1K/6-31+G(d,p) level of theory.[53]

Table 3. *Quantum tunneling factors evaluated for backbiting reactions and updated rate coefficient values. Data are calculated at 330 K and are based on the activation energies and frequency factors obtained with both the used functionals.*

Reaction	B3LYP/6-311+G(d,p)		MPWB1K/6-31G(d,p)	
	Q_{tun}	k_{bb} s^{-1}	Q_{tun}	k_{bb} s^{-1}
1:3 backbiting	$8.11 \ 10^3$	$1.20 \ 10^{-9}$	$3.94 \ 10^4$	$2.10 \ 10^{-9}$
3:1 backbiting		$9.04 \ 10^{-11}$		$7.09 \ 10^{-11}$
1:5 backbiting	$3.73 \ 10^1$	$4.34 \ 10^1$	$9.25 \ 10^1$	$1.90 \ 10^2$
5:1 backbiting		8.21		$2.73 \ 10^1$
1:7 backbiting	$7.56 \ 10^1$	$4.89 \ 10^{-4}$	$2.13 \ 10^2$	$7.68 \ 10^{-2}$
7:1 backbiting		$9.07 \ 10^{-5}$		$9.03 \ 10^{-3}$
5:9 backbiting	$3.51 \ 10^1$	$2.80 \ 10^1$	$6.13 \ 10^1$	$1.63 \ 10^3$
9:5 backbiting		$3.82 \ 10^1$		$2.04 \ 10^3$

As already mentioned, MCRs can induce chain scission reactions, especially at high temperature. In this work, the so called *β*-scission reactions from a selected group of MCRs, and in particular the ones involved in the backbiting reactions discussed above, have been examined. Namely, three different polymer chains made of six repeating units and with the radical located on carbon atom 3, 5, and 7 have been taken into account. With reference to the carbon atom numeration in **Figure 8**, both right and left β-scissions from such radical chains have been simulated.

The computational results reported in **Table 1** and **Table 2** show that these secondary pathways play a significant role only at high temperature due to the large values of the corresponding activation energies. In terms of rate coefficients, all the examined reactions are quite similar, with exception of the 3-right scission that exhibits a smaller rate constant value. This reaction is quite disfavored due to the formation of an unstable low-molecular weight radical, as shown in **Figure 9c**. On the whole, the values of β-scission rate constants calculated in this work with the B3LYP functional are about one order of magnitude larger than those evaluated in a previous work,[121] while the values estimated using the MPWB1K functional are about three orders of magnitude smaller. The estimated rate constants of these scission reactions involving MCRs can be compared with those of the same reactions involving chain-end radicals, which are indicated as depolymerization, whose rate coefficients are reported in **Table 1** and **Table 2**. These values are consistent with those predicted for the β-scission reactions, and in particular very close to those reported for the 3-left β-scission reaction.

The unconventional HH addition of a monomer unit to a chain-end radical is the first step in many complex mechanisms that can lead to the formation of structural defects. Moreover, this reaction is involved in one of the most relevant mechanisms of chain transfer to monomer.[52] A computational study of the HH propagation of chain-end radicals made of five repeating units has shown that the rate constant of this reaction is about two orders of magnitude smaller than that of the conventional head-to-tail (HT) propagation, as again shown in **Table 1** and **Table 2**; the same behavior has been previously reported in the literature.[52] However, the same rate constant is about two orders of magnitude larger than that of transfer to monomer experimentally available at 330 K.[128] As a result, this reaction cannot be considered the rate-determining step of the mechanism of chain transfer to monomer. The transition state configuration of HH propagation reaction involving chain-end radicals is reported in **Figure 9d**.

As explained before, branching reactions are responsible for the formation of labile degradation points, like tertiary chlorines; moreover, they affect the polymer morphology producing non-linear chains. With the aim of investigating these reactions, the first propagation step of an MCR, indicated as HT propagation[I] in the

tables, and the following two monomer additions, indicated respectively as HT propagation[II] and HT propagation[III], have been studied, and the results are shown in **Table 1** and **Table 2**. Focusing on the parameters obtained with the B3LYP functional, the rate constant of the first propagation step of MCR is five orders of magnitude smaller than that of chain-end radical, in agreement with our previous results.[121] The ratio between the same two rate constants predicted using the MPWB1K functional is reduced to three orders of magnitude only, in agreement with the computational results from a different literature source.[52] Although a comparison with experimental data is needed to discriminate the reliability of the two computational results, the rate constant value of the third propagation step of MCR evaluated with the MPWB1K functional is very close to that of propagation of chain-end radical predicted using the same functional as discussed before. This consistency, which adds reliability to the predictions made through the MPWB1K method, is supported by the fact that the former reaction is actually a propagation of chain-end radical. The transition state configuration of the first HT propagation step of MCR is shown in **Figure 9e**.

Finally, the HH propagation of an MCR has been simulated, taking into account the monomer addition to a PVC active chain made of six repeating units and with the radical located in the center of the backbone. The rate constants computed using both functionals are about four orders of magnitude smaller than those calculated for the first step of HT propagation of MCRs, as reported in **Table 1** and **Table 2**. The transition state configuration of the HH propagation reactions involving MCRs is shown in **Figure 9f**.

As a conclusive remark to the first part of the work, the results of the extensive computational analysis of the main reactions involving chain-end and MCRs can be summarized as follows:

- *β*-scission as well as depolymerization reactions can be neglected at low temperature, due to their high activation energies;
- the only intramolecular transfer reaction able to compete with the propagation of chain-end radicals and, more significantly, of MCRs is the *j:j±*4 backbiting;

- HH propagation of chain-end radicals is indirectly related to chain transfer to monomer, and its rate constant is intermediate between those of propagation and backbiting reactions;
- HH propagation of MCRs can be assumed negligible, being propagation and backbiting the most probable "termination" pathways of this type of radicals.

These conclusions have been accounted for in the development of the kinetic model presented in the next paragraph, which is aimed at verifying the actual impact of the different reactions on the final polymer properties. Moreover, this modeling analysis is supposed to shed light on the reliability of the rate coefficients computationally evaluated in this part of the work as well as on the discrepancies between the data found in the literature through an indirect comparison with experimental evidences. Such investigation was encouraged by the fact that a direct comparison with experimental data is rarely accessible when reactions involving MCRs are considered.

4.2.3. Kinetic Model

In the most conventional kinetic scheme of FRP chain-end radicals only are accounted for, and such species take part to reactions like initiation, propagation, and termination. In the specific case of PVC, the most relevant termination mechanism is chain transfer to monomer.[129-133] Since this work is mainly focused on MCRs, the kinetic scheme has been updated in order to include a selection of the most relevant reactions involving this type of radicals. Such selection has been based on literature evidences as well as on our own computational results discussed above. Specifically, the kinetic model shown in the followings provides that:

- chain transfer to monomer reaction is included, being this the dominant termination event; moreover, it is inclusive of the HH propagation contribution according to the mechanism discussed above;
- MCRs are involved in bimolecular terminations but only with chain-end radicals (i.e., cross-terminations); in agreement with previous literature,[13, 14] the rate constant of bimolecular homo-termination of MCRs can be estimated

as two orders of magnitude smaller than that of cross-termination, and has therefore been neglected. Moreover, the rate coefficient of cross-termination is assumed equal to that of homo-termination of chain-end radicals;

- MCRs are not involved in HH propagation reactions, being HT propagation and backbiting much faster steps;
- chain transfer to polymer reactions are neglected;[134]
- forward and backward j:$j\pm4$ backbiting reactions are included as representative of internal backbiting between MCRs;
- the other reactions characterized by the largest activation energies according to the computational predictions, β-scission and depolymerization, are neglected.

Monomer concentration has been assumed constant during the polymerization; this way, the reaction environment typical of a polymer-rich phase in equilibrium with pure monomer has been simulated. The resulting reaction scheme is as follows:

Initiator decomposition $I_2 \xrightarrow{k_d} 2I\cdot$

Initiation reaction $I\cdot + M \xrightarrow{k_i} R_{1,1}$

Chain-end propagation $R_{n,1} + M \xrightarrow{k_p} R_{n+1,1}$

Propagation of MCR $(k \geq 2, n \geq 2k-1)$ $R_{n,k} + M \xrightarrow{k_p^{MCR}} R_{n+1,1}$

Chain transfer to monomer $R_{n,1} + M \xrightarrow{k_{fM}} P_n + R_{1,1}$

Termination by coupling $R_{n,1} + R_{m,1} \xrightarrow{k_{tc}} P_{n+m}$

$(n \geq 3)$ $R_{n,i} + R_{m,1} \xrightarrow{k_{tc}} P_{n+m}$

Termination by disproportionation $R_{n,1} + R_{m,1} \xrightarrow{k_{td}} P_n + P_m$

$(n \geq 3)$ $R_{n,i} + R_{m,1} \xrightarrow{k_{td}} P_n + P_m$

1:5 backbiting $(n \geq 3)$ $R_{n,1} \underset{k_{bb,51}}{\overset{k_{bb,15}}{\rightleftarrows}} R_{n,2}$

Internal Backbiting $(k \geq 2, n \geq 2k+1)$ $R_{n,k} \underset{k_{bb,j+4:j}}{\overset{k_{bb,j:j+4}}{\rightleftarrows}} R_{n,k+1}$

In the previous scheme, I_2 is the initiator, $I^·$ its active fragment, $R_{n,1}$ the chain-end propagating radical, $R_{n,k}$ the MCR, and P_n the dead polymer chain. The subscripts n and k indicate the number of monomer units and the radical position along the chain, respectively; note that $k = 1+(j-1)/4$, where j is the number of the carbon atom which brings the radical and the numbering of the carbon atoms starts from the radical end of the chain. This index has been selected in order to describe the four-position jump of the radical along the chain in terms of carbon atoms due to backbiting reactions using consecutive integer numbers. Given the chain length n, the largest possible value of k is $K = n/2$ (with even n) or $K = (n+1)/2$ (with odd n). At the same time, given k, the smallest number of monomer units N consistent with a given value of k (i.e., needed to ensure the existence of the k-th position) is $N = 2k-1$.

In the kinetic scheme reported above, the rate constants of backbiting reactions have been presumed all different depending upon the position of the radical along the chain. Actually, all these reactions have very similar rate constants with the exception of those involving a chain-end radical. Moreover, the reaction rates are practically the same in both the directions: therefore, $k_{bb,j:j+4} = k_{bb,j+4:j}$ for any $j > 1$ and they are indicated as k_{bb}. The population balance equations for initiator, chain-end radicals, MCRs, and dead polymer have been written as in **Equations 4.1-4.9**.

$$\frac{dI_2}{dt} = -k_d I_2 \tag{4.1}$$

$$\frac{dI^·}{dt} = 2f k_d I_2 - k_i M I^· \tag{4.2}$$

$$\frac{dR_{1,1}}{dt} = k_i M I^· - k_p M R_{1,1} - (k_{tc} + k_{td}) R_{1,1} \sum_{n=1}^{\infty} R_{n,1}$$
$$+ k_{fM} M \sum_{n=2}^{\infty} R_{n,1} - \frac{k_{tc} + k_{td}}{2} R_{1,1} \sum_{n=3}^{\infty} \sum_{k=2}^{K} R_{n,k} \tag{4.3}$$

$$\frac{dR_{2,1}}{dt} = -k_p M R_{2,1} + k_p M R_{1,1} - k_{fM} M R_{2,1}$$
$$- (k_{tc} + k_{td}) R_{2,1} \sum_{m=1}^{\infty} R_{m,1} \tag{4.4}$$
$$- \frac{k_{tc} + k_{td}}{2} R_{2,1} \sum_{n=3}^{\infty} \sum_{k=2}^{K} R_{n,k}$$

$$\frac{dR_{n,1}}{dt} = k_p M (R_{n-1,1} - R_{n,1}) - k_{fM} M R_{n,1} - k_{bb15} R_{n,1} + k_{bb51} R_{n,2}$$
$$+ k_p^{MCR} M \sum_{k=2}^{K} R_{n-1,k} - (k_{tc} + k_{td}) R_{n,1} \sum_{m=1}^{\infty} R_{m,1} \tag{4.5}$$
$$- \frac{k_{tc} + k_{td}}{2} R_{n,1} \sum_{m=3}^{\infty} \sum_{k=2}^{K} R_{m,k}$$

$$\frac{dR_{n,2}}{dt} = \left(-k_{bb51} - k_{bb} - k_p^{MCR} M\right) R_{n,2} + k_{bb} R_{n,3} + k_{bb15} R_{n,1}$$
$$- \frac{k_{tc} + k_{td}}{2} R_{n,2} \sum_{m=1}^{\infty} R_{m,1} \tag{4.6}$$

$$\frac{dR_{n,k}}{dt} = \left(-2k_{bb} - k_p^{MCR} M\right) R_{n,k} + k_{bb} R_{n,k+1} + k_{bb} R_{n,k-1}$$
$$- \frac{k_{tc} + k_{td}}{2} R_{n,k} \sum_{m=1}^{\infty} R_{m,1} \tag{4.7}$$

$$\frac{dR_{n,K}}{dt} = \left(-k_{bb} - k_p^{MCR} M\right) R_{n,K} + k_{bb} R_{n,K-1}$$
$$- \frac{k_{tc} + k_{td}}{2} R_{n,K} \sum_{m=1}^{\infty} R_{m,1} \tag{4.8}$$

$$\frac{dP_n}{dt} = k_{fM} R_{n,1} M + k_{td} R_{n,1} \sum_{m=1}^{\infty} R_{m,1} + \frac{k_{tc}}{2} \sum_{j=1}^{n-1} R_{j,1} R_{n-j,1}$$
$$+ \frac{k_{td}}{2} \left(R_{n,1} \sum_{m=3}^{\infty} \sum_{k=2}^{K} R_{m,k} + \sum_{k=2}^{K} R_{n,k} \sum_{m=1}^{\infty} R_{m,1} \right) \tag{4.9}$$
$$+ \frac{k_{td}}{2} \sum_{j=1}^{n-1} R_{j,1} \sum_{k=2}^{K} R_{n-j,k}$$

The resulting set of ordinary differential equations has been numerically solved through the method of moments. The equations of the moments of the first three orders (i.e., 0, 1, and 2) have been written for the dead polymer as well as for the two radical species, chain-end radicals, and MCRs. The moments of the different species have been defined as shown in **Equations 4.10-4.12**, with $j = 0$, 1, and 2.

$$\lambda_j^{R1} = \sum_{n=1}^{\infty} n^j R_{n,1} \tag{4.10}$$

$$\lambda_j^{Ri} = \sum_{k=2}^{\infty} \sum_{n=2k-1}^{\infty} n^j R_{n,k} = \sum_{n=3}^{\infty} \sum_{k=2}^{K} n^j R_{n,k} \tag{4.11}$$

$$\mu_j = \sum_{n=1}^{\infty} n^j P_n \tag{4.12}$$

These moments are evaluated for chain lengths from one to infinity for chain-end radicals and dead polymer, while those of MCRs are defined from minimum chain lengths large enough to be able to accommodate at least one tertiary radical (i.e., $n = 3$). The resulting moment equations are summarized in the system composed by **Equations 4.13-4.23**; note that the two species $R_{1,1}$ and $R_{2,1}$ had to be considered separately in order to correctly evaluate all transitions from chain-end radicals to MCRs.

$$\frac{dR_{1,1}}{dt} = k_i MI^{\cdot} - k_p M R_{1,1} - (k_{tc} + k_{td}) R_{1,1} \left(\lambda_0^{R1} + \frac{\lambda_0^{Ri}}{2} \right)$$
$$+ k_{fM} M \left(\lambda_0^{R1} - R_{1,1} \right) = 0 \tag{4.13}$$

$$\frac{dR_{2,1}}{dt} = -k_p M R_{2,1} + k_p M R_{1,1} - k_{fM} M R_{2,1}$$
$$- (k_{tc} + k_{td}) R_{2,1} \left(\lambda_0^{R1} + \frac{\lambda_0^{Ri}}{2} \right) = 0 \tag{4.14}$$

$$\frac{d\lambda_0^{R1}}{dt} = k_i MI^{\cdot} - k_{bb15}\left(\lambda_0^{R1} - R_{1,1} - R_{2,1}\right) + k_{bb51}\sum_{n=3}^{\infty} R_{n,2}$$
$$- (k_{tc} + k_{td})(\lambda_0^{R1})^2 + k_P^{MCR}M\lambda_0^{Ri}$$
$$- \frac{k_{tc} + k_{td}}{2}\lambda_0^{R1}\lambda_0^{Ri} = 0 \tag{4.15}$$

$$\frac{d\lambda_0^{Ri}}{dt} = k_{bb15}\left(\lambda_0^{R1} - R_{1,1} - R_{2,1}\right) - k_{bb51}\sum_{n=3}^{\infty} R_{n,2} - k_P^{MCR}M\lambda_0^{Ri}$$
$$- \frac{k_{tc} + k_{td}}{2}\lambda_0^{R1}\lambda_0^{Ri} = 0 \tag{4.16}$$

$$\frac{d\lambda_1^{R1}}{dt} = k_i MI^{\cdot} - k_{bb15}\left(\lambda_1^{R1} - R_{1,1} - 2R_{2,1}\right) + k_{bb51}\sum_{n=3}^{\infty} nR_{n,2}$$
$$- (k_{tc} + k_{td})\lambda_0^{R1}\lambda_1^{R1} + k_P^{MCR}M\left(\lambda_0^{Ri} + \lambda_1^{Ri}\right)$$
$$+ k_p M\lambda_0^{R1} + k_{fM}M(\lambda_0^{R1} - \lambda_1^{R1}) - \frac{k_{tc} + k_{td}}{2}\lambda_1^{R1}\lambda_0^{Ri} \tag{4.17}$$

$$\frac{d\lambda_1^{Ri}}{dt} = k_{bb15}\left(\lambda_1^{R1} - R_{1,1} - 2R_{2,1}\right) - k_{bb51}\sum_{n=3}^{\infty} nR_{n,2} - k_P^{MCR}M\lambda_1^{Ri}$$
$$- \frac{k_{tc} + k_{td}}{2}\lambda_0^{R1}\lambda_1^{Ri} \tag{4.18}$$

$$\frac{d\lambda_2^{R1}}{dt} = k_i MI^{\cdot} - k_{bb15}\left(\lambda_2^{R1} - R_{1,1} - 4R_{2,1}\right) + k_{bb51}\sum_{n=3}^{\infty} n^2 R_{n,2}$$
$$- (k_{tc} + k_{td})\lambda_0^{R1}\lambda_2^{R1}$$
$$+ k_P^{MCR}M\left(\lambda_2^{Ri} + \lambda_0^{Ri} + 2\lambda_1^{Ri}\right)$$
$$+ k_p M(\lambda_0^{R1} + 2\lambda_1^{R1}) + k_{fM}M(\lambda_0^{R1} - \lambda_2^{R1})$$
$$- \frac{k_{tc} + k_{td}}{2}\lambda_2^{R1}\lambda_0^{Ri} \tag{4.19}$$

$$\frac{d\lambda_2^{Ri}}{dt} = k_{bb15}\left(\lambda_1^{R1} - R_{1,1} - 4R_{2,1}\right) - k_{bb51}\sum_{n=3}^{\infty} n^2 R_{n,2}$$
$$- k_P^{MCR}M\lambda_2^{Ri} - \frac{k_{tc} + k_{td}}{2}\lambda_0^{R1}\lambda_2^{Ri} \tag{4.20}$$

$$\frac{d\mu_0}{dt} = k_{fM}\,M\lambda_0^{R1} + \frac{k_{tc}}{2}(\lambda_0^{R1})^2 + k_{td}(\lambda_0^{R1})^2 + \frac{k_{tc}}{2}\lambda_0^{R1}\lambda_0^{Ri}$$
$$+ k_{td}\lambda_0^{R1}\lambda_0^{Ri} \tag{4.21}$$

$$\frac{d\mu_1}{dt} = k_{fM} M\lambda_1^{R1} + (k_{tc} + k_{td})\lambda_0^{R1}\lambda_1^{R1} + \frac{k_{tc} + k_{td}}{2}\lambda_0^{R1}\lambda_1^{Ri}$$
$$+ \frac{k_{tc} + k_{td}}{2}\lambda_1^{R1}\lambda_0^{Ri} \tag{4.22}$$

$$\frac{d\mu_2}{dt} = k_{fM} M\lambda_2^{R1} + k_{tc}\left[(\lambda_1^{R1})^2 + \lambda_0^{R1}\lambda_2^{R1} + \lambda_1^{R1}\lambda_1^{Ri}\right]$$
$$+ k_{td}\lambda_0^{R1}\lambda_2^{R1} + \frac{k_{tc} + k_{td}}{2}\left(\lambda_0^{R1}\lambda_2^{Ri} + \lambda_2^{R1}\lambda_0^{Ri}\right) \tag{4.23}$$

The values of all model parameters have been set as follows. The monomer concentration in the reaction locus has been considered constant and equal to 5.82 mol L^{-1}. This value has been estimated from the Flory-Huggins equation assuming pure monomer in the monomer-rich phase, and it corresponds to the typical value of suspension polymerization at conversion below 70-80%.[129, 135] The polymerization temperature has been set to 330 K, and an initial concentration of initiator (AIBN) of 5.82 10^{-4} mol L^{-1}, corresponding to a molar ratio initiator/monomer equal to 10^{-4}, has been chosen.[135]

Table 4. *Rate coefficient values calculated at 330 K and used in the simulations. Data computationally determined in this work with the MPWB1K/6-31G(d,p) functional[a] as well as taken from literature[b]. Reversible internal backbiting rate constant value evaluated as the average between those of 5:9 and 9:5 backbiting reactions.*

Reaction		k
		L mol^{-1} s^{-1} or s^{-1}
Chain-end propagation[a]	k_p	1.73 10^4
j:j±4 reversible internal backbiting[a]	k_{bb}	1.84 10^3
1:5 backbiting[a]	k_{bb15}	1.90 10^2
5:1 backbiting[a]	k_{bb51}	2.73 10^1
Propagation of MCR[a]	k_p^{MCR}	1.43 10^1
Chain transfer to monomer[b], [128]	k_{fM}	1.37
Termination by coupling[b], [128]	k_{tc}	7.10 10^7
Termination by disproportionation[b], [128]	k_{td}	7.10 10^7
Initiator decomposition[b], [136]	k_d	6.37 10^{-5}
Initiation reaction[a]	k_i	1.73 10^4

All values of the rate coefficients have been taken from the literature or equal to those estimated by quantum chemistry calculations; all the selected values are summarized in **Table 4**. In particular, the values calculated using the MPWB1K/6-31G(d,p) functional and basis set including the tunneling effect have been considered.

4.2.4. Model Results

In order to solve the system of **Equations 4.13-4.23**, a series of summations involving MCRs in a specific position, $R_{n,2}$, needs to be evaluated. For this purpose, the concentrations of MCRs in any positions, $R_{n,k}$, have been expressed as a function of that of the chain-end radicals, $R_{n,1}$, as follows. Let one consider **Equations 4.6-4.8** above. Since the backbiting and propagation terms are much larger than the termination one, roughly by two orders of magnitude, the latter has been neglected. Moreover, applying the quasi-steady-state (QSS) assumption, a tridiagonal system of finite-difference equations is obtained, as shown in **Equations 4.24-4.26** with $2 < k < K$.

$$\left(k_{bb51} + k_{bb} + k_p^{MCR}M\right)R_{n,2} = k_{bb}R_{n,3} + k_{bb15}R_{n,1} \tag{4.24}$$

$$\left(2k_{bb} + k_p^{MCR}M\right)R_{n,k} = k_{bb}R_{n,k+1} + k_{bb}R_{n,k-1} \tag{4.25}$$

$$\left(k_{bb} + k_p^{MCR}M\right)R_{n,K} = k_{bb}R_{n,K-1} \tag{4.26}$$

This system has been solved analytically, thus obtaining the generic $R_{n,k}$ as a linear function of the corresponding $R_{n,1}$ for any k between 2 and K, according to **Equation 4.27**. The γ_k constant coefficients are defined as combinations of the rate constants of backbiting and propagation of MCR, as detailed by **Equations 4.28-4.31**, with $\alpha_1 = \beta_K = 1$. Moreover, these parameters are function of the temperature only, under the assumption of a constant monomer concentration.

$$R_{n,k} = R_{n,1}\gamma_k = R_{n,1} \frac{k_{bb15}(k_{bb})^{k-2}\beta_k}{\left(k_{bb} + k_p^{MCR}M\right)\alpha_{K-1} - (k_{bb})^2\alpha_{K-2}} \tag{4.27}$$

$$\alpha_k = \alpha_{k-1}\left(2k_{bb} + k_p^{MCR}M\right) - (k_{bb})^2\alpha_{k-2} \tag{4.28}$$

$$\beta_k = \beta_{k+1}\left(2k_{bb} + k_p^{MCR} M\right) - (k_{bb})^2 \beta_{k+2} \tag{4.29}$$

$$\alpha_2 = k_{bb51} + k_{bb} + k_p^{MCR} M \tag{4.30}$$

$$\beta_{K-1} = k_{bb} + k_p^{MCR} M \tag{4.31}$$

With the aim of evaluating the overall concentration of MCRs in a specific position, whatever the chain length, **Equation 4.27** has been used as defined in **Equation 4.32**, which shows that all $R_{n,1}$ values, with n ranging from $2k$-1 to ∞, are needed to evaluate R_k. Specifically, focusing on $k = 2$ (i.e., k corresponding to the only unknown term involved in the system of **Equations 4.13-4.23**) the corresponding summations have been readily expressed as a function of variables already included in the balance equations, as shown in **Equations 4.33-4.35**, therefore "closing" the system of equations.

$$R_k = \sum_{n=2k-1}^{\infty} R_{n,k} = \sum_{n=2k-1}^{\infty} R_{n,1}\, \gamma_k = \gamma_k \sum_{n=2k-1}^{\infty} R_{n,1} \tag{4.32}$$

$$\sum_{n=3}^{\infty} R_{n,2} = \sum_{n=3}^{\infty} R_{n,1}\, \gamma_2 = \gamma_2 \sum_{n=3}^{\infty} R_{n,1} = \gamma_2\left(\lambda_0^{R1} - R_{1,1} - R_{2,1}\right) \tag{4.33}$$

$$\sum_{n=3}^{\infty} n R_{n,2} = \gamma_2\left(\lambda_1^{R1} - R_{1,1} - 2R_{2,1}\right) \tag{4.34}$$

$$\sum_{n=3}^{\infty} n^2 R_{n,2} = \gamma_2\left(\lambda_2^{R1} - R_{1,1} - 4R_{2,1}\right) \tag{4.35}$$

Equation 4.32 has been also used to calculate the distribution of R_k as a function of the radical position k. Such distribution, normalized to the total concentration of active species R_t, is shown in **Figure 10**. Note that this distribution corresponds to the constant values of temperature and monomer concentration mentioned above. Even though the fraction of chain-end radicals is the largest, it is only slightly larger than 30%. Therefore, MCRs represent almost the remaining 70% of active species, indeed a surprisingly high amount.

Starting from the chain-end, such radicals can shift along the polymer chain due to the fast *j:j±4* backbiting; however, their concentrations become smaller and smaller at increasing distance from the chain end, being the fraction of MCRs at *k* larger than 20 (about position 40 in terms of repeating units) practically negligible. It should be noted that this result is consistent with backbiting rate coefficients accounting for the quantum tunneling correction: the picture is largely different if this correction is neglected.
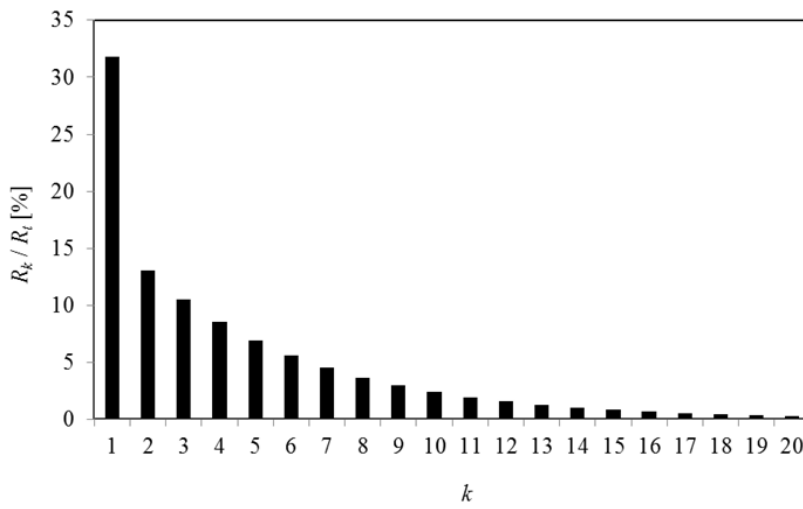
Figure 10. *Percentage of radicals as a function of their position along the chain (k). Column chart relative to the parameters and reaction rate coefficients evaluated at 330 K with the MPWB1K/6-31G(d,p) method.*

Let us now examine the total concentrations of chain-end and mid-chain radicals. Applying the QSS assumption to the *zero*-order moment equations of both types of radicals and combining them with **Equation 4.33**, two non-linear equations in the variables λ_0^{R1} and λ_0^{Ri} have been obtained. Once more, neglecting the bimolecular termination term with respect to propagation and backbiting for MCRs as well as the concentrations of the shortest chain-end radicals, $R_{1,1}$ and $R_{2,1}$, with respect to their total concentration, λ_0^{R1}, **Equations 4.36-4.37** have been obtained.

$$\lambda_0^{R1} = \sqrt{\frac{2fk_dI_2}{k_{tc}+k_{td}}} \left(1 + \frac{k_{bb15} - k_{bb51}\gamma_2}{2\,k_p^{MCR}\,M} \right)^{-\frac{1}{2}} \tag{4.36}$$

$$\lambda_0^{Ri} = \frac{(k_{bb15} - k_{bb51}\gamma_2)(\lambda_0^{R1} - R_{1,1} - R_{2,1})}{k_p^{MCR} M} \qquad (4.37)$$

Equations 4.36-4.37 provide the total concentration of chain-end radicals and MCRs, respectively. Notably, the concentration of chain-end radicals is affected by the presence of MCRs, and **Equation 4.36** reduces to the classical QSS formula of FRP when backbiting reactions are absent. Moreover, if one considers that 1:5 backbiting is much more favored than 5:1, and that the value of the constant coefficient γ_2 is smaller than one, the ratio of mid-chain to chain-end radical concentrations reduces to the ratio between the two rate constants of 1:5 backbiting and propagation of MCR, as shown in **Equation 4.38**.

$$\frac{\lambda_0^{Ri}}{\lambda_0^{R1}} \approx \frac{k_{bb15}}{k_p^{MCR} M} \qquad (4.38)$$

This equation provides a very direct way to correlate the relative amount of MCRs produced in the system with the reaction rate constants most determining their reactivity. Secondary reactions, and in particular backbiting, result in a kind of "protection" of the radicals that migrate to a tertiary carbon atom when involved in 1:5 backbiting. Such radicals can change their position along the polymer backbone by backbiting without terminating, thus being accumulated. Notably, the relative extent of the propagation of MCR to backbiting determines their conversion rate to chain-end radicals, which represents a limitation to their accumulation.

Due to the very small tendency of MCRs to propagate in comparison with chain-end radicals, the direct contribution of the former radicals to the overall polymerization rate as well as to the average molecular weight of the polymer is negligible. However, since secondary reactions affect the concentration of chain-end radicals, the same two quantities are indirectly affected. In order to clarify this last point, the kinetic model has been used to predict the polymerization rate (R_p) as well as the polymer number average molecular weight (*Mn*) and the polydispersity index (*PDI*). Namely, two simulations have been carried out using the parameter values in **Table 4** with and without including backbiting reactions, thus with and without considering MCRs.

As shown in **Figure 11**, the overall polymerization rate decreases when secondary reactions are included. The net effect of MCRs and secondary reactions on this quantity has been evaluated as smaller than a factor of two. Such impact is therefore quite limited, and the use of a model not accounting for MCRs but with slightly different values of some rate constants (e.g., twofold propagation rate constant or fourfold termination rate constant) would provide the same prediction, thus making a fair model discrimination very difficult.
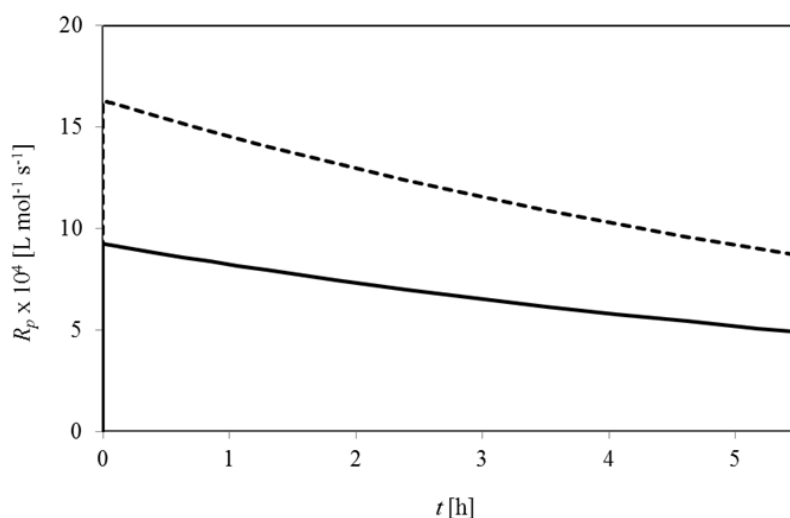
Figure 11. *Effect of secondary reactions and mid-chain radicals on the overall polymerization rate (R_p). Curve relative to calculations with (solid line) and without (dashed line) considering secondary reactions.*

With regard to the polymer molecular weight, the results reported in **Figure 12** show that this parameter is slightly affected by secondary reactions involving MCRs at 330 K. Moreover, the *PDI* value is not modified by secondary reactions: this is an expected result since the latter quantity is determined by the dominant termination mechanism, which is chain transfer to monomer. Once more, the unambiguous identification of the presence and impact of MCRs as well as the corresponding reactions on quantities such as rate of polymerization and polymer molecular weight is indeed quite difficult.
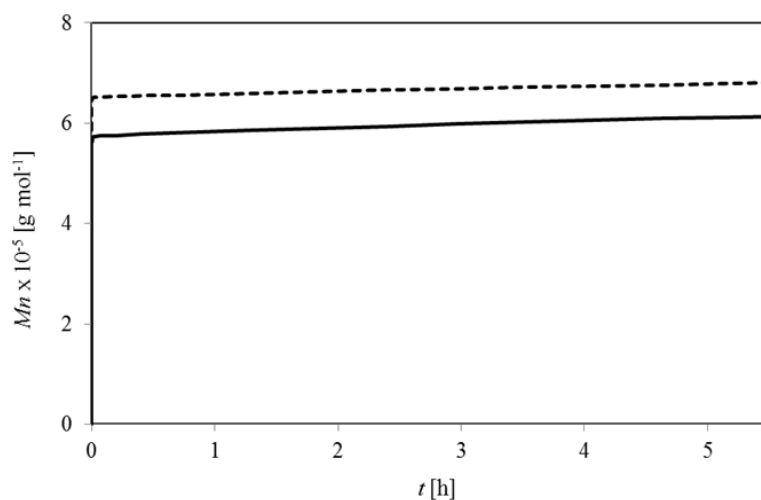
Figure 12. *Effect of secondary reactions and mid-chain radicals on the number average molecular weight (Mn). Curve relative to calculations with (solid line) and without (dashed line) considering secondary reactions.*

Following the last argument above, the modeling analysis has been extended to more specific polymer features, better suited to validate the selected kinetic scheme and the parameter values estimated by the computational methods. Namely, the formation of branches has been considered, being this quantity strictly related to the secondary reactions discussed above and its extent easily detected by suitable experimental techniques. As mentioned before, SCBs are mainly formed by propagation following the reaction of intramolecular chain transfer. Since every MCR propagation step corresponds to the formation of a branch, their overall production rate is given by **Equation 4.39**.

$$\frac{dB}{dt} = k_P^{MCR} M \lambda_0^{Ri} \tag{4.39}$$

Let one focus the attention on a specific type of branch: the butyl branches, which are mainly originated through the propagation reaction of the MCRs with the radical located on the fifth carbon atom (i.e., at $k = 2$). Since the total concentration of this type of radicals is given by **Equation 4.33**, the production rate of butyl branches is expressed by **Equation 4.40**.

71

$$\frac{dB_{Bu}}{dt} = k_P^{MCR} M \sum_{n=3}^{\infty} R_{n,2} = k_P^{MCR} M \gamma_2 \left(\lambda_0^{R1} - R_{1,1} - R_{2,1} \right) \tag{4.40}$$

The density of such branches is commonly considered, expressed as the number of butyl branches per thousand monomer units in the polymer chains. Such quantity, indicated as N_{Bu}, has been evaluated as in **Equation 4.41**.

$$N_{Bu} = 1000 \, \frac{B_{Bu}}{\mu_1 + \lambda_1^{R1} + \lambda_1^{Ri}} \tag{4.41}$$

Through estimating this cumulative quantity by time integration of the corresponding balance, a practically constant value is predicted. Therefore, it is worth analyzing the corresponding instantaneous value. With reference to the equations of the moments and **Equation 4.40**, the relation shown in **Equation 4.42** has been obtained.

$$N_{Bu}^{inst} = 1000 \, \frac{k_p^{MCR} M \sum_{n=3}^{\infty} R_{n,2}}{k_p M \, \lambda_0^{R1}} \approx 1000 \, \frac{k_p^{MCR}}{k_p} \gamma_2 \tag{4.42}$$

Equation 4.42 shows that N_{Bu}^{inst} is a function of temperature only. Therefore, its value is equal to that of the corresponding cumulative property, N_{Bu}, at constant temperature, which is the case under examination. Similar expressions have been obtained investigating the FRP of alkyl acrylates.[8, 9] The density of butyl branches estimated through the last previous equation and using the parameter values in **Table 4** is equal to 0.34 at 330 K. This result is in a good agreement with the literature, where values ranging from 0.5 to 1.7 are reported from ^{13}C NMR measurements on a series of commercial PVC samples produced by suspension polymerization.[49, 137]

Equation 4.42 allows also understanding how temperature affects the amount of such defects. The higher activation energy of k_p^{MCR} compared to that of k_p makes the ratio between the two parameters strongly direct-proportion dependent upon temperature, even though this influence on N_{Bu} is slightly smoothed by the coefficient γ_2, which exhibits a slight inverse-proportion dependence upon temperature. Overall, a

temperature increase of only twenty degrees results in N_{Bu} increase of almost 30%, thus in a remarkable effect on the chain regularity.

4.2.5. Conclusion

A quantum chemistry investigation of the secondary reactions producing and involving MCRs in PVC polymerization has been performed, focusing on a set of side steps possibly responsible of the formation of microstructural defects in the polymer. Two DFT functionals have been adopted to perform the computational investigation: the B3LYP/6-311+G(d,p) method and the novel MPWB1K functional with 6-31G(d,p) basis set. Rate constants of propagation, backbiting, and chain scission reactions have been estimated to elucidate the differences in reactivity between chain-end radicals and MCRs. Specifically, 1:5, 5:1, and 5:9 backbiting reactions turned out to be the most significant reaction steps involving MCRs. Moreover, their kinetics has shown to be affected by relevant tunneling effect, and has been found to be in competition with the kinetics of propagation of the same radicals.

A kinetic model of PVC polymerization within the polymer-rich phase typical of the reacting droplets in suspension polymerization has been developed including the investigated secondary steps in the reaction scheme. A remarkable impact of such reactions on the relative amount of the two types of radicals, chain-end and mid-chain, has been observed. In particular, large amounts of MCRs can accumulate in the reacting system due to the "protection" of the radical activity when positioned along the polymer chain. Although such radicals do not show significant effects on the molecular weight buildup, they affect the chain-end radical concentration, thus they influence the polymerization rate.

The amount of branches originated along the polymer chains is the most significant quantity suited to identify the contribution of secondary reactions. The density of butyl branches predicted considering this kinetic scheme and the selected parameters is in good agreement with the experimental values, thus validating the general reliability of the computational approach.[122]

4.3. Relevance of Quantum Tunneling on Backbiting

Quantum tunneling in hydrogen transfer reactions active in FRP is investigated at a theoretical level. Three systems are examined: PE, PS, and PVC. Kinetic parameters of backbiting reactions are evaluated using quantum chemistry. Tunneling corrections are estimated adopting the 1D Eckart model, which provides a reasonable accuracy along with a limited computational effort. The relevance of quantum tunneling in the investigated systems is highlighted, with focus on the temperature dependence of the tunneling correction in the typical polymerization conditions of the investigated monomers. Obtained results clearly show that tunneling plays an important role in the kinetics estimation of hydrogen abstractions in FRP.[105]

4.3.1. Introduction

Quantum tunneling characterizes hydrogen transfer reactions in the way that has been detailed previously, with reference to the dedicated paragraph in Chapter 3; therefore, its relevance is at issue in those reaction systems that host hydrogen abstraction phenomena. Among them, intramolecular hydrogen transfer plays often an important role in the combustion of hydrocarbons. In fact, the formation of some reaction products in this process can be explained only in terms of isomerization reactions. Hydrogen shift reactions strongly influence also paraffin pyrolysis, hydrocarbon oxidation, and the mechanism of those processes involving radical intermediates.[50, 138-142]

The relevance of isomerization reactions is associated to the resulting changes in the location of the radical site, which can lead to branching on the reaction pathway. Moreover, hydrogen shifts are the predominant monomolecular reactions under low-temperature conditions. Furthermore, even when the temperature increases and β-scission reactions acquire relevance, isomerizations still remain critical steps determining the dissociation of alkyl radicals.[143] Finally, the determination of the rate coefficients of isomerization reactions is a prerequisite for modeling of combustion devices, such as engines and furnaces operating with hydrocarbon fuels.

In regard to the FRP field, recent studies convincingly proved the existence of MCRs mainly originated through the so-called backbiting reactions.[6, 13, 144] A backbiting reaction consists in a hydrogen transposition to the chain-end of a radical macromolecule, and it is energetically favored because of the higher stability of the MCR with respect to the chain-end radical. The products of these isomerization reactions are usually well stabilized by the existence of a tertiary carbon radical, and the reactions in which they are involved can affect the final properties of the polymer to a significant extent.

Despite the importance of intramolecular hydrogen transfer reactions, and even if experimental measurements on alkyl radicals have been recently reported,[145-148] few data on the kinetics of these reactions are available in the literature. The difficulties related to the experimental investigation of isomerization reactions are mainly due to the great instability of the produced intermediates that makes critical the direct measurement of their reaction rates. In the specific case of FRP, the reactivity difference between secondary and tertiary carbon radicals makes it difficult even the estimation of rate coefficients when using PLP-SEC.[28] Recently, the most advanced PLP-EPR technique has helped to overcome those issues, being able also to provide a measurement of the relative population of the two different radicals.[14]

In these complex processes, for which a theoretical investigation of the kinetics is often necessary to interpret experimental evidences, computational studies represent a new tool for the determination of the rate coefficients of hydrogen transfer reactions. In this scenario, one of the most critical aspects is represented by the evaluation of the tunneling contribution to the rate constant. The role of quantum tunneling in alkyl radical isomerizations has been recently highlighted by Tsang and co-workers.[145, 146, 149] In particular, they concluded that a large body of literature data estimated at low temperature (i.e., reaction rate coefficients with small pre-exponential factors and activation energies) can be reconciled with high-temperature data by taking into account the quantum tunneling correction.[150]

Although some computational studies on the determination of the tunneling effect in isomerization reactions of linear alkyl radicals are available in literature,[151-154] along with few studies on PVC,[49, 53] no works are reported about the investigation of this topic in FRP systems involving widely used monomers such as St and

acrylates. Considering that the tunneling contribution increases against a decrease of the reaction temperature,[151, 152] this phenomenon might gain relevance in the milder conditions of FRP rather than in hydrocarbon cracking or pyrolysis processes. All of the hydrogen transposition reactions are supposed to be affected by quantum tunneling, and in particular backbiting, which is typical in the FRP of the mentioned monomers.[7, 13]

Hence, this work is aimed at investigating the relevance of quantum tunneling on backbiting reactions in FRP, with particular attention to its temperature dependence. Firstly, ethylene is selected as a benchmark monomer in order to validate the computational approach. This choice has been mainly due to the limited number of atoms involved, which allows a considerable reduction of the computational effort and the possibility to use higher-level theories. Moreover, this system offers a wide availability of experimental and computational backbiting rate coefficient values to be compared with the computational predictions.[146, 155, 156] Afterwards, the method is applied to the investigation of the tunneling effect in St and vinyl chloride polymerization, starting from the computational data about backbiting reactions in these FRP systems reported in the literature.[7, 121]

The tunneling coefficients used to correct the rate constants of backbiting reactions are estimated adopting the Eckart model.[109] This 1D approach associates a reasonable accuracy to a limited computational effort, as it requires the estimation of the activation energy and imaginary frequency only. Although the difference between the predictions with Eckart and more refined theories is usually about a factor of five at 300 K, there are a few examples in which differences with SCT calculations are much smaller due to fortuitous self-cancellation of errors implicit in the Eckart model. Moreover, this difference is reduced at the higher-temperature values typical of FRP systems (i.e., usually above 330 K).

4.3.2. Computational Results

The computational investigation has been initially focused on 1:3, 1:5, and 1:7 backbiting reactions involving linear and branched PE radicals consisting of eight and nine monomer units, referred to as linear and branched hexadecyl radicals,

respectively. In addition, the 1:5 radical shift from an SBR to the main-chain has been investigated. Reaction schemes of the examined backbiting steps involving PE chains are shown in **Figure 13**. The tunneling factors have been estimated at 473 K, which is a temperature typical of ethylene radical polymerization.
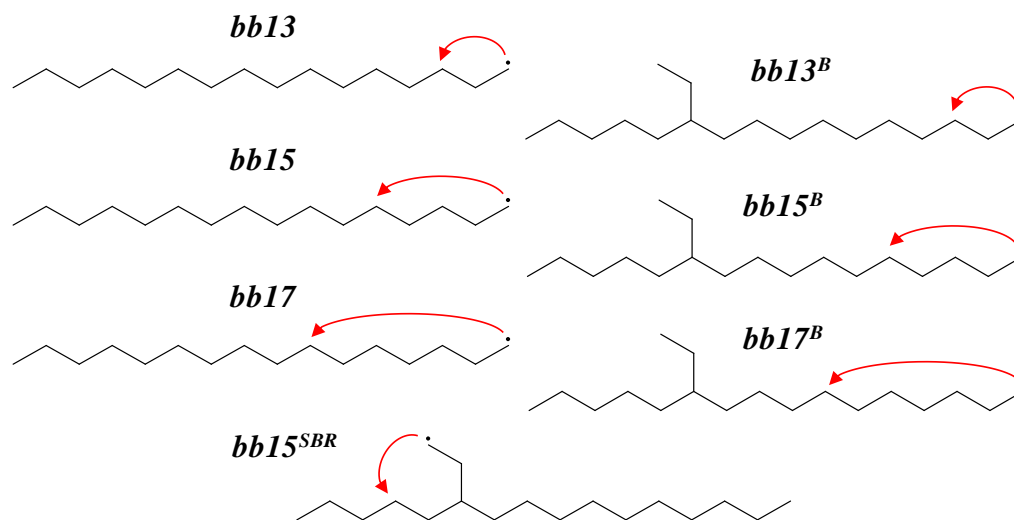
Figure 13. *Reaction schemes of backbiting reactions involving polyethylene chains. Reaction symbolism referred to: 1:3 (bb13), 1:5, (bb15), and 1:7 (bb17) backbiting on linear chain; 1:3 (bb13^B), 1:5 (bb15^B), and 1:7 (bb17^B) backbiting on branched chain; 1:5 backbiting of short-branch radical (bb15^{SBR}).*

With the aim of validating the computational method adopted in this study, the benchmark reaction of 1:5 backbiting of a 1-octyl radical has been investigated first, adopting a higher level of theory. Specifically, the CBS-QB3 method was used for the estimation of activation energy, and the HR approximation for the definition of the pre-exponential factor was considered, in addition to the conventional procedure (i.e., B3LYP method and HO model), according to the computational details provided in Chapter 3. Calculations about this reaction have been performed at two temperature values (i.e., 473 K and 1000 K), in order to have a comparison with the computational predictions for the hexadecyl radical at 473 K as well as with the experimental high-temperature measures. In **Table 5** the activation energy values estimated using the two different methods for the benchmark reaction are reported, along with the result at the B3LYP level for 1:5 backbiting of the 1-hexadecyl radical.

Table 5. *Activation energy values calculated at the B3LYP/6-31G(d,p) and CBS-QB3 level of theory for the benchmark reaction and for 1:5 backbiting on the longer polyethylene chain.*

Reaction	Method	E_a
		kJ mol^{-1}
1:5 backbiting on 1- octyl radical	CBS-QB3	61.6
1:5 backbiting on 1- octyl radical	B3LYP/6-31G(d,p)	58.4
1:5 backbiting on 1- hexadecyl radical	B3LYP/6-31G(d,p)	57.6

The results in **Table 5** show that all of activation energy values are within 4 kJ mol^{-1}, which is a reasonable uncertainty for this class of reactions. Based on the activation energy and imaginary frequency values obtained with the CBS-QB3 calculations, the Eckart tunneling factor has been estimated to be 3.55 at 473 K and 1.31 at 1000 K for the investigated reaction. These values are in agreement with the literature data chosen for comparison and evaluated with the more refined SCT method.[150]

Afterwards, the HR model has been used to estimate the rate constant of the benchmark 1:5 backbiting reaction. In **Table 6** the internal rotation partition function values are reported, along with other details.

Table 6. *Calculated internal rotation partition functions, dihedral atom sequences, assigned vibrational frequencies, and reduced inertia moments related to the hindered rotor motions of the reactant and transition state involved in the benchmark 1:5 backbiting of 1-octyl radical.*

Reaction	$Q_{int,rot}$	$Q_{int,rot}$	Dihedral Atoms	Frequency	RIM
	473 K	*1000 K*		*cm^{-1}*	*Å^2 amu*
φ_1-*reactant*	5.54	7.83	2, 1, 4, 7	58.1	1.72
φ_2-*reactant*	13.84	31.30	1, 4, 7, 8	116.1	31.64
φ_3-*reactant*	12.69	34.58	4, 7, 8, 11	80.2	54.40
φ_4-*reactant*	16.39	44.72	7, 8, 11, 14	50.9	91.01
φ_5-*reactant*	12.66	34.59	8, 11, 14, 17	144.2	54.78
φ_6-*reactant*	10.01	27.19	11, 14, 17, 20	164.2	34.71
φ_5-*transition state*	14.90	38.11	8, 11, 14, 17	75.4	51.07
φ_6-*transition state*	10.22	27.59	11, 14, 17, 20	146.4	34.83

In particular, dihedral atoms, assigned vibrational frequency values, and reduced inertia moments (*RIM*) related to the corresponding torsion motions for reactant and transition state structures are reported with reference to the configurations shown in **Figure 14**. Considering the HR model instead of the HO approximation, the pre-exponential factor of the reference reaction is reduced by 38 and 65 times at 473 K and 1000 K, respectively. This result shows that the uncoupled HR model can have a significant impact on the rate constant estimation, both at high and reduced temperatures.
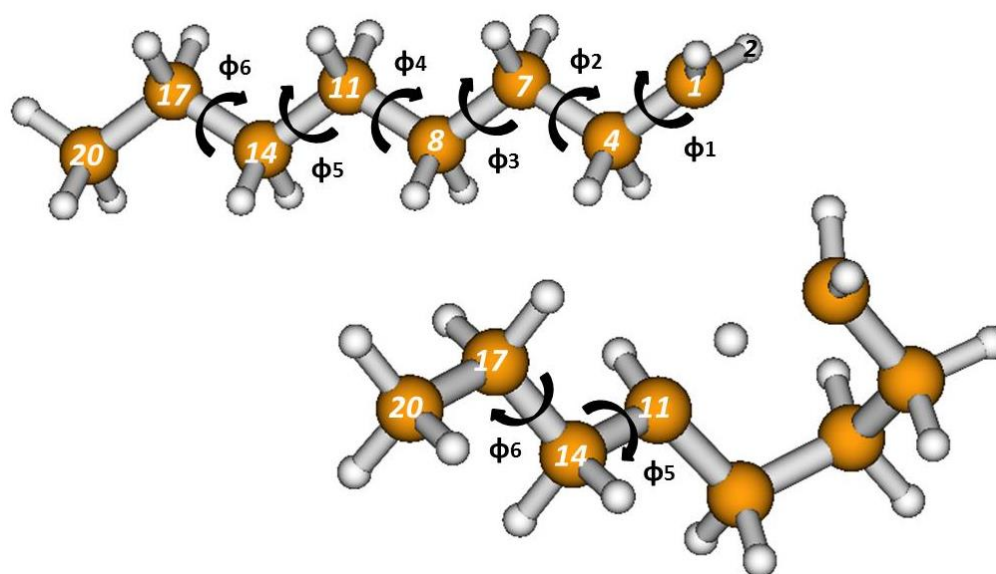
Figure 14. *Optimized geometries of reactant (top) and transition state (bottom) structures relative to the 1:5 backbiting reaction involving 1-octyl radical. Detail of the torsion motions around the dihedral angles at issue, according to the HR model adopted.*

The 1:5 backbiting rate constant calculated at 1000 K including the HR model and using CBS-QB3 energies is about seven times smaller than the experimental value relative to the 1-octyl radical isomerization, which has been determined in high-temperature single pulse shock tube experiments,[146] as shown in **Table 7**. Such difference between the two values includes both computational and experimental uncertainties. Moreover, an underestimation of the experimental rate constant was in part expected, as the use of an uncoupled rotor approximation for a multiple rotor

system is likely to lead to an overestimation of the stability of the reactant. It is also interesting to observe that the error introduced by the use of the HR model is not much different from the one that would be obtained using the harmonic approximation (i.e., a factor of nine).

Since at low temperature the HO approximation is expected to increase in accuracy, it has been decided to use it for the remainder of the calculations together with B3LYP/6-31G(d,p) energies, which were found to be in a reasonable agreement with CBS-QB3 energies for this class of reactions. These calculations are likely to have an uncertainty factor of about ten.

Table 7. *Rate constant values for the 1:5 backbiting reaction on 1-octyl radical computationally evaluated at the higher level of theory and experimental value taken from the literature.*

Rate Constant	$k_{bb, 473 K}$ s^{-1}	$k_{bb, 1000 K}$ s^{-1}
Calculated (this work)	$6.65 \ 10^3$	$4.33 \ 10^6$
Experimental data[146]	$8.57 \ 10^3$	$2.95 \ 10^7$

In **Table 8** the evaluated tunneling factors for the backbiting reactions involving PE radicals along with the corresponding backbiting rate constants comprehensive of tunneling corrections are reported, with reference to the symbolism defined in **Figure 13**.

Concerning 1:5 transfer reactions, the backbiting rate constant appears to be reduced by the presence of a branch along the chain, while it is increased if the radical shift occurs from an SBR. The tunneling factors evaluated at 473 K are in the range of 3.2-3.5, with the exception of 1:3 backbiting. The latter reaction exhibits a larger imaginary frequency, so that the tunneling correction is enhanced. Furthermore, the estimated tunneling correction for 1:5 backbiting is in agreement with the corresponding data reported by Tsang et al., concerning the six-member transition state shift on *n*-alkyl radical, which has been estimated as 4.0 through SCT calculations at 473 K.[150]

Table 8. *Calculated values of activation energy, imaginary frequency associated to the transition state structure, tunneling factor, and rate coefficient for the forward (fw) and backward (bw) backbiting reactions involving polyethylene radicals. Rate coefficients are calculated at 473 K and comprehensive of the tunneling correction.*

Reaction	$E_{a,fw}$	$E_{a,bw}$	Frequency	Q_{tun}	$k_{bb,fw}$	$k_{bb,bw}$
	kJ mol^{-1}	*kJ mol^{-1}*	*cm^{-1}*		*s^{-1}*	*s^{-1}*
bb13	153.9	171.1	2097.9*i*	$1.22\ 10^1$	$2.49\ 10^{-3}$	$1.18\ 10^{-5}$
bb13^B	155.1	171.6	2099.4*i*	$1.23\ 10^1$	$2.38\ 10^{-4}$	$6.39\ 10^{-6}$
bb15	57.6	75.9	1669.1*i*	3.46	$2.31\ 10^6$	$3.07\ 10^3$
bb15^B	58.9	75.5	1670.9*i*	3.48	$3.24\ 10^5$	$9.11\ 10^3$
bb15^{SBR}	47.8	60.6	1652.9*i*	3.28	$1.35\ 10^7$	$5.48\ 10^5$
bb17	72.7	90.0	1596.9*i*	3.17	$1.44\ 10^4$	$1.14\ 10^2$
bb17^B	73.4	90.4	1601.5*i*	3.19	$4.29\ 10^3$	$6.25\ 10^1$

The second set of reactions considered concerns PS, particularly the computational data evaluated at the B3LYP/6-31G(d,p) level reported in a previous work.[7] The tunneling effect has been evaluated for 1:3, 1:5, 1:7, and 7:3 backbiting reactions, where two different atactic configurations have been adopted for the esamer polymer backbone (i.e., *m-m-r-m-r* and *r-r-m-r-r*), as shown in **Figure 15**.
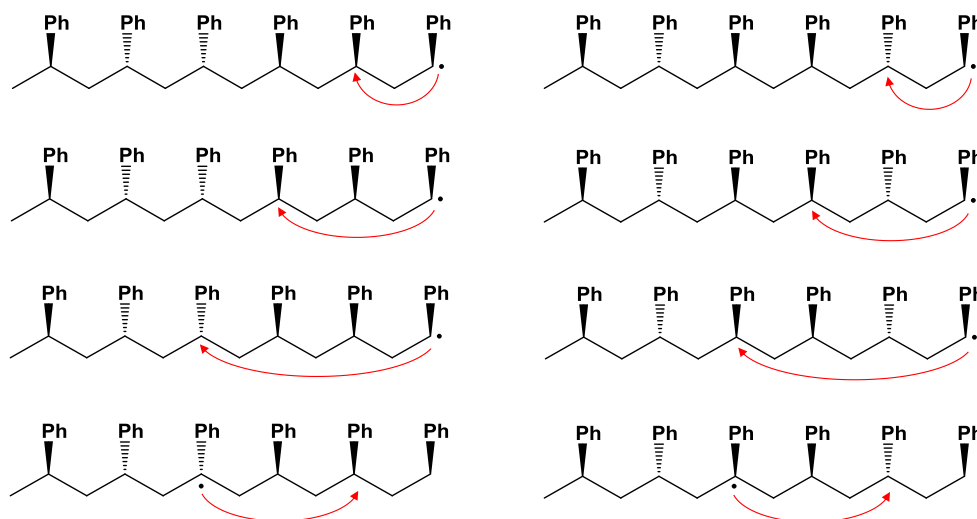
Figure 15. *Reaction schemes of backbiting reactions involving polystyrene chains with atactic configuration m-m-r-m-r (left) and r-r-m-r-r (right), with the order of the diads starting from the radical end of the chain. From top to bottom: 1:3, 1:5, 1:7, and 7:3 backbiting.*

The tunneling corrections to backbiting rate constants of PS have been estimated at 573 K, temperature at which simulations were performed in the previous work. The calculated tunneling coefficients are comprised between the values 1.9 (1:5 backbiting) and 3.8 (1:3 backbiting), as shown in **Table 9**. These results underline a poor increase of the backbiting rate constants due to the tunneling effect, which is limited to a factor of two, mainly due to the high-temperature conditions adopted.

Table 9. *Calculated values of activation energy, imaginary frequency associated to the transition state structure, tunneling factor, and rate coefficient for the forward (fw) and backward (bw) backbiting reactions involving polystyrene radicals. Rate coefficients are calculated at 573 K and comprehensive of the tunneling correction. Superscripts a) and b) are referred to atactic polymer configurations m-m-r-m-r and r-r-m-r-r, respectively.*

Reaction	$\mathbf{E_{a,fw}}$ $kJ\,mol^{-1}$	$\mathbf{E_{a,bw}}$ $kJ\,mol^{-1}$	**Frequency** cm^{-1}	$\mathbf{Q_{tun}}$	$\mathbf{k_{bb,fw}}$ s^{-1}	$\mathbf{k_{bb,bw}}$ s^{-1}
1:3 backbiting[a]	171.8	181.6	2013.8i	3.79	$2.69\,10^{-4}$	$1.18\,10^{-4}$
1:3 backbiting[b]	185.4	185.5	1960.0i	3.49	$2.48\,10^{-5}$	$4.05\,10^{-5}$
1:5 backbiting[a]	91.9	92.1	1481.6i	1.91	$1.00\,10^{3}$	$1.01\,10^{3}$
1:5 backbiting[b]	78.7	82.3	1476.5i	1.89	$1.30\,10^{4}$	$2.47\,10^{4}$
1:7 backbiting[a]	85.7	93.5	1639.0i	2.23	$2.35\,10^{3}$	$1.83\,10^{2}$
1:7 backbiting[b]	86.0	93.8	1612.0i	2.16	$1.60\,10^{3}$	$3.82\,10^{1}$
7:3 backbiting[a]	95.5	99.5	1666.1i	2.30	$3.95\,10^{2}$	$3.43\,10^{2}$
7:3 backbiting[b]	85.0	98.7	1572.8i	2.08	$1.01\,10^{4}$	$3.77\,10^{3}$

Finally, the tunneling effect on PVC has been investigated, and its relevance at low-temperature conditions examined. Previous studies have been performed investigating several backbiting reactions and the corresponding tunneling effect in this system.[49, 53, 122] In particular, it was proven the strong influence on vinyl chloride polymerization of quantum tunneling in affecting backbiting reaction kinetics, which significantly influences the radical chain distribution. In this work, the tunneling corrections have been evaluated at 330 K on the basis of the rate coefficients of 1:3, 1:5, 1:7, and 5:9 backbiting reactions of PVC, which have been investigated at the B3LYP/6-31G(d,p) level of theory in a previous works.[121, 122] This way, the reported results are consistent with those of the previous investigations performed on both PE

and PS systems. Reaction schemes of the examined backbiting steps involving PVC chains are reported in **Figure 16**.
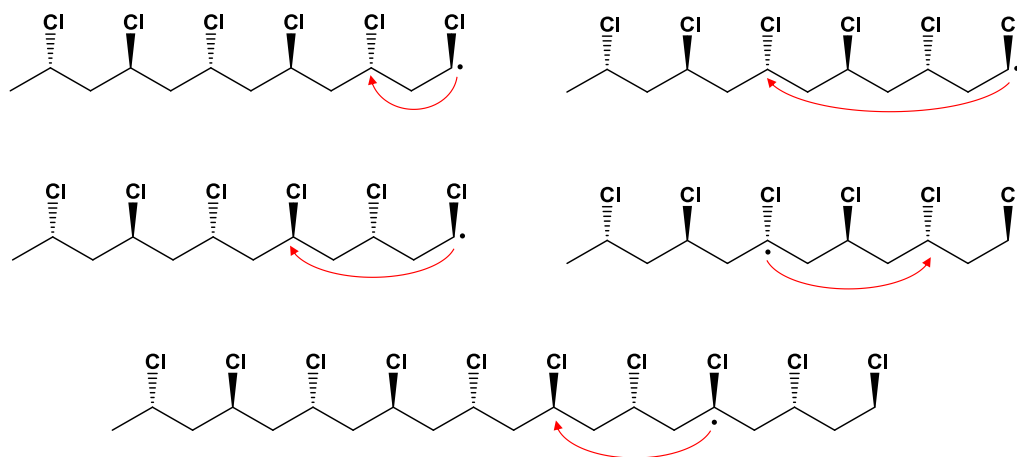
Figure 16. *Reaction schemes of backbiting reactions involving syndiotactic poly (vinyl chloride) chains. From top to bottom: 1:3 (left) and 1:7 (right) backbiting; 1:5 (left) and 7:3 (right) backbiting;5:9 backbiting*.

An initial comparison has been made between the tunneling factors evaluated at different levels of theory (i.e., based on the activation energy and imaginary frequency data obtained from the use of different computational methods). The results shown in **Table 10** are in agreement with those reported in our previous work and obtained with the B3LYP/6-311+G(d,p) method, while the tunneling factors evaluated with the MPWB1K/6-31G(d,p) method in the same paper are in general larger by two to five times.[122] This difference is due to the higher values of imaginary frequencies of the transition states evaluated by the latter computational method.

Furthermore, the evaluated tunneling corrections to 1:3 and 1:5 backbiting reactions have been compared with the data reported in another work.[53] Such reference values, obtained with the Eckart method and based on parameters calculated at the G3(MP2)-RAD//MPW1K/6-31+G(d,p) level of theory, are in agreement with the tunneling factors evaluated in our previous work with the MPWB1K method. In conclusion, it is worth noting that in this polymerization system operating at low temperature the tunneling effect is relevant, and it is responsible of an increase of the 1:5 backbiting rate constant by ten to one hundred times.

Table 10. *Calculated values of activation energy, imaginary frequency associated to the transition state structure, tunneling factor, and rate coefficient for the forward (fw) and backward (bw) backbiting reactions involving poly (vinyl chloride) radicals. Rate coefficients are calculated at 330 K and comprehensive of the tunneling correction.*

Reaction	$E_{a,fw}$ $kJ\ mol^{-1}$	$E_{a,bw}$ $kJ\ mol^{-1}$	Frequency cm^{-1}	Q_{tun}	$k_{bb,fw}$ s^{-1}	$k_{bb,bw}$ s^{-1}
1:3 backbiting	160.1	168.1	$2110.7i$	$7.70\ 10^3$	$2.06\ 10^{-9}$	$8.77\ 10^{-11}$
1:3 backbiting	71.6	76.2	$1748.2i$	$3.32\ 10^1$	$6.74\ 10^1$	7.64
1:7 backbiting	101.3	105.8	$1773.1i$	$6.63\ 10^1$	$6.08\ 10^{-4}$	$7.09\ 10^{-5}$
7:3 backbiting	72.5	76.1	$1756.3i$	$3.48\ 10^1$	$2.01\ 10^1$	6.82
5:9 backbiting	72.0	71.7	$1749.1i$	$3.21\ 10^1$	$3.89\ 10^1$	$4.18\ 10^1$

With the aim of investigating how the tunneling effect is able to enhance the backbiting reaction rates in relation to the peculiarities of the different reacting radical molecules, the tunneling factors have been finally calculated for the three systems as a function of temperature. A comparison between the tunneling corrections to the reaction rate constants of 1:3, 1:5, and 1:7 backbiting on PE, PS, and PVC linear radical chains is shown in **Table 11**.

Table 11. *Temperature dependence of the tunneling factors evaluated for 1:3, 1:5, and 1:7 backbiting reactions involving polyethylene, polystyrene, and poly (vinyl chloride) radicals. Backbiting along the main-chain of linear radicals is considered for polyethylene, while atactic polymer configuration r-r-m-r-r is adopted for polystyrene.*

Reaction		Q_{tun} 298 K	Q_{tun} 373 K	Q_{tun} 473 K	Q_{tun} 573 K	Q_{tun} 673 K
1:3 backbiting	*PE*	$1.93\ 10^5$	$2.78\ 10^2$	$1.22\ 10^1$	4.32	2.69
	PS	$7.28\ 10^4$	$1.25\ 10^2$	8.27	3.49	2.34
	PVC	$2.63\ 10^5$	$3.24\ 10^2$	$1.28\ 10^1$	4.43	2.73
1:5 backbiting	*PE*	$5.04\ 10^1$	8.93	3.46	2.34	1.87
	PS	$2.39\ 10^1$	5.53	2.65	1.89	1.60
	PVC	$1.07\ 10^2$	$1.24\ 10^1$	4.09	2.54	1.96
1:7 backbiting	*PE*	$4.83\ 10^1$	7.88	3.17	2.16	1.75
	PS	$6.61\ 10^1$	8.70	3.30	2.16	1.76
	PVC	$3.43\ 10^2$	$1.76\ 10^1$	4.52	2.62	1.98

As expected, for all the investigated reactions the tunneling factor strongly decreases along with the temperature growth. Moreover, the tunneling corrections to 1:3 backbiting are generally higher than those of the other two backbiting reactions, which are rather comparable. However, the strong enhancing effect on 1:3 backbiting rate constants due to quantum tunneling should be compared with the corresponding rate coefficients, which are significantly small. Thus, the tunneling effect is more relevant in the enhancement of 1:7 and, in particular, 1:5 backbiting rate coefficients. Focusing on the different radical molecules involved in hydrogen transfer reactions, PVC radicals are characterized by a stronger tunneling contribution to their backbiting rate constants compared with the other systems, though this difference is reduced at high temperature.

Finally, the temperature dependence of the calculated 1:5 backbiting rate coefficient involving the 1-hexadecyl radical has been examined, in order to show directly the quantum tunneling effect on the rate constant value. The results relative to the investigation of backbiting reaction involving a chain-end linear radical are reported in **Figure 17**.
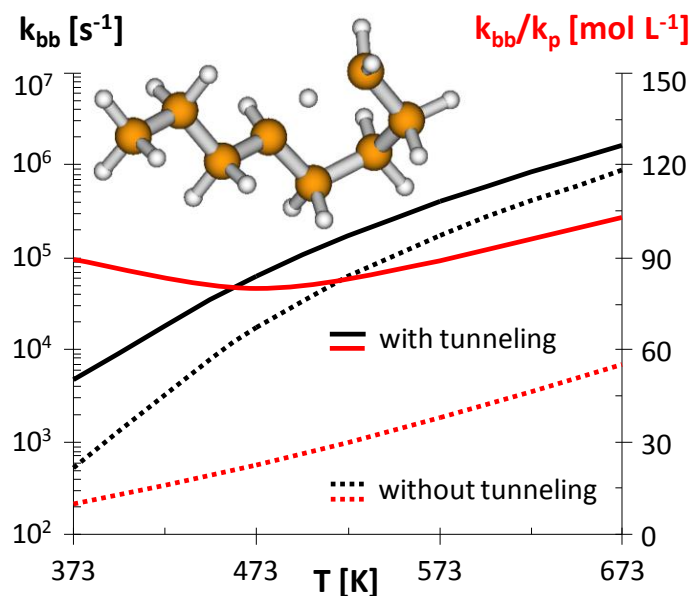
Figure 17. *Temperature dependence of 1:5 backbiting rate constant (k_{bb}) and ratio of 1:5 backbiting to chain-end propagation rate coefficients (k_{bb}/k_p) with and without considering the tunneling correction, referred to backbiting of 1-hexadecyl radical.*

85

While the tunneling effect is shown to be quite regular in the enhancement of the backbiting rate constant along with temperature, it is interesting to focus on its influence on the backbiting on propagation[27] rate coefficient ratio (k_{bb}/k_p), which is a significant parameter in order to understand the real competition between backbiting and the overall reaction kinetics. Without considering the tunneling correction, such ratio increases with temperature, since backbiting is characterized by larger activation energy with respect to propagation. On the contrary, the inverse-proportion dependence of the tunneling factor upon temperature gives a k_{bb}/k_p ratio that is rather independent upon temperature inside the selected temperature range.

4.3.3. Conclusion

In this work, an investigation of quantum tunneling relevance in FRP systems has been performed. Focusing on backbiting reactions, the quantum tunneling effect has been evaluated through the Eckart model, which proved to have a reasonable accuracy in the estimation of the tunneling factors. Rate coefficients of backbiting in PE have been initially evaluated in order to assess the reliability of the adopted computational approach based on the DFT. Then, tunneling corrections have been estimated for this system as well as for PS and PVC, based on backbiting rate coefficients obtained from previous works. As expected, quantum tunneling is relevant in enhancing the backbiting probability, especially at mild polymerization temperatures.

The temperature dependence of quantum tunneling corrections has been also studied, focusing the attention to its contribution on the ratio of 1:5 backbiting to propagation of PE. The increase with temperature of this parameter has resulted to be significantly smoothed by quantum tunneling. While the computational evaluation of backbiting rate constant values might be affected by an uncertainty intrinsic of the DFT method, the quantum tunneling effect on this secondary reaction is clearly showed. However, a development of alternative and more refined computational approaches to better estimate pre-exponential factors is still required in order to obtain accurate estimation of the absolute rate constants.[105]

4.4. Insight into Butyl Acrylate Polymerization

Secondary reactions involved in the FRP of butyl acrylate are investigated using quantum chemistry. First, various backbiting reactions are studied by adopting a simplified molecular model suitable for treating long polymer chains. The predicted reaction kinetics suggest the possibility of a radical migration along the PBA chain as a consequence of subsequent *j:j±4* hydrogen abstractions, which are characterized by low activation energy. Moreover, branching propagation and β-scission reactions originating from MCRs are investigated using a complete PBA model composed of five monomer units. The reaction kinetics involving SBRs is also examined, and a novel backbiting step leading to the formation of short branches is proposed.[123]

4.4.1. Introduction

The relevance of MCRs in FRP processes has been thoroughly investigated in the last decade, with a particular emphasis on acrylates, due to the close correlation of these radicals with the branching and gel formation observed in the resulting polymers.[2, 21, 22] The impact of MCRs on the polymerization process is determined by the extent of secondary reactions, which are especially active at high temperatures and are responsible for the origination of MCRs as well as their resulting reactivity.[2, 23, 122] MCRs show a remarkably lower reactivity in comparison to chain-end radicals due to a greater stabilization associated with the tertiary carbon radical with respect to a secondary carbon one.

However, MCRs can also be involved in a wide range of reactions subsequent to their formation. The mechanisms and kinetics of such reactions are often unknown, whereas their effects on the final polymer properties are more clearly observable, even when the polymerization is carried out under mild conditions. Therefore, an accurate knowledge of the secondary reaction kinetics is of paramount importance for the polymerization of systems that are characterized as being of high industrial relevance, and for those that are subjected to the effects of these reactions to such an extent that the original properties can be significantly modified. In this context, acrylates are of

great interest, and among them BA is undoubtedly one of the most widely used and studied monomers.[11, 13, 14, 28, 30, 31]

The development of increasingly advanced experimental techniques for the estimation of reaction rate coefficients has made it possible to obtain parameter values for a wide range of polymer systems.[24, 27] In the case of BA, not only has an extensive investigation led to the determination of accurate propagation rate coefficient,[26] but it has also allowed researchers to obtain a reliable prediction of the kinetics of these secondary reactions.[14] Among these reactions, backbiting is certainly one of the most interesting in many respects. The importance of intramolecular transfer to polymer reactions in FPR processes has been previously described in the first half of the last century.[4, 5] This reaction is primarily responsible for the formation of MCRs, along with random intermolecular chain transfers to polymer.[2] Moreover, the effectiveness of backbiting reactions in BA polymerization has made investigations into propagation kinetics at temperatures greater than ambient a difficult task for many years.[9, 28, 29, 157]

Once an MCR is formed, it is subject to the classical steps of propagation and termination; otherwise, it may undergo other monomolecular reactions, such as chain-scission and further backbiting events. Propagation and termination of MCRs have been studied experimentally in the past few decades through PLP techniques coupled with SEC or EPR. This work has been conducted in parallel with investigations on backbiting.[13, 14, 31] In particular, the relative extent of the propagation of MCRs to that of chain-end radicals is a key parameter in the determination of the polymerization rate and the branching density of the final polymer.[8, 9, 157]

Reaction kinetics of the secondary reactions involving MCRs are hardly observable at the experimental level because neither the reactants nor the products are easily detectable. Therefore, accurate rate parameters of the so-called β-scission and internal backbiting reactions are still unknown for BA. Even when the rate coefficient values of secondary reactions are determined experimentally and well established, it should be noted that they are often referred to as mean values rather than a single reaction step. Concerning a complex kinetic polymerization scheme in which the relevance of MCRs is non-negligible, secondary reactions such as backbiting and propagation of tertiary radicals include a certain number of steps or possible reaction pathways that the experimental analysis is often unable to distinguish between.

Aside from the experimental approach, computational investigations based on quantum mechanics can provide a strong contribution to achieving estimates of secondary reaction kinetics. This approach at a theoretical level has proven to be effective in determining the rate constant parameters for specific reaction steps with reasonable accuracy. Although previous works have shown that there is still some uncertainty in the prediction of the absolute rate coefficients, usually associated with the estimation of the pre-exponential factor, it is worth noting that this method does satisfactorily evaluate the rate constant ratios, as well as the relative impact of reaction rates within a given polymerization system.[7, 46, 52, 53, 105, 122]

In this work, quantum chemistry is used to investigate backbiting reactions occurring in BA polymerization. In particular, the established procedure is adopted to study secondary reactions in St,[7] acrylonitrile,[51] and vinyl chloride[121, 122] is extended to now examine BA. Reaction kinetics of intramolecular chain transfer reactions characterized by various transition state ring sizes and involving both chain-end and tertiary radicals is examined. Moreover, reaction kinetics of monomer addition to MCR is investigated as well as those of the subsequent competitive reaction steps of backbiting and propagation of SBR. Finally, β-scission reactions are studied, and the overall computational results are compared with the existing experimental data. The combined B3LYP/6-31G(d,p)//MPWB1K/6-31G(d,p) method is adopted in this work, while the HO model is used for the definition of the pre-exponential factors, according to the computational details described in Chapter 3.

4.4.2. Computational Results

As a preliminary investigation, the selected DFT method has been validated by comparing the computational results with the experimental values about BA propagation rate constant. Parameter values of $E_a = 18.0 \pm 0.1$ kJ mol^{-1} and $A = 2.26 \pm 0.05$ 10^7 L mol^{-1} s^{-1} were assumed as benchmark data for this reaction, whereby a rate constant value of 1.58 10^4 L mol^{-1} s^{-1} at 298 K is calculated.[26, 28] Since the determination of the propagation rate coefficients using quantum chemistry may be affected by the radical chain length, this comparison has been performed with a computational model involving monomer addition steps to a radical chain composed

by one to four BA units. As shown in **Table 12**, the calculated rate constant value increases with increasing chain length of the PBA radical due to the combined effects of slight changes in the pre-exponential factor and activation energy values.

Table 12. *Calculated values of reaction enthalpy, activation energy, pre-exponential factor, and rate coefficient for propagation involving poly (butyl acrylate) radicals at increasing chain length. Rate parameters are calculated at 298 K.*

Reaction		ΔH	E_a	$Log_{10}(A)$	k_p
		kJ mol⁻¹	*kJ mol⁻¹*		*L mol⁻¹ s⁻¹*
$R_1 + M \rightarrow R_2$	$k_{p,1}$	-98.3	19.5	5.297	$7.55 \ 10^1$
$R_2 + M \rightarrow R_3$	$k_{p,2}$	-103.9	16.6	6.090	$1.55 \ 10^3$
$R_3 + M \rightarrow R_4$	$k_{p,3}$	-106.9	18.3	6.558	$2.20 \ 10^3$
$R_4 + M \rightarrow R_5$	$k_{p,4}$	-102.2	17.8	6.748	$4.17 \ 10^3$

Although a classic chain-length effect in a strict sense (i.e., a decrease in propagation rate constant value down to an asymptotic value after a few monomer additions) is not observable in these results, it is interesting to notice that the calculated rate constant of the fourth propagation step approaches the experimental value, being $k_{p,4}$ smaller than the PLP data at 298 K by less than a factor of four. Moreover, the predicted value of activation energy is in very good agreement with the experimental data. Finally, although the computational method is not well suited to determine whether the chain-length effect is actually present in the system, a more reliable description of the radical reactivity is obtained by considering a sufficient number of monomer units. This argument has led to the definition of a molecular model suitable for describing the long polymer chains required for investigating secondary reactions.

Turning the focus of the study to intramolecular chain transfer, the 1:3, 1:5, 1:7, and 7:3 forward and backward backbiting reactions have been first investigated, as it has already been done in our previous works.[7, 51, 121] Reaction schemes of the selected backbiting steps are reported in **Figure 18**, where the representative model for this system of reactions is shown. Such a simplified approach has been selected in order to minimize the number of electrons involved without losing any peculiar

characteristics of the reactive moiety involved in the backbiting process. In detail, the monomer units directly involved in the hydrogen transfer are true BA units, whereas the other units in the chain are simple ethyl groups.

Figure 18. *Reaction schemes of 1:3, 1:5, 1:7, and 7:3 backbiting reactions involving poly (butyl acrylate) chains investigated according to the simplified molecular model*.

All of the determined kinetic parameters, reaction enthalpies, activation energies for both forward and backward reactions, and pre-exponential factors are reported in **Table 13**. As it has already reported in other polymer systems, 1:3 backbiting reaction exhibits the largest activation energy, because of the formation of a highly strained four-member ring transition state, followed by 1:7 backbiting reaction. On the contrary, smaller activation energies have been found for the reactions involving a six-member ring transition state (i.e., 1:5 and 7:3 backbiting reactions). It is worth noting that the activation energy of 7:3 backbiting falls between the corresponding values of forward and backward 1:5 backbiting steps. This behavior can be explained observing that the radical shift occurs between two tertiary carbons, thus it is expected to be more favorable than the shift between a tertiary and a secondary carbon. This is a result of the smaller stability of a secondary radical than a tertiary radical. Likewise, the backward shift from a secondary carbon to a tertiary

carbon is expected to be the fastest step, indeed this behavior is observed in all of the investigated 1:*j* backbiting reactions.

Table 13. *Calculated values of tunneling factor, reaction enthalpy, activation energy, pre-exponential factor, and rate coefficient for forward and backward 1:3, 1:5, 1:7, 1:9, 1:11, and 1:13 as well as reversible 7:3 and 5:9 backbiting reactions involving poly (butyl acrylate) radicals according to the simplified molecular model. Rate constants and kinetic parameters are calculated at 298 K.*

Reaction		Q_{tun}	ΔH $kJ\ mol^{-1}$	E_a $kJ\ mol^{-1}$	$Log_{10}(A)$	k_{bb} s^{-1}
1:3 backbiting	$k_{bb1:3}$	$1.92\ 10^4$	-21.8	140.9	12.455	$1.07\ 10^{-8}$
	$k_{bb3:1}$		21.8	162.8	12.422	$1.44\ 10^{-12}$
1:5 backbiting	$k_{bb1:5}$	25.44	-21.4	55.0	11.455	$1.64\ 10^3$
	$k_{bb5:1}$		21.4	76.4	11.528	$3.52\ 10^{-1}$
1:7 backbiting	$k_{bb1:7}$	59.39	-20.6	83.9	10.223	$1.92\ 10^{-3}$
	$k_{bb7:1}$		20.6	104.4	10.260	$5.37\ 10^{-7}$
7:3 backbiting	$k_{bb7:3}$	27.03	0.0	63.3	10.456	6.24
5:9 backbiting	$k_{bb5:9}$	27.91	0.0	61.1	10.465	$1.62\ 10^1$
1:9 backbiting	$k_{bb1:9}$	$2.65\ 10^2$	-16.3	107.6	8.760	$2.11\ 10^{-8}$
	$k_{bb9:1}$		16.3	123.1	9.072	$8.28\ 10^{-11}$
1:11 backbiting	$k_{bb1:11}$	$2.61\ 10^2$	-20.0	100.1	8.674	$3.47\ 10^{-7}$
	$k_{bb11:1}$		20.0	120.3	8.633	$9.07\ 10^{-11}$
1:13 backbiting	$k_{bb1:13}$	$3.69\ 10^2$	-19.5	108.2	8.581	$1.51\ 10^{-8}$
	$k_{bb13:1}$		19.5	127.6	7.929	$1.37\ 10^{-12}$

In the literature, a rate coefficient of 133.2 s^{-1} at 298 K is found for backbiting reaction in BA.[14] A comparison with the results in **Table 13** shows that the predicted rate constant value for the fastest backbiting step (i.e., 1:5 backbiting reaction) is one order of magnitude greater than the experimental data. This discrepancy can be attributed to several aspects concerning the evaluation of the pre-exponential factor. The tunneling factors calculated from the Eckart model lose accuracy at low temperature and may result in an overestimation of the backbiting rate coefficient at 298 K. Neglecting the HR treatment may be another source contributing to an

overestimation of the backbiting rate coefficient, although the values obtained are within one order of magnitude at the low-temperature values for these calculations.[105]

Although a loss of accuracy in the calculation of the absolute values of backbiting rate coefficients may also occur because of the approximation introduced by the simplified model, its application to the description of intramolecular chain transfer reactions has allowed the investigation of other important features of backbiting involving longer chains. Focusing on the six-member transition state hydrogen shifts, the further migration of a tertiary radical along the chain subsequent to 1:5 backbiting reaction (i.e., the 5:9 backbiting reaction) has been investigated, and it is shown in **Figure 19**.
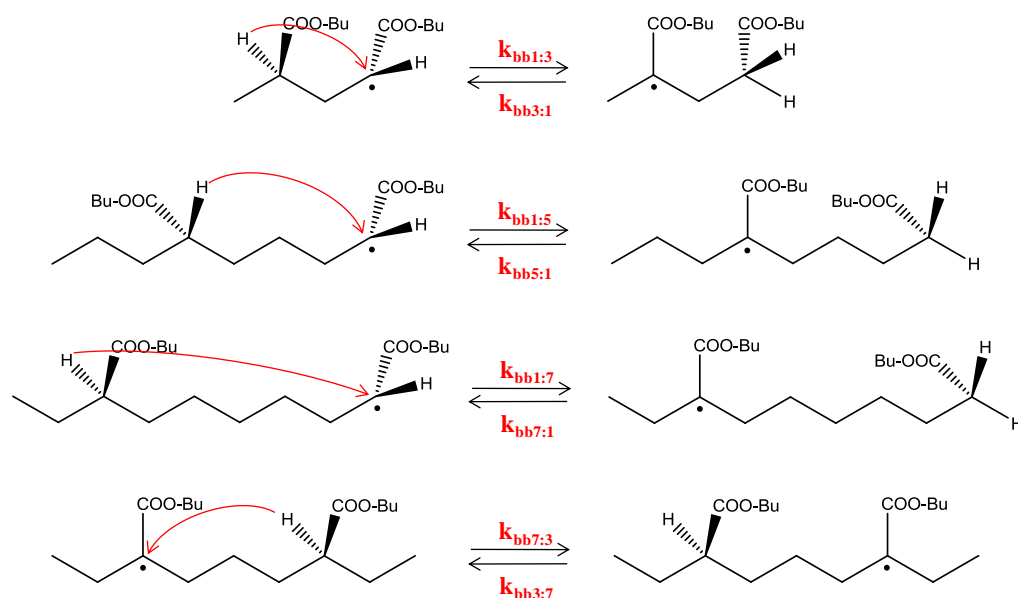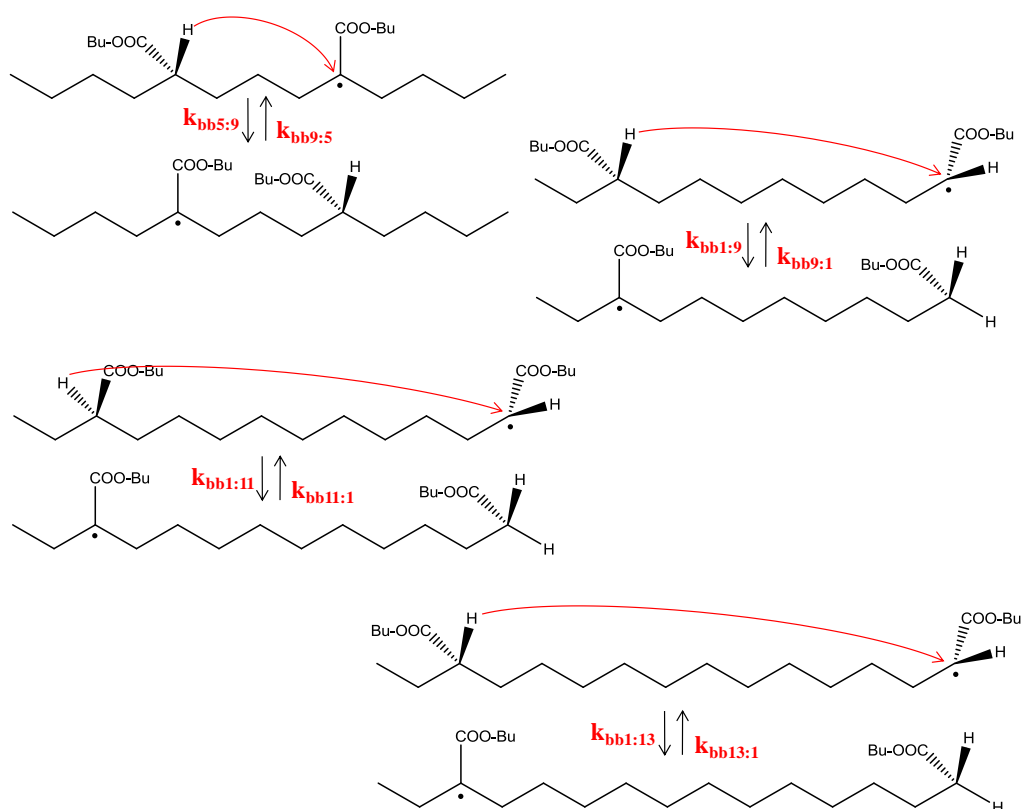

Figure 19. *Reaction schemes of 5:9, 1:9, 1:11, and 1:13 backbiting reactions involving poly (butyl acrylate) chains investigated according to the simplified molecular model.*

The rate parameters of 5:9 backbiting reaction reported in **Table 13** are very close to those of 7:3 backbiting. Therefore, the same comparison that has been made between 7:3 and 1:5 radical shifts can be extended to 5:9 backbiting. These results strongly support the hypothesis of a radical migration along the growing polymer chain through consecutive j:$j\pm4$ backbiting reactions in competition with the other reactions that MCRs may be subjected to.

With the aim of testing the probability of alternative pathways to j:$j\pm4$ backbiting reactions for the radical migration along the chain, the 1:9, 1:11, and 1:13 radical shifts have been investigated with the simplified model, as detailed in **Figure 19**. The calculated rate coefficients of the 1:j shifts reported in **Table 13** are similar to those of 1:3 backbiting reaction, rendering these hydrogen transfer steps almost negligible. However, it is interesting to note how the activation energy values of the 1:j backbiting reactions follow the trend of the internal ring strain values of the cycloalkanes associated with the transition state configurations of the investigated backbiting steps,[158, 159] as reported in **Table 14**. Particularly, this behavior is well observed only up to the 1:9 backbiting reaction, for the reasons that are discussed in the followings.

The internal strain of the larger molecules approaches zero as for cyclohexane, but for the corresponding backbiting reactions the activation energy still remains greater than that required for the 1:5 backbiting reaction. Such misbehaviors can be due to the distortion effect of the C-H-C angle in the transition state. In fact, the ring strain of cycloalkanes is mostly due to the deviation in bond angles from the ideal tetrahedral value of 109.5°. Larger ring molecules can accommodate atomic displacements that approximate this angle. On the contrary, in backbiting reactions the ring strain increases from the presence of the C-H-C angle in the transition state that significantly deviates from the ideal tetrahedral value, even in larger transition state rings. The only exception is observed in the 1:3 backbiting reaction, where the C-H-C angle is close to 109.5°, though for a very strained square geometry. Among all the other cases, the six-member transition state leads to a smaller C-H-C angle, thus slowing down the ring strain. This effect yields a smaller activation energy for j:$j\pm4$ backbiting reactions with respect to the other hydrogen shift pathways, supporting the

conclusion that a radical migration through the BA chains is more likely to occur through consecutive 1:5 backbiting reaction steps.

Table 14. *Calculated values of activation energy, rate coefficient, size of the C-H-C angle in the transition state, and ring strain of the cycloalkane corresponding to the transition state ring for 1:3, 1:5, 5:9, 1:7, 1:9, 1:11, and 1:13 backbiting reactions involving poly (butyl acrylate) radicals according to the simplified molecular model. Rate constants are calculated at 298 K.*

Reaction	**E_a**	**k_{bb}**	**C-H-C Angle**	**Alkane Ring Strain**	
	kJ mol^{-1}	*s^{-1}*		*kJ mol^{-1}*	
1:3 backbiting	140.9	$1.07 \ 10^{-8}$	103.7°	109	*Cyclobutane*
1:5 backbiting	55.0	$1.64 \ 10^{3}$	156.7°	0	*Cyclohexane*
5:9 backbiting	61.1	$1.62 \ 10^{1}$	158.2°	0	*Cyclohexane*
1:7 backbiting	83.9	$1.92 \ 10^{-3}$	176.9°	42	*Cyclooctane*
1:9 backbiting	107.6	$2.11 \ 10^{-8}$	168.1°	58	*Cyclodecane*
1:11 backbiting	100.1	$3.47 \ 10^{-7}$	168.8°	10	*Cyclododecane*
1:13 backbiting	108.2	$1.51 \ 10^{-8}$	178.5°	0	*Cyclotetradecane*

While the formation of the MCRs and the radical location inside the chain are mainly regulated by backbiting kinetics, other features of BA polymerization such as the mid-chain to chain-end radical distribution or the formation of branches are determined by the extent of other competitive reactions that may involve the MCRs. The addition of monomer to an MCR made up of four BA units has been investigated by adopting a complete molecular model similar to that used for the study of propagation of chain-end radicals. The rate parameters shown in **Table 15** are quite different from the experimental values of $E_a = 28.6 \pm 0.3$ kJ mol^{-1} and $A = 1.22 \pm 0.3$ 10^6 L mol^{-1} s^{-1},[13, 14] although the predicted rate coefficient at 298 K is greater than the experimental data by less than a factor of two. It should be noted that the pre-exponential factor evaluated in this work is temperature-dependent, and that the rate coefficients calculated in the range of temperatures of the SP-PLP-EPR analysis (273-333 K) using both computational and experimental rate parameters show a difference of about a factor of three.

Table 15. *Calculated values of reaction enthalpy, activation energy, pre-exponential factor, and rate coefficient for propagation of mid-chain radical, propagation and 1:5 backbiting of short-branch radical, and β-scission reactions involving poly (butyl acrylate) radicals according to the complete molecular model. Rate constants and kinetic parameters are calculated at 298 K.*

Reaction		$Log_{10}(A)$	E_a	$Log_{10}(A)$	k
			$kJ \, mol^{-1}$		$L \, mol^{-1} \, s^{-1} \, or \, s^{-1}$
Propagation of MCR	$k_{p,MCR}$	-79.2	7.9	2.643	$1.82 \ 10^1$
Propagation of SBR	$k_{p,SBR}$	-96.3	20.2	5.069	$3.32 \ 10^1$
1:5 backbiting of SBR	$k_{bb1:5,SBR}$	-1.9	54.6	12.566	$1.85 \ 10^4$
	$k_{bb5:1,SBR}$	1.9	55.3	12.378	$8.92 \ 10^3$
β-scission	$k_{\beta S}$	114.0	116.9	12.460	$9.22 \ 10^{-9}$

A key parameter in the determination of the branching density is represented by the ratio of MCR propagation rate constant to that of chain-end radical propagation. Adopting the rate parameters calculated in this work, a value of 0.4% is obtained at 298 K for this ratio, whereas the experimental ratio under the same conditions is six times smaller. Despite the approximations in the computational approach (i.e., the choice of applying the HO model and the limited number of BA units that were permitted to be considered at this theoretical level), as well as the known level of inaccuracy intrinsic to the method, this result is quite satisfactory. Because of the propagation of MCR, the newly formed chain-end radical near a tertiary carbon is supposed to exhibit reactivity that is intermediate between that of a linear chain-end radical and that of an MCR.

With the aim of verifying this hypothesis, both propagation and 1:5 backbiting reactions of the formed SBR have been investigated, as detailed in **Table 15**. The SBR adds monomer slightly faster than an MCR, though it is not as effective as the linear chain-end radical. According to what has been proposed in a previous work,[122] it is expected that from the third monomer addition step on the MCR the propagation rate constant will approach the value of chain-end propagation. On the contrary, 1:5 backbiting of SBR is faster than backbiting of a linear chain-end radical by one order of magnitude. While the activation energy values are very close, the former reaction exhibits a larger pre-exponential factor that is in agreement with a configuration of the

reactant that is closer to that of the transition state. The backward 5:1 shift also takes place faster than that of a linear chain, because of a smaller activation energy reflecting the fact that the SBR is close enough to the branching point to feel the stabilizing effect of the tertiary carbon. As a further confirmation of this result, the enthalpy change of the backbiting reaction under investigation is found to be close to the zero value of internal backbiting, which is known to involve only MCRs.

Based on these results, comparisons have been made between the ratios of backbiting to propagation rate constants, with reference to the reactions involving chain-end radicals, MCRs, and SBRs. In the first case, the 1:5 backbiting rate constant of chain-end radical is 39% of the chain-end radical propagation rate coefficient. This ratio is greater than the value calculated using the experimental rate coefficients, for the reasons previously discussed. As far as MCRs are concerned, the 5:9 backbiting rate constant is 89% of the corresponding propagation rate coefficient. The rate constant ratio here is increases by a factor of two in comparison to the previous case, thus implying that both reaction kinetic mechanisms are slowed down almost to the same extent in terms of degrees of magnitude when moving from chain-end to mid-chain radicals. However, it is surprising to notice that the ratio between the reaction rate coefficients involving SBRs is three orders of magnitude greater than the previous values, suggesting that this type of radical is far more likely to backbite than to propagate, even if considering a bulk monomer concentration. For these reasons, 1:5 backbiting of SBR is proposed in this work as a relevant mechanism of intramolecular hydrogen transfer leading to the formation of short-chain branches.

At last, β-scission reaction of an MCR made up of four BA units has been studied, and the investigation of the secondary reactions that may involve MCRs has been finalized. The result reported in **Table 15** clearly shows how this reaction is negligible almost at the same extent of the greatly strained 1:3 backbiting reaction at 298°C. The transition state structures of the reactions investigated with the complete molecular model are reported in **Figure 20**.
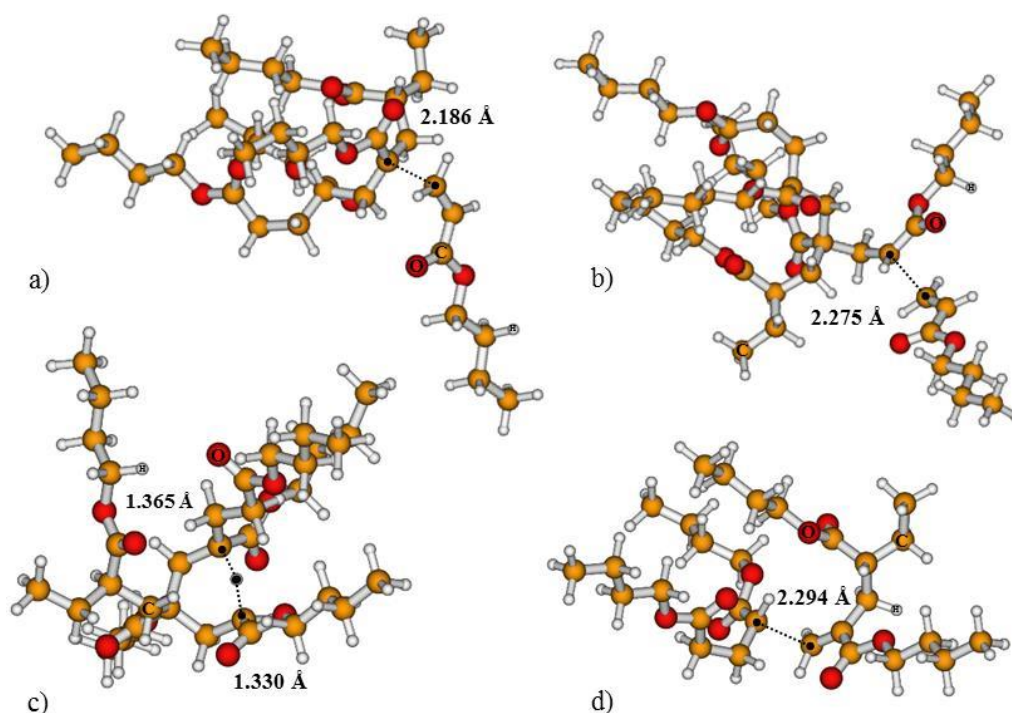
Figure 20. *Optimized geometries of the transition state structures relative to the secondary reactions involving poly (butyl acrylate) chains investigated with the complete molecular model. Reactions of: a) propagation of mid-chain radical; b) propagation of short-branch radical; c) 1:5 backbiting of short-branch radical; d) β-scission.*

4.4.3. Conclusion

A detailed quantum chemistry investigation of secondary reactions active in the FRP of BA has been carried out, with special focus on backbiting and propagation of MCRs. Various backbiting steps have been investigated by adopting a simplified molecular model in order to describe the long polymer chains. In particular, the $j:j\pm4$ hydrogen shifts involving the formation of relatively stable transition state rings have been characterized. It has been shown that a radical migration along the backbone may occur through a series of these fast backbiting reactions rather than by $1:j$ intramolecular transfers of the radical from the chain-end to an internal position.

Moreover, a novel backbiting reaction from the SBR produced after MCR propagation has been analyzed. This 1:5 hydrogen shift has turned out to be more favorable than the 1:5 backbiting reaction involving linear chain-end radicals, because the geometry of the reactant is closer to the configuration of the transition state. Reaction kinetics of MCR propagation has also been characterized, along with the determination of the rate coefficients of the consecutive monomer additions on the newly formed SBR. Backbiting has been found to be more competitive with propagation when moving from chain-end to mid-chain radicals and is, by far, the most relevant reaction with regard to SBR.[123]

——————————————— ——————————— ———————— ————— ————— — —

CHAPTER 5

——————————————— ——————————— ———————— ————— ————— — —

Pushing toward Prediction

——————————————— ——————————— ———————— ————— ————— — —

5.1. Summary

Quantum chemistry has been applied to the investigation of acrylate-based systems in order to study the kinetics of challenging reactions that are not directly observable by experiments. In the first part of this chapter, the attention has been focused on relevant secondary reactions active in copolymers. To this end, a terpolymer system composed by MA, MMA, and St monomer units has been adopted in order to examine the effect of copolymer composition on the kinetics of backbiting, propagation, and β-scission steps. The physicochemical behavior of different radical species with respect to the investigated reactions has been determined, providing the estimation of a large number of kinetic parameters.

Afterwards, reactions of atom transfer from PBA active chains to various CTAs have been investigated, with the aim of shedding light on their features when radicals of various nature and size are involved. Particularly, the different reactivity of chain-end and mid-chain radicals with respect to the chain transfer reaction has been discussed, taking into account CTAs representative of the common classes of halocarbons and thiols. The results have led to a deeper understanding of the mechanism of MCR patching by the action of CTAs in the context of branching in acrylate polymerization.

5.2. Secondary Reactions in Acrylic Copolymers

Recently, increasing attention is being focused on the influence of secondary reactions on the free radical polymerization features as well as on the properties and microstructure of the final polymer, particularly in the context of acrylate copolymers. One of the most challenging aspects of this research is the accurate determination of the corresponding reaction kinetics. In this paper, this problem is addressed using quantum chemistry. The reaction rate coefficients of various backbiting, propagation, and β-scission steps are estimated considering different chain configurations of a terpolymer system composed of methyl acrylate, styrene, and methyl methacrylate. The results clarify the different physicochemical behavior of chain-end, mid-chain, and short-branch radicals. The estimated kinetic parameters provide new insights into free radical polymerization kinetics, and they can be used to predict relative radical stability and reactivity for the different radical chain configurations considered.

5.2.1. Introduction

The industrial and commercial relevance of poly (acrylates) and their large production worldwide reflect the wide applicability of these materials. Acrylate-based polymers are primarily used for surface treatments (e.g., coatings, films, latex paints and pigments), biomedical applications (e.g., drug delivery systems and biocompatible adhesives), and additives for processing (e.g., thickeners, flocculants, binding and plasticizing agents). Moreover, acrylate-based polymers are employed in the manufacture of a large variety of materials that display remarkable performance characteristics (e.g., synthetic rubbers and fibers, glues, and acrylic glass) because of their breakage resistance and elasticity. Poly (acrylates) are primarily produced by FRP, and a large set of acrylic esters with different functionalities can be combined with themselves or other vinyl monomers (e.g., St, methacrylates, vinyl chloride, and fluorinated monomers) to obtain high-performance copolymer formulations. The copolymerization of acrylic monomers with St for the manufacture of automotive coatings belongs in this context.[160]

The polymerization behavior of acrylic compounds can differ significantly from the ideal because of the demonstrated effect of backbiting and other secondary reactions. In this regard, not only is the polymerization process affected but also the investigation of the reaction kinetics can be subject to the interference of the intramolecular chain transfer.[26, 28] Particularly critical cases include high-temperature processes, such as those performed to obtain low-molecular weight resins and oligomers.[11, 23] Moreover, a close correlation has been observed between the peculiarity of the most relevant secondary steps and certain features of the resulting polymer, such as the degree of branching and the formation of gel fractions.[8, 21, 22]

The importance of investigating the kinetics of secondary reactions and the determination of their rate coefficients has recently become evident.[2] The development of PLP analysis has resulted in numerous attempts to estimate accurate rate coefficients for reactions that involve or form MCRs. Interesting results have been obtained, particularly for BA.[8, 13, 14, 31] Moreover, the computational study of polymerization kinetics using quantum chemistry has facilitated the in-depth investigation of the kinetics of specific steps of the secondary reactions of acrylic polymers in addition to polymerization systems not yet examined using the experimental PLP analysis.[51-54, 121, 123]

Most previous studies on secondary reactions in acrylate polymerization have only focused on homopolymer systems. However, it is interesting to consider the secondary steps that are active in copolymer formulations. Several studies on acrylate copolymer systems at high temperature have been performed, in particular concerning the polymerization of BA and St.[23, 160, 161] Under these polymerization conditions, the activity of the MCRs of PBA is enhanced, whereas their kinetics is likely to be affected by the presence of a St monomer and by St units in the chains. Moreover, β-scission reactions originate a significant portion of polymer chains with terminal double bonds, which act as macromonomers with respect to further initiation reactions. Other studies have been conducted on BA-St copolymerization at low temperature and noted the effect of a decrease in the polymerization rate and the gel content as a result of the presence of St.[162-164] Kinetic modeling of terpolymer resins that include methacrylates has been performed to determine the impact of the secondary reactions on the polymerization properties in addition to PLP studies on

estimating the composition-averaged propagation rate coefficient.[165, 166] Furthermore, Monte Carlo simulations have been recently used to investigate the kinetic behavior of acrylic functional copolymers to correlate the secondary reaction kinetics with the polymer microstructure and composition.[167]

Despite these attempts to accurately model copolymerization features, the detailed evaluation of secondary reaction kinetics and MCR reactivity are complicated if the additional parameter of copolymer composition is considered. For instance, in the case of backbiting, the probability of a radical shift along the backbone is likely to be affected not only by the nature of the radicals involved (i.e., chain-end or mid-chain radicals) but also the different monomer units that may be found in the proximity of these radicals. Nevertheless, at this stage, computational tools have proven to be a useful means to overcome the limits of the experimental approach. Therefore, in this paper, a quantum chemistry approach is applied to investigate the physicochemical features of the secondary reactions kinetics in acrylic-based copolymers with a focus on the intramolecular chain-transfer, propagation, and β-scission reactions as well as the difference in reactivity between chain-end radicals, MCRs, and SBRs.

Specifically, terpolymer chains composed of units of MA, St, and MMA are considered. MA and MMA have been selected as representative monomers of the acrylate and methacrylate families to perform simulations that adopt polymer chain models with a reasonable number of atoms. A comprehensive kinetic copolymerization scheme is presented, and the specific reaction rate coefficients are estimated using a consolidated computational procedure. This paper aims at evaluating physicochemical parameters that are not accessible using an experimental approach, but which are of substantial interest in the development of complex kinetic models of acrylate copolymerization.

A combined B3LYP/6-31G(d,p)//MPWB1K/6-31G(d,p) method is adopted in this work, while the HO model is used for the definition of the pre-exponential factors, according to the computational details described in Chapter 3.

5.2.2. Terpolymer Molecular Model

The rate coefficients of backbiting, propagation, and β-scission reactions have been estimated taking into account the polymer chains in a syndiotactic configuration, according to our previous studies (i.e., the conformation of the backbone that exhibits an intermediate kinetic behavior among the atactic configurations that are commonly obtained through FRP),[122, 123] and composed of a number of monomer units sufficient to describe the reacting system, as shown in **Figure 21**, **Figure 22**, and **Figure 23**.
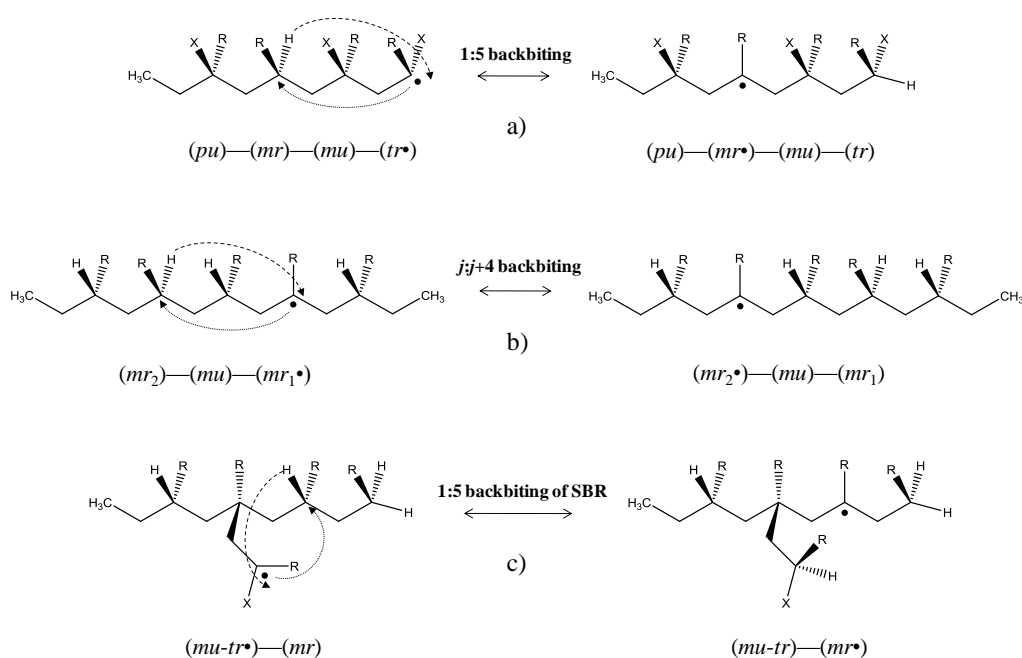
Figure 21. *Reaction schemes of the investigated backbiting steps, and detail of the replacement units.*

In the reported reaction schemes, the following notation is adopted to define the replacement units: *tr* is the terminal unit of a chain-end radical; *mr* is an MCR unit; *mu* is an intermediate unit between chain-end and mid-chain radical sites; *pu* is a penultimate unit adjacent only to one radical site; *mo* is an attaching monomer. Moreover: for MA units, *R* is $COOCH_3$ and *X* is H; for St units, *R* is C_6H_5 and *X* is H; for MMA units, *R* is $COOCH_3$ and *X* is CH_3.
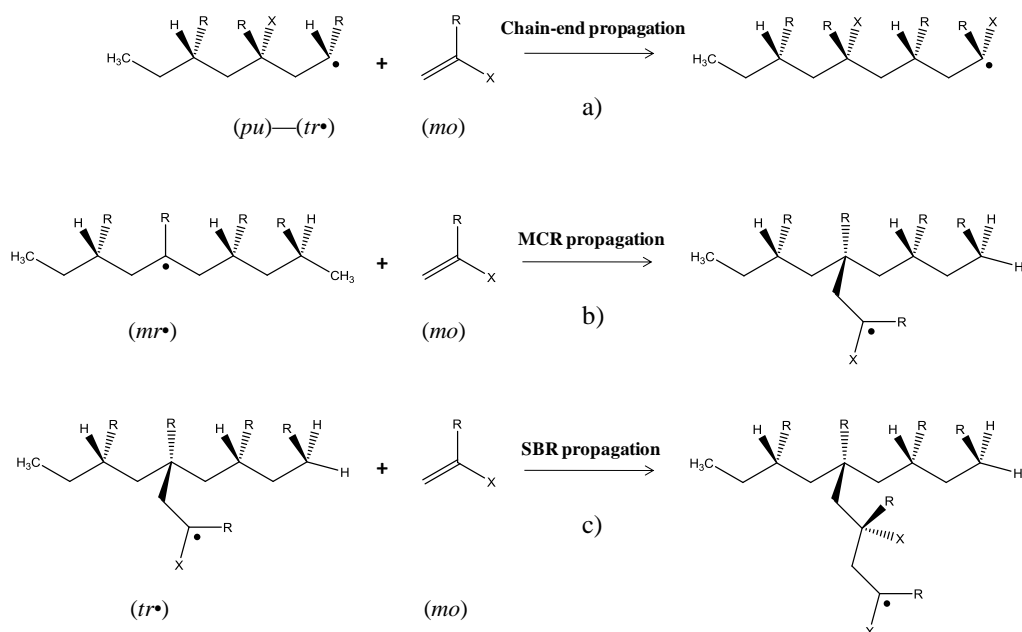
105

Figure 22. *Reaction schemes of the investigated propagation steps, and detail of the replacement units.*

Specifically, 1:5 backbiting and MCR propagation have been simulated considering linear tetramer radicals (**Figure 21a** and **Figure 22b**), whereas the reactions of backbiting and the further propagation of SBRs have been studied taking into account the pentamer branched radicals originated after the propagation of the MCRs (**Figure 21c** and **Figure 22c**). Internal $j{:}j\pm4$ backbiting and β-scission have been modeled by adopting larger suitably designed MCRs (**Figure 21b** and **Figure 23**). Finally, chain-end propagation has been studied considering linear trimer radicals (**Figure 22a**).
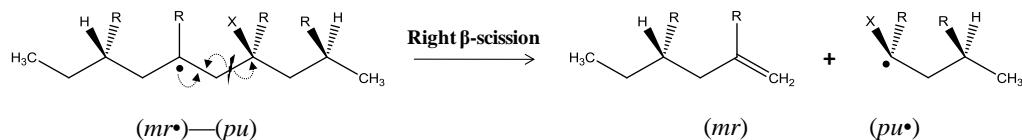
Figure 23. *Reaction scheme of the investigated β-scission steps, , and detail of the replacement units.*

As a general procedure applied to all of the kinetic steps investigated, the rate coefficients of reactions that involve poly (methyl acrylate) (PMA) homopolymer chains have been adopted as benchmark values to investigate the relative effect of the replacement units in the resulting copolymer chains. This choice was made in an attempt to provide a comprehensive estimation of the kinetic parameters for a copolymer system in which the acrylate plays a dominant role. Therefore, the effect of St and MMA comonomers has been studied with the aim of emphasizing their behavior as modifiers of the polymerization process.

5.2.3. Backbiting Kinetics and Radical Stability

The computational results for the investigated hydrogen shift reactions and the corresponding nomenclature (*A.0-A.9* for 1:5 backbiting of the chain-end radical, *B.0-B.2* for internal *j:j±4* backbiting, and *C.0-C.4* for 1:5 backbiting of SBR) are reported in **Table 16**.

For the benchmark 1:5 backbiting on the PMA homopolymer (reaction *A.0*), the obtained rate coefficient is comparable with that of PBA, according to our previous work.[123] Based on the literature, such agreement between PMA and PBA backbiting kinetics is expected.[2, 54] However, the lack of accurate experimental data specifically for the backbiting of PMA prevents a better validation of the computational result.

The first analysis of the copolymer composition effect on 1:5 backbiting kinetics has been performed by changing the terminal and mid-chain MA units, with reference to **Figure 21a**. If the terminal unit is replaced with St (reaction *A.1*), the 1:5 shift becomes two orders of magnitude slower than for the PMA homopolymer, which agrees with the greater stability of the St radical because of its resonance in the aromatic ring. A similar but stronger effect is observed for an MMA replacement unit (reaction *A.2*), where the terminal radical is now located on a less reactive tertiary carbon with respect to the secondary carbon that characterizes both MA and St terminal radical units. When the mid-chain unit is replaced by St (reaction *A.3*), the rate coefficient is again reduced compared with the benchmark reaction *A.0* (although to a shorter extent) because of the reduced tendency of the benzyl hydrogen in being

abstracted. Both effects are combined in reaction *A.4*, in which both terminal and mid-chain units are replaced with St. This reaction is characterized by a strongly decreased backbiting probability, which is comparable with that of hydrogen abstraction PS and exhibits an activation energy value that agrees with previous quantum chemistry calculations for PS 1:5 backbiting.[7]

Table 16. *Calculated values of activation energy, rate coefficient, radical equilibrium parameter, and forward (fw)-to-backward (bw) backbiting rate constant ratio for the investigated backbiting reactions. In the reaction formulas, the characters A, S, and M correspond to methyl acrylate, styrene, and methyl methacrylate units, respectively. Rate constants and parameters are evaluated at 323 K.*

Reaction		E_a	k_{bb}	ΔE^*	K_{eq}
		$kJ\ mol^{-1}$	s^{-1}		
A.0	$AAA\dot{A} \leftrightarrow A\dot{A}AA$	50.7	$4.12\ 10^3$	7.1	$1.29\ 10^2$
A.1	$AAA\dot{S} \leftrightarrow A\dot{A}AS$	68.4	$4.53\ 10^1$	-0.5	$1.21\ 10^{-2}$
A.2	$AAA\dot{M} \leftrightarrow A\dot{A}AM$	81.2	$2.19\ 10^{-1}$	-4.2	$1.78\ 10^{-3}$
A.3	$ASA\dot{A} \leftrightarrow A\dot{S}AA$	58.5	$1.60\ 10^2$	10.1	$6.05\ 10^2$
A.4	$ASA\dot{S} \leftrightarrow A\dot{S}AS$	84.9	$4.85\ 10^{-2}$	1.2	$5.25\ 10^{-2}$
A.5	$ASA\dot{M} \leftrightarrow A\dot{S}AM$	85.9	$9.62\ 10^{-3}$	-2.0	$1.22\ 10^{-3}$
A.6	$SAA\dot{A} \leftrightarrow S\dot{A}AA$	55.1	$1.81\ 10^3$	3.4	2.88
A.7	$MAA\dot{A} \leftrightarrow M\dot{A}AA$	47.9	$2.36\ 10^4$	5.9	$3.29\ 10^1$
A.8	$AAS\dot{A} \leftrightarrow A\dot{A}SA$	49.2	$2.59\ 10^3$	11.6	$1.67\ 10^2$
A.9	$AAM\dot{A} \leftrightarrow A\dot{A}MA$	50.4	$3.18\ 10^3$	4.7	$1.04\ 10^1$
B.0	$AAAA\dot{A} \leftrightarrow A\dot{A}AAA$	69.8	$1.09\ 10^1$	0.0	1.00
B.1	$AAA\dot{S}A \leftrightarrow A\dot{A}ASA$	91.6	$5.43\ 10^{-3}$	-3.8	$6.32\ 10^{-2}$
B.2	$ASA\dot{S}A \leftrightarrow A\dot{S}ASA$	101.0	$1.38\ 10^{-3}$	0.0	1.00
C.0	$A(A\dot{A})AA \leftrightarrow A(AA)\dot{A}A$	59.1	$7.44\ 10^3$	2.3	1.05
C.1	$A(A\dot{S})AA \leftrightarrow A(AS)\dot{A}A$	64.9	$7.40\ 10^1$	-9.2	$1.13\ 10^{-5}$
C.2	$A(A\dot{M})AA \leftrightarrow A(AM)\dot{A}A$	81.3	$4.53\ 10^{-1}$	-5.0	$5.70\ 10^{-4}$
C.3	$A(A\dot{A})SA \leftrightarrow A(AA)\dot{S}A$	74.7	$1.11\ 10^2$	6.9	$1.06\ 10^4$
C.4	$A(A\dot{S})SA \leftrightarrow A(AS)\dot{S}A$	99.8	$7.19\ 10^{-3}$	-3.9	$2.18\ 10^{-2}$

Eventually, the combined effects of a chain-end unit of MMA and a mid-chain unit of St, which result in the strongest decrease in the 1:5 backbiting probability, are clearly demonstrated by reaction *A.5*. The presence of St and MMA in the penultimate and intermediate unit positions slightly affects the backbiting rate coefficient. More specifically, a penultimate unit of St appears to inhibit the abstraction of the tertiary hydrogen on the nearby MA unit (reaction *A.6*), whereas an MMA penultimate unit (reaction *A.7*) enhances the rate coefficient with respect to that of the benchmark reaction *A.0*.

Previous studies noted the importance of considering the internal backbiting reaction in addition to the conventional 1:5 shift among hydrogen transfer steps that involve a six-member transition state ring.[122, 123] Reversible *j:j*±4 backbiting reactions (**Figure 21b**) have been investigated using the rate coefficient determined for PMA (reaction *B.0*) as a benchmark rate coefficient. This reaction exhibits a rate constant value that is substantially smaller than that of reaction *A.0* because the reactant is a less reactive tertiary radical and one order of magnitude smaller than the corresponding value previously calculated for PBA.[123] In reaction *B.1*, the reactant radical is on a St unit, which implies a decrease in the backbiting probability toward a tertiary MA radical with respect to reaction *B.0*. The same behavior with respect to the internal backbiting that involves PMA is observed for reaction *B.2* of the hydrogen transfer between two MCRs of St. These results are consistent with the observations reported for backbiting on terminal radicals (reactions *A.1* and *A.3*). Moreover, the activation energy value of the backbiting between two MA units requires approximately 20 kJ mol^{-1} less than the backbiting between MA and St units. This difference in activation energy is increased homogeneously up to approximately 30-35 kJ mol^{-1} in the case of backbiting between two St units.

The last series of backbiting investigated concerns the hydrogen transfer reaction that occurs on SBR (**Figure 21c**). The 1:5 shift on the branched chain-end radical of PMA (reaction *C.0*) is faster than the conventional 1:5 backbiting of a linear chain (reaction *A.0*) by nearly a factor of two. Although the activation energy value of the former reaction is higher, in that case, the backbiting probability is enhanced by the closer configuration of the reactant and transition state, which determines an increase in the pre-exponential factor, as discussed in our previous study on BA.[123]

Regarding the other investigated reactions, all of the corresponding rate coefficients are smaller than that of reaction *C.0*, which was selected as a benchmark value for the backbiting of SBR, as for 1:5 backbiting. A comparison of the rate coefficients of the backbiting of SBR with the parameters of the corresponding 1:5 shift reactions indicates that if only the terminal unit is replaced (reactions *C.1* and *C.2*) negligible changes in the activation energy are observed, whereas the rate coefficients are slightly enhanced. In contrast, for reactions *C.3* and *C.4*, in which the mid-chain unit is also modified, the energy barrier increases to a degree similar to that observed for the benchmark reaction *C.0* compared with *A.0*.

To generalize the results and classify the investigated reactions according to the relative order of reactivity, the radical stability between the reactants and the products of the investigated backbiting steps has been studied. For this purpose, a radical equilibrium parameter (*ΔE**) has been defined as in **Equation 5.1**, which considers the energy difference between the reactant and the product with reference to a forward backbiting reaction $R \rightarrow P$. Notably, *ΔE** is unaffected by the sources of inaccuracy that typically characterize the evaluation of the pre-exponential factors using quantum chemistry calculations. Thus, this parameter is well suited to determine the radical stability with good accuracy.

$$\Delta E^* = \frac{-(E_P - E_R)}{R\,T} = \frac{E_{a,bw} - E_{a,fw}}{R\,T} \tag{5.1}$$

Radical equilibrium parameters have been calculated for all of the investigated backbiting reactions, as reported in **Table 16**. A comparison of the calculated *ΔE** parameters referred to the most relevant backbiting reactions (i.e., leaving aside penultimate and intermediate unit effects) is shown in **Table 17**. In sum, a terminal unit of any monomer type is more inclined to shift the radical to an MCR of St than to an MCR of MA, whereas SBRs tend to become MCRs to a lesser extent than the corresponding chain-end radicals. Moreover, the *ΔE** values are only positive (i.e., the equilibrium is in favor of the MCR) for 1:5 backbiting from terminal units of MA and for reaction *A.4*, reproducing of the hydrogen transfer in PS. Regarding the backbiting from an MCR of MA, the radical is more likely to be shifted toward MMA than St

and, again, more likely toward St than MA. Additionally, the MCR is more likely to be transferred toward another MCR than to an SBR and, again, more likely toward an SBR than to a terminal unit. The only exception is reaction *C.1*, whose equilibrium appears to be more shifted to the terminal St unit than both the corresponding backbiting to an MCR (reaction *B.1*) and the corresponding backbiting to an SBR of MMA (reaction *C.2*). Finally, the same observations made concerning an MCR of MA can be extended to the backbiting that occurs from an MCR of St, with reference to the order of *ΔE** values reported in **Table 17**. An exception in this case is represented by reaction *C.4*. Thus, with respect to SBRs, the terminal unit of St is far more effective in stabilizing the radical and enhancing the backward backbiting reaction (reactions *C.1* and *C.4*).

Table 17. *Sequence of the calculated radical equilibrium parameters for the most relevant backbiting reactions investigated, referred to a specific radical unit. The subscript bw denotes the backward backbiting step and indicates that the corresponding ΔE* value from Table 16 must be considered with the opposite sign.*

Radical Unit	**ΔE***
Chain-end, MA	A.3 > A.0 > C.3 > C.0
Chain-end, St	A.4 > A.1 > C.4 > C.1
Chain-end, MMA	A.5 > A.2 > C.2
Mid-chain, MA	$C.1_{bw} > C.2_{bw} > A.2_{bw} > B.1_{bw} > A.1_{bw} > B.0 > C.0_{bw} > A.0_{bw}$
Mid-chain, St	$C.4_{bw} > A.5_{bw} > B.2 > A.4_{bw} > B.1 > C.3_{bw} > A.3_{bw}$

Because the prediction of radical reactivity with respect to the backbiting equilibrium has been demonstrated to agree with the physicochemical behavior of the radical species, in this work, the kinetic study has been focused on the estimation of the backbiting equilibrium constant (K_{eq}) for the investigated reactions. This parameter, which is a function of *ΔE**, is defined as the ratio of the forward to the backward backbiting rate coefficients, according to **Equation 5.2**.

$$K_{eq} = \frac{k_{bb,fw}}{k_{bb,bw}} = \frac{A_{fw}}{A_{bw}} \cdot e^{\left(\frac{E_{a,bw} - E_{a,fw}}{RT}\right)} = \frac{Q_{vib}^P \, Q_{rot}^P}{Q_{vib}^R \, Q_{rot}^R} \cdot e^{\Delta E^*} \qquad (5.2)$$

The value of K_{eq} quantifies the backbiting equilibrium and accounts for the effect of pre-exponential factors, unlike ΔE^*. Therefore, the calculated K_{eq} values can be used as additional kinetic parameters to characterize the backbiting reactions. Because these parameters are evaluated as the ratios between absolute rate coefficients, they can be considered free from certain systematic errors introduced in the pre-exponential factor that are often responsible for decreased accuracy in quantum chemistry calculations.

The equilibrium constants of 1:5 backbiting reported in **Table 16** clarify that when the terminal radical unit of MA is replaced (reactions *A.1*, *A.2*, *A.4*, and *A.5*) not only is the forward backbiting kinetics slowed but the equilibrium is also strongly shifted toward reactants, with K_{eq} values on the order of 10^{-2} to 10^{-3}. Regarding the replacement of penultimate and intermediate units, the effect is milder (reactions *A.3*, *A.6-A.9*), and although the corresponding equilibrium constant values are decreased compared with reaction *A.0*, they are still larger than one (i.e., the backbiting equilibrium continues to be shifted toward the MCR). Concerning internal backbiting, reaction *B.1* follows the behavior of the corresponding 1:5 shift (reaction *A.1*) even if the forward and backward rate coefficients are considerably slowed because of MCR involvement. Finally, for SBRs, the stabilizing effect on the chain-end radical that results from the nearby branch and the corresponding enhancement of the backward reaction rate are reflected in a global shift of the equilibrium toward the reactant compared with the corresponding kinetics of 1:5 backbiting. The only exception is reaction *C.3*, in which the presence of an MCR on an St unit strongly decreases the backward shift.

5.2.4. Propagation and β-Scission Results

Kinetic parameters and rate constants for all of the investigated propagation reactions along with the corresponding nomenclature (*D.0-D.6* for the propagation from a chain-end radical, *E.0-E.4* for the propagation from an MCR, and *F.0-F.5* for the propagation from an SBR) are reported in **Table 18**. The effect of the polymer composition on the propagation probability was studied by replacing chain-end and mid-chain radical units, the attaching monomer, and the penultimate unit (**Figure 22**).

Table 18. *Calculated values of activation energy, pre-exponential factor, and rate coefficient for the investigated propagation reactions. In the reaction formulas, the characters A, S, and M correspond to methyl acrylate, styrene, and methyl methacrylate units, respectively. Rate constants and parameters are evaluated at 323 K.*

Reaction		E_a	A	k_p
		$kJ\ mol^{-1}$	$L\ mol^{-1}\ s^{-1}$	$L\ mol^{-1}\ s^{-1}$
D.0	$A\dot{A}A + mo_A \rightarrow AAA\dot{A}$	14.9	$3.42\ 10^5$	$1.35\ 10^3$
D.1	$AA\dot{S} + mo_A \rightarrow AAS\dot{A}$	28.8	$3.49\ 10^5$	7.61
D.2	$AA\dot{A} + mo_S \rightarrow AAA\dot{S}$	7.5	$1.94\ 10^4$	$1.19\ 10^3$
D.3	$AA\dot{S} + mo_S \rightarrow AAS\dot{S}$	28.2	$1.89\ 10^5$	5.30
D.4	$AA\dot{A} + mo_M \rightarrow AAA\dot{M}$	9.7	$1.62\ 10^5$	$4.39\ 10^3$
D.5	$AS\dot{A} + mo_A \rightarrow ASA\dot{A}$	16.0	$4.40\ 10^5$	$1.14\ 10^3$
D.6	$AM\dot{A} + mo_A \rightarrow AMA\dot{A}$	10.0	$6.43\ 10^4$	$1.53\ 10^3$
E.0	$A\dot{A}AA + mo_A \rightarrow A(A\dot{A})AA$	17.3	$1.30\ 10^4$	$2.08\ 10^1$
E.1	$A\dot{S}AA + mo_A \rightarrow A(S\dot{A})AA$	36.8	$6.40\ 10^4$	$7.27\ 10^{-2}$
E.2	$A\dot{A}AA + mo_S \rightarrow A(A\dot{S})AA$	16.2	$5.25\ 10^3$	$1.25\ 10^1$
E.3	$A\dot{S}AA + mo_S \rightarrow A(S\dot{S})AA$	39.0	$3.61\ 10^4$	$1.78\ 10^{-2}$
E.4	$A\dot{A}AA + mo_M \rightarrow A(A\dot{M})AA$	19.9	$9.14\ 10^3$	5.63
F.0	$A(A\dot{A})AA + mo_A \rightarrow A(AA\dot{A})AA$	16.0	$5.63\ 10^5$	$1.46\ 10^3$
F.1	$A(A\dot{S})AA + mo_A \rightarrow A(AS\dot{A})AA$	30.8	$1.03\ 10^5$	1.07
F.2	$A(A\dot{A})AA + mo_S \rightarrow A(AA\dot{S})AA$	16.0	$3.19\ 10^5$	$8.27\ 10^2$
F.3	$A(A\dot{S})AA + mo_S \rightarrow A(AS\dot{S})AA$	38.4	$8.49\ 10^4$	$5.29\ 10^{-2}$
F.4	$A(A\dot{A})AA + mo_M \rightarrow A(AA\dot{M})AA$	11.6	$2.02\ 10^5$	$2.70\ 10^3$
F.5	$A(A\dot{M})AA + mo_A \rightarrow A(AM\dot{A})AA$	23.9	$7.96\ 10^4$	$1.09\ 10^1$

First, the chain-end propagation reaction of the PMA homopolymer has been examined, with reference to **Figure 22a**. The obtained rate coefficient (reaction *D.0*) is one order of magnitude smaller than the experimental data.[168] The underestimation of the propagation rate coefficient is primarily the result of uncertainty in the determination of the pre-exponential factor, according to what has been observed for BA.[123] A radical unit of St in place of MA decreases the rate constant value by approximately two orders of magnitude (reaction *D.1*), whereas the effect on the rate coefficient of the replacement of the attaching MA monomer with St (reactions *D.2* and *D.3*) is nearly negligible. The ratio between the experimental values of the

propagation rate constants of MA and St is approximately a hundred,[168, 169] which is only a factor of two smaller than the ratio between the computational values calculated in this paper ($k_{p,D.0}$ / $k_{p,D.3}$). This result confirms that a systematic error is largely responsible for the underestimation of the single propagation rate coefficients, whereas the estimation error is decreased for the rate constant ratios.[43, 45, 46, 122, 123] By replacing the attaching monomer unit with MMA (*D.4*) and the penultimate unit with St or MMA (reactions *D.5* and *D.6*), significant effects on the propagation rate coefficient with respect to the benchmark MA propagation are not observed. Among all of the propagation reactions that involve an MA radical, those steps characterized by a replacement monomer unit (reactions *D.2* and *D.4*) exhibit decreased activation energy values because of the larger electron density in the double bond of St and MMA compared with MA. Regarding penultimate units (reactions *D.5* and *D.6*), while an St replacement unit determines a decrease in the propagation rate coefficient, an MMA unit has the opposite effect. This different behavior of the two monomers with respect to the reactivity of the adjacent reacting site agrees with the conclusion regarding the penultimate unit effect on 1:5 backbiting, in which the rate coefficient with respect to a PMA chain was increased by an MMA penultimate unit but decreased by an St penultimate unit.

The propagation of an MCR of MA is two orders of magnitude slower than that of the corresponding chain-end radical, and the rate coefficient of reaction *E.0* is close to that obtained for BA.[123] Based on **Figure 22b**, St and MMA replacement units change the MCR propagation rate coefficient homogeneously in the same way that they affect the chain-end radical propagation, although the effects are more strongly focused on the reduction of the rate constant value compared with the benchmark MA propagation (reaction *E.0*). The ratios of $k_{p,E.i}$ to $k_{p,E.0}$ (where *E.i* refers to an MCR propagation reaction with generic replacement units) are globally smaller than those of the corresponding chain-end propagation reactions (i.e., the ratios of $k_{p,D.i}$ to $k_{p,D.0}$, where *D.i* refers to a generic chain-end propagation among the reactions investigated), indicating that the stabilizing effect of replacement units on the MCR reactivity is more effective than on chain-end radicals. Moreover, as long as MCRs are involved, a replacement monomer unit does not affect the activation energy of the propagation of the MCRs (reactions *E.2* and *E.4*).

114

In the last set of propagation reactions studied (*F.0-F.5*), the reactivity of the SBRs has been investigated to understand how the replacement units affect the tendency of the propagation rate constant to approach the chain-end propagation value as the propagating MCR is converted into a chain-end radical. With reference to **Figure 22c**, the SBR propagation of the MA homopolymer (reaction *F.0*) immediately reaches the chain-end propagation value. This process can be generalized to all of the propagation steps that involve an MA propagating unit (reactions *F.2* and *F.4*). However, if the chain-end radical is an St or MMA unit (reactions *F.1*, *F.3*, and *F.5*), the propagation rate constant is still smaller than that of a chain-end radical by at least one order of magnitude. Nevertheless, in these cases, it is expected that the propagation rate coefficient approaches the value of the corresponding chain-end radicals starting from the third monomer addition step from an MCR.[122]

Finally, the reaction kinetics of the β-scission steps that occur from MCRs has been investigated. The obtained rate constants, parameters, and the corresponding nomenclature (G.0-G.5) are reported in **Table 19**. The replacement units of St and MMA are selected to investigate different compositions of the MCR and the resulting products, with reference to **Figure 23**.

Table 19. *Calculated values of activation energy, pre-exponential factor, and rate coefficient for the investigated β-scission reactions. In the reaction formulas, the characters A, S, and M correspond to methyl acrylate, styrene, and methyl methacrylate units, respectively, whereas the superscript DB identifies a terminal double bond. Rate constants and parameters are evaluated at 323 K.*

Reaction		E_a	A	$k_{\beta S}$
		$kJ\ mol^{-1}$	s^{-1}	s^{-1}
G.0	$A\dot{A}AA \rightarrow AA^{DB} + A\dot{A}$	115.6	$1.02\ 10^{14}$	$2.09\ 10^{-5}$
G.1	$A\dot{S}AA \rightarrow AS^{DB} + A\dot{A}$	115.9	$1.37\ 10^{13}$	$2.51\ 10^{-6}$
G.2	$A\dot{A}SA \rightarrow AA^{DB} + A\dot{S}$	119.0	$1.75\ 10^{13}$	$9.80\ 10^{-7}$
G.3	$A\dot{S}SA \rightarrow AS^{DB} + A\dot{S}$	128.4	$1.28\ 10^{13}$	$2.24\ 10^{-8}$
G.4	$A\dot{A}MA \rightarrow AA^{DB} + A\dot{M}$	104.4	$4.43\ 10^{12}$	$5.74\ 10^{-5}$
G.5	$A\dot{S}MA \rightarrow AS^{DB} + A\dot{M}$	109.8	$2.26\ 10^{13}$	$3.91\ 10^{-5}$

Because right and left β-scission reactions exhibit nearly the same activation energy if the MCR is sufficiently far from the chain-end, the composition of the reactants was changed to cover all of the desired chain configurations, whereas, in agreement with results reported in the literature, only right β-scission reactions are investigated.[7, 123] The benchmark reaction *G.0* exhibits an activation energy value that is comparable with that of BA, whereas a difference in the pre-exponential factor results in a β-scission rate coefficient that is larger than that of BA by two orders of magnitude.[123] Regarding other reactions in which the MA units are replaced with St or MMA in the intermediate and penultimate positions, the pre-exponential factor is decreased by at least one order of magnitude. By replacing one of these units with St (reactions *G.1* and *G.2*), the activation energy value is not affected compared with reaction *G.0*. In contrast, by replacing both units of St (reaction *G.3*), the activation energy value increases, which results in a rate coefficient that is smaller than that of PMA by three orders of magnitude. Finally, if the penultimate unit is MMA (reactions *G.4* and *G.5*), the activation energy is decreased. Thus, the corresponding rate coefficient value is increased compared with the benchmark reaction *G.0*. In the latter cases, the presence of a penultimate unit of MMA in addition to the MCR appears to be responsible for the enhanced β-scission probability, which agrees with the penultimate unit effect observed for the backbiting process and the propagation kinetics.

5.2.5. Conclusion

With reference to an acrylate-based terpolymer system, various secondary reactions have been investigated using a computational method based on quantum chemistry. Backbiting, propagation, and β-scission reactions have been examined with respect to differences in the nature of the radicals. Starting with PMA, the physicochemical behavior of active terpolymer chains in which relevant MA units (i.e., the chain-end and mid-chain radical sites, the penultimate unit, the intermediate unit, and the attaching monomer) were replaced with St and MMA has been investigated.

Both St and MMA radicals were found to decrease the backbiting probability with respect to MA because of an increase in the radical stability and a strengthening of the C-H bond on the tertiary carbon. The replacement of units adjacent to the radical sites causes slight deviations from the benchmark backbiting rate coefficient of PMA, although St and MMA have opposite effects if the penultimate unit effect is considered. For internal backbiting and backbiting on SBR, the composition effect on the reaction kinetics is comparable with that observed for 1:5 backbiting. Copolymer composition was also demonstrated to affect the competition between forward and backward backbiting, in which radicals on the St and MMA units result in a shift of the equilibrium toward reactants.

The propagation reactions appeared to be primarily affected by changing the chain-end radical unit, whereas other composition effects are nearly negligible. The reaction rate coefficients of the MCR propagation are homogeneously decreased with respect to chain-end radicals. However, the effects of the replacement units were demonstrated to be more effective on MCR reactivity. Regarding SBRs, the propagation rates attain values determined for chain-end radicals if the terminal unit is MA. In other cases, a stronger chain-length effect was found.

Finally, the rate coefficients of β-scission reactions were found to be homogeneously decreased by replacing MA units with St and MMA as a result of a decrease in the corresponding pre-exponential factors. Particularly, the β-scission kinetics appeared to be affected primarily by the presence of penultimate MMA units, which determines and enhances the rate coefficient.

All of the reported results could be used to describe the physicochemical behavior of the secondary reaction active in acrylate-based copolymerization, providing that reasonable kinetic predictions could be made a priori. Calculated rate coefficients could be adopted as a reliable first source of parameters for a detailed description of the investigated terpolymer system to characterize the kinetics of various secondary reaction pathways in the context of acrylate-based copolymerization modeling.

5.3. Chain Transfer to Agent Kinetics

Reactions of chain transfer to agent are conventionally used to regulate the polymer molecular weight during radical polymerization processes, due to the interaction between CTAs and chain-end growing radicals. In acrylate polymerization, the presence of a large amount of MCRs opens the way for alternative kinetic pathways involving CTAs, which can result in a modification of the overall kinetics as well as the final polymer properties. In this work, chain transfer reactions from BA radicals of various size and nature to a set of selected CTAs are investigated using quantum chemistry. The different reactivity of chain-end and mid-chain radicals is emphasized, with particular focus on the kinetic effect of the radical chain length. Eventually, the mechanism of MCR patching and its relevance in decreasing the branching density are critically examined, with reference to the estimated kinetic parameters and experimental evidences about BA polymerization.

5.3.1. Introduction

One of the primary parameters determining the physical properties of macromolecular compounds is the polymer chain length, which is generally defined by the MWD along with its average properties. In a conventional reaction scheme of chain-growth polymerization, these basic features are mainly regulated by the relative extent of propagation and termination events, under the assumption of a steady-state behavior characterizing the active species. However, a premature termination of the growing chains may occur due to secondary mechanism of chain transfer, therefore leading to a reduction or modification of the polymer MWD and its average properties with respect to the expected values.[1]

In FRP, the propagation of a radical chain can be arrested by the conventional events of bimolecular termination by coupling or disproportionation. Otherwise, a radical molecule can be involved in the chain transfer reaction of an atom species. This transfer event generally occurs from another molecule in the system (e.g., monomer, solvent, or a macromolecular chain), which thus becomes a radical, or even within the radical chain itself, as in the case of backbiting. The macroscopic effects of

chain transfer reactions on the polymerization features are determined mainly by the rate of the atom transfer step to the rate of re-initiation of the newly formed radical. Although chain transfer may occur from any molecule within the polymerization system itself, a CTA can be intentionally added in order to trace the molecular weight modification back to a specific contribution. In fact, through the setup of parameters such as the choice of the CTA and its relative amount, chain transfer reactions can be made the dominant stopping mechanisms of the radical chain growth.

CTAs are widely used to control the MWD during FRP, in combination with an appropriate configuration of temperature and other reaction conditions, and find wide application in emulsion processes for the production of latexes.[170, 171] Moreover, they are adopted in controlled-radical polymerization (CRP) systems, in order to have a strong control of the MWD characterized by narrow polydispersity and the possibility to produce block copolymers.[172] Among the most recent applications, CTAs have demonstrated their effectiveness in controlling the polymer chain architecture. Particularly, the formation of branches can be substantially reduced with the addition of a sufficient amount of CTA.[20]

Considering the wide range of applications of CTAs, it is highly valuable the knowledge of their reactivity, which is strongly related to their chemical structure. The most important classes of CTAs are thiols, also referred to as mercaptans, and halocarbons. What makes them extremely reactive with respect to radical molecules is the presence of a weak S-H or C-Hal bond (generally with Hal = Cl, Br, or I), which promotes the chain transfer of the hydrogen or halogen atom to a growing radical chain. The reactivity of the most common CTAs can be compared based on the relative strength of their labile bonds, while the chain transfer kinetics determined by experimental analysis are often in agreement with the theoretical predictions. However, while on the one hand the effect of the CTA on chain transfer kinetics is deducible in principles, on the other hand it is more complicated to predict the influence of the nature of the propagating radical. In this sense, the monomer species composing the radical chain as well as its chain length are supposed to give a contribution on the reaction kinetics, as like as the selected CTA, not to mention the nature of the radical carbon that is discussed hereinafter.

Recent studies have shown that MCRs can be subject to most of the reactions that usually take place on chain-end radicals, contributing to quantify the corresponding kinetics.[2, 14, 52, 122] Therefore, it is expected to have them involved also in chain transfer to agent mechanisms. Reaction kinetics of secondary steps involving MCRs is not easy to be determined, particularly as long as the investigation is aimed at evaluating rate coefficients of specific reactions. This goal is still hardly achievable at the experimental level, due to the complexity of the reaction network that allows only an indirect deduction of most rate parameters, which is usually performed through data fitting.

Otherwise, a detailed evaluation of the reaction kinetics of a wide range of chain transfer events can be more easily accessible with the use of computational methods, which allow investigating single reaction steps focusing on the active reaction site. In particular, the application of quantum chemistry methods based on the DFT to the investigation of polymerization kinetics has been extensively carried out in the past decades. This theoretical approach has been applied in the estimation of kinetic parameters of several reaction classes, more recently with a close attention on chain transfer events.[54, 122, 123] With the aim of shedding light on the peculiar chain transfer mechanism involving CTAs, a computational investigation of their reactivity is performed in this work. The investigation is focused on the reactions of ethanethiol (EtSH), tetrachloromethane (CCl_4), and tetrabromomethane (CBr_4) transfer agents abstracting from radical chains of BA of different size and nature. Specifically, a comprehensive overview of chain transfer to agent kinetics involving both chain-end and mid-chain radicals is provided, through the examination of the reactivity of common CTAs and a relevant acrylate polymer.

5.3.2. Computational Results

Reactions of atom chain transfer to the selected CTAs from radical molecules of various natures have been investigated. Specifically, a preliminary study has been carried out considering a methyl radical reactant, with the aim of testing the capability of the computational method in predicting accurate rate coefficients for relatively simple systems already characterized experimentally. Subsequently, the attention has been turned to the reactivity of a BA monomer radical. In this regard, a first discrimination between the reactivity of chain-end and mid-chain radicals has been performed. The last chain transfer reactions have been modeled considering longer PBA radicals (i.e. trimers of both types), in order to obtain a more realistic description of the reaction kinetics within the feasibility limits of the quantum chemistry approach. A summarizing picture of the reactions investigated is provided in **Figure 24**, where *R* is a $COOC_4H_9$ group and *A-X* is the CTA (with *X* = H, Cl, or Br as long as *A* stands for the fragment EtS, CCl_3, or CBr_3, respectively).
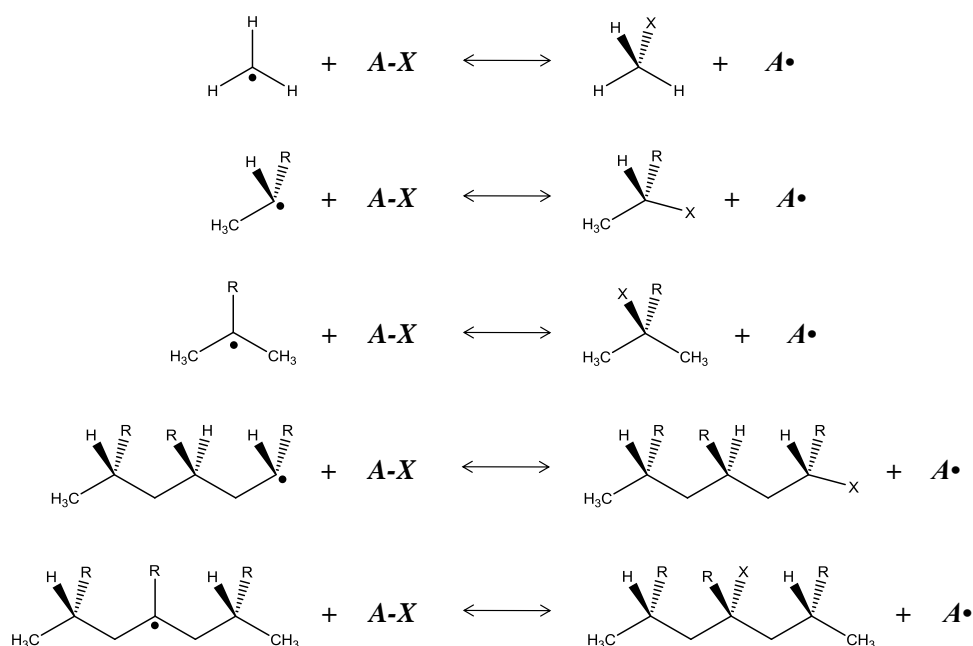
Figure 24. *Reaction schemes of the investigated chain transfer to agent steps. From top to bottom: radical transfer from a methyl radical, a monomer chain-end radical of butyl acrylate, a monomer mid-chain radical of butyl acrylate, a trimer chain-end radical butyl acrylate, and a trimer mid-chain radical of butyl acrylate.*

In the first part of this computational investigation, chain transfer reactions from a methyl radical to EtSH, CCl4, and CBr4 molecules have been studied adopting different quantum chemistry methods to perform single point calculations, while molecular structures were optimized indiscriminately at the B3LYP/6-31G(d,p) level (with the exception of the CBS-QB3 method that performs also geometry optimization). This was an attempt to check which methods are better adequate to predict the behavior of the different CTAs. Transition state configurations corresponding to the investigated reactions are shown in **Figure 25**.
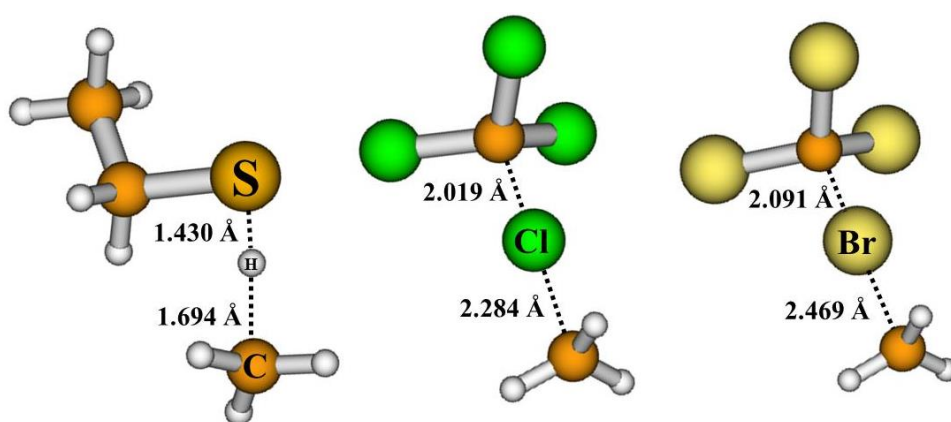
Figure 25. *Optimized geometries of the transition state structures relative to the investigated reactions of chain transfer to agent involving a methyl radical. From left to right: chain transfer to ethanethiol, tetrachloromethane, and tetrabromomethane.*

Focusing on the reaction involving the mercaptan first, and the corresponding data reported in **Table 20**, a good agreement with the experimental parameters is observed considering the results at the MPWB1K/6-31G(d,p) level. While the B3LYP alone fails in the estimation of the activation energy, the pre-exponential factor is very well predicted. Although the computationally-determined pre-exponential factor is temperature-dependent, the calculated parameter keeps within 10% of the experimental data inside the corresponding temperature range of analysis.[173] Concerning the calculations performed with the other two methods (i.e., MPWB1K/6-31G(d,p) and CBS-QB3) the activation energy is overestimated by 4-5 kJ mol^{-1}, which is however a range of uncertainty that is assumed reasonable for quantum chemistry calculations.[105]

Table 20. *Calculated values of quantum tunneling factor, reaction enthalpy, activation energy, pre-exponential factor, and rate coefficient for the chain transfer reaction involving ethanethiol and a methyl radical. Comparison between experimental data and estimates at different levels of theory, with reference to the computational methods adopted for single point calculations. Rate coefficients and kinetic parameters are evaluated at 323 K.*

Method	Q_{tun}	ΔH $kJ\ mol^{-1}$	E_a $kJ\ mol^{-1}$	A $L\ mol^{-1}\ s^{-1}$	k $L\ mol^{-1}\ s^{-1}$
Experimental data	-	-	9.7	$2.51\ 10^8$	$6.70\ 10^6$
B3LYP/6-31G(d,p)	1.11	-92.2	5.2	$2.50\ 10^8$	$3.98\ 10^7$
MPWB1K/6-31G(d,p)	1.12	-92.2	11.1	$2.50\ 10^8$	$4.58\ 10^6$
MPWB1K/6-311G(d,p)	1.12	-85.2	15.1	$2.50\ 10^8$	$1.02\ 10^6$
CBS-QB3	1.12	-76.0	13.2	$2.50\ 10^8$	$2.02\ 10^6$

Concerning halocarbons, the results about CCl_4 that are reported in **Table 21** lead to discussions that are similar to those concerning EtSH. In this case, the calculated pre-exponential factor is smaller than the experimental value by a factor of two, although the latter parameter is fitted on a wide range of temperatures (i.e., up to 523 K). On the other hand, the activation energy calculated at the MPWB1K/6-31G(d,p) level agrees with the experimental value,[174] whereas the estimates with the MPWB1K/6-31G(d,p) and CBS-QB3 methods are within 4 kJ mol⁻¹.

Table 21. *Calculated values of reaction enthalpy, activation energy, pre-exponential factor, and rate coefficient for the chain transfer reaction involving tetrachloromethane and a methyl radical. Comparison between experimental data and estimates at different levels of theory, with reference to the computational methods adopted for single point calculations. Rate coefficients and kinetic parameters are evaluated at 323 K.*

Method	ΔH $kJ\ mol^{-1}$	E_a $kJ\ mol^{-1}$	A $L\ mol^{-1}\ s^{-1}$	k $L\ mol^{-1}\ s^{-1}$
Experimental data	-	41.4	$1.26\ 10^9$	$2.53\ 10^2$
B3LYP/6-31G(d,p)	-89.8	25.6	$5.61\ 10^8$	$4.00\ 10^4$
MPWB1K/6-31G(d,p)	-93.7	41.5	$5.61\ 10^8$	$1.09\ 10^2$
MPWB1K/6-311G(d,p)	-86.6	45.6	$5.61\ 10^8$	$2.33\ 10^1$
CBS-QB3	-56.6	37.0	$5.61\ 10^8$	$5.75\ 10^2$

The last CTA that has been examined is CBr_4, and the corresponding results are reported in **Table 22**. Focusing on the activation energy, not only is the B3LYP clearly inadequate in predicting this parameter (i.e., a negative value of this parameter is obtained), but also the other approaches are not enough accurate. The activation energy for the reaction at issue is globally underestimated by a factor of two in the best case. However, a careful analysis shows that the pre-exponential factor is also miscalculated by two orders of magnitude in the same direction, therefore the corresponding rate coefficient results to be in a fair agreement with the experimental data as long as the MPWB1K/6-311G(d,p) and CBS-QB3 methods are concerned.[175] Moreover, considering the entire range of temperature adopted of the experimental study, the predicted rate coefficient for the reaction involving CBr_4 at the CBS-QB3 level is different from the experimental data by less than a factor of three, which is indeed an appreciable result.

Table 22. *Calculated values of reaction enthalpy, activation energy, pre-exponential factor, and rate coefficient for the chain transfer reaction involving tetrabromomethane and a methyl radical. Comparison between experimental data and estimates at different levels of theory, with reference to the computational methods adopted for single point calculations. Rate coefficients and kinetic parameters are evaluated at 323 K.*

Method	ΔH	E_a	A	k
	$kJ\ mol^{-1}$	$kJ\ mol^{-1}$	$L\ mol^{-1}\ s^{-1}$	$L\ mol^{-1}\ s^{-1}$
Experimental data	-	33.1	1.58E+11	7.02E+05
B3LYP/6-31G(d,p)	-73.9	-2.5	1.54E+09	3.83E+09
MPWB1K/6-31G(d,p)	-75.8	7.1	1.54E+09	1.08E+08
MPWB1K/6-311G(d,p)	-97.7	16.3	1.54E+09	3.57E+06
CBS-QB3	-61.5	15.5	1.54E+09	4.73E+06

Although the accuracy of the obtained rate parameters does not agree with what expected from the investigation of a relatively simple molecular system, the presence of bromine atoms can be a certain source of inaccuracy in this context, due to the high level of detail that is required in the description of large and greatly polarizable halogens. However, the choice of the best appropriate quantum chemistry

method in this work was dictated by the need of maintaining a reasonable computational feasibility adequate for treating polymer systems. To this end, the CBS-QB3 approach provides very accurate energy calculations, whereas its computing demand is still acceptable when dealing with methyl radicals but not as much reasonable with macromolecular species. Therefore, the results at the CBS-QB3 level of theory were considered as benchmark data for the discrimination among other DFT approaches that are indeed better feasible in treating polymer systems. Hence, considering that the performance of the CBS-QB3 method in the energy estimation is close to that of MPWB1K/6-311G(d,p) with reference to the results in **Table 22**, the latter approach has been selected for the characterization of CBr_4 reactivity. Otherwise, the MPWB1K/6-31G(d,p) has been considered adequate for the investigation of reactions involving CCl_4 and EtSH. In accordance with these remarks, the selected computational methods have been used for the study of the further chain transfer reactions involving larger radicals.

In the second part of the computational study, reactions of radical transfer from BA monomer radicals to the selected CTAs have been investigated, taking into account the reactivity of secondary and tertiary carbon radicals. The corresponding results are reported in **Table 23**, while the transition state configurations of the reactions at issue are shown in **Figure 26**.

Table 23. *Calculated values of tunneling factor, reaction enthalpy, activation energy, pre-exponential factor, rate coefficient, and forward-to-backward rate constant ratio for the chain transfer to agent reactions involving a monomer radical of butyl acrylate. Rate coefficients and kinetic parameters are evaluated at 323 K.*

CTA	Radical	Q_{tun}	E_a	A	k	K_{eq}
			$kJ\ mol^{-1}$	$L\ mol^{-1}\ s^{-1}$	$L\ mol^{-1}\ s^{-1}$	
EtSH	*Chain-end*	2.98	26.0	4.01E+06	7.42E+02	3.18E+05
	Mid-chain	3.64	25.1	2.81E+05	8.81E+01	1.35E+02
CCl₄	*Chain-end*	-	63.9	1.08E+07	5.08E-04	4.94E+06
	Mid-chain	-	64.6	2.64E+06	9.49E-05	5.25E+04
CBr₄	*Chain-end*	-	35.4	1.61E+07	3.03E+01	5.24E+07
	Mid-chain	-	36.1	3.92E+06	5.71E+00	1.57E+05

This study is aimed at highlighting the difference in reactivity, with respect to chain transfer reactions, between methyl radicals and true monomer units, and between the two different types of radicals in their simplest configuration. Focusing on chain-end radicals first, the presence of a monomer unit bringing the radical instead of a less stable methyl moiety reduces the chain transfer probability due to the combined increase of activation energy (by 15-22 kJ mol^{-1}) and decrease of pre-exponential factor (by about two orders of magnitude). The latter feature agrees with having a less accessible radical moiety for the atom transfer event on the monomer radical compared to the methyl radical.

Figure 26. *Optimized geometries of the transition state structures relative to the investigated reactions of chain transfer to agent involving a monomer chain-end radical (top) and a mid-chain radical (bottom) of butyl acrylate. From left to right: chain transfer to ethanethiol, tetrachloromethane, and tetrabromomethane.*

126

Considering monomer BA radicals, the differences in reactivity between chain-end and mid-chain ones are quite restrained (i.e., less than one order of magnitude between the corresponding reaction rate coefficients). This feature comes from the fact that such monomer radicals are not large enough to model accurately the different stability of secondary and tertiary carbon radicals. Moreover, the gaps between the estimated rate coefficients of the two types of radical are comparable among all of the chain transfer agents examined, despite the largely different values observed for the absolute rate constants (which range from 10^{-4} to 10^{3} L mol^{-1} s^{-1}). It is interesting to examine also the corresponding backward reaction kinetics (i.e. atom abstraction from the patched radicals). The equilibrium between chain transfer to agent reactions and the corresponding reverse steps has been investigated, leading to the definition of rate constant ratios (K_{eq}) of forward-to-backward rate coefficients, which are reported in **Table 23**. The calculated values of K_{eq} suggest that the backward steps are generally slower than the forward one, as expected. However, their competition with the forward kinetics acquires relevance when moving to MCRs.

In the last investigation, the kinetic study of chain transfer reactions involving monomer radicals has been extended to the reactivity of trimer PBA chains, in order to investigate more realistically the polymer systems at issue and better characterize the different nature of chain-end and mid-chain radicals. Transition state configurations corresponding to the investigated reactions are shown in **Figure 27**. The results reported in **Table 24** show that three monomer units defining the radical chains are sufficient to model the difference in reactivity between secondary and tertiary carbon radicals. When moving from trimer chain-end to trimer mid-chain radicals, activation energy values are increased by 9-18 kJ mol^{-1} while pre-exponential factors are reduced by one order of magnitude, with the largest difference characterizing the reactions with CBr$_4$. Concerning halocarbons, the differences between the two models (i.e., monomer versus trimer radicals) are mainly focused in the estimated rate coefficient of chain transfer involving MCRs, which are smaller considering the trimer. On the contrary, concerning EtSH, the reactivity of the chain-end radial appears to be largely affected by the chain-length model adopted than the MCR.
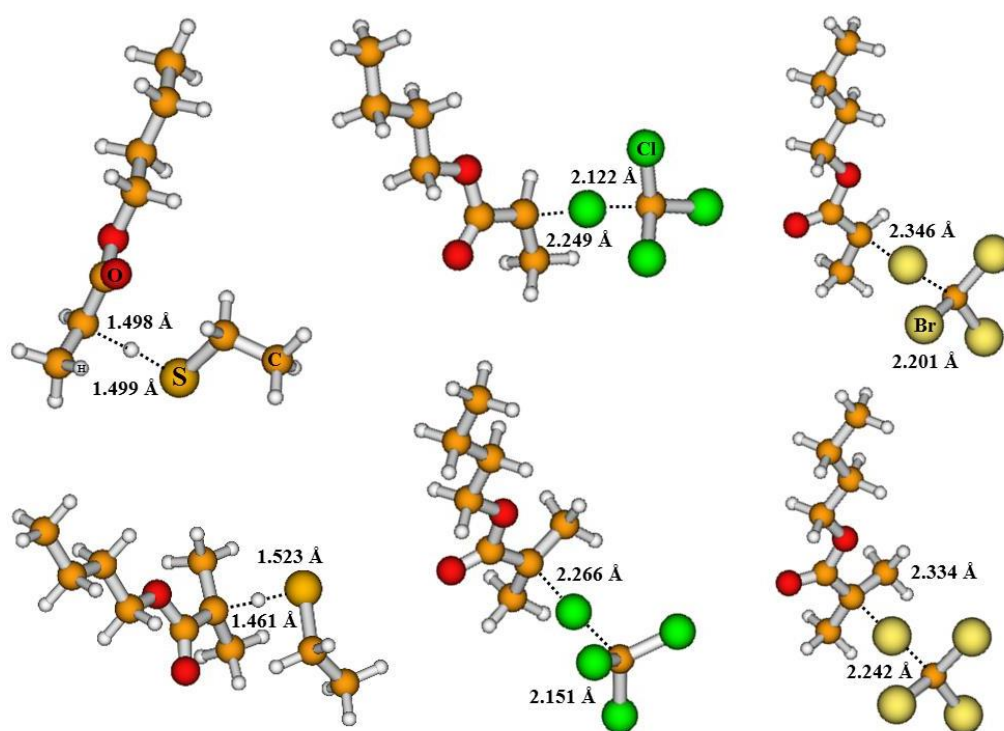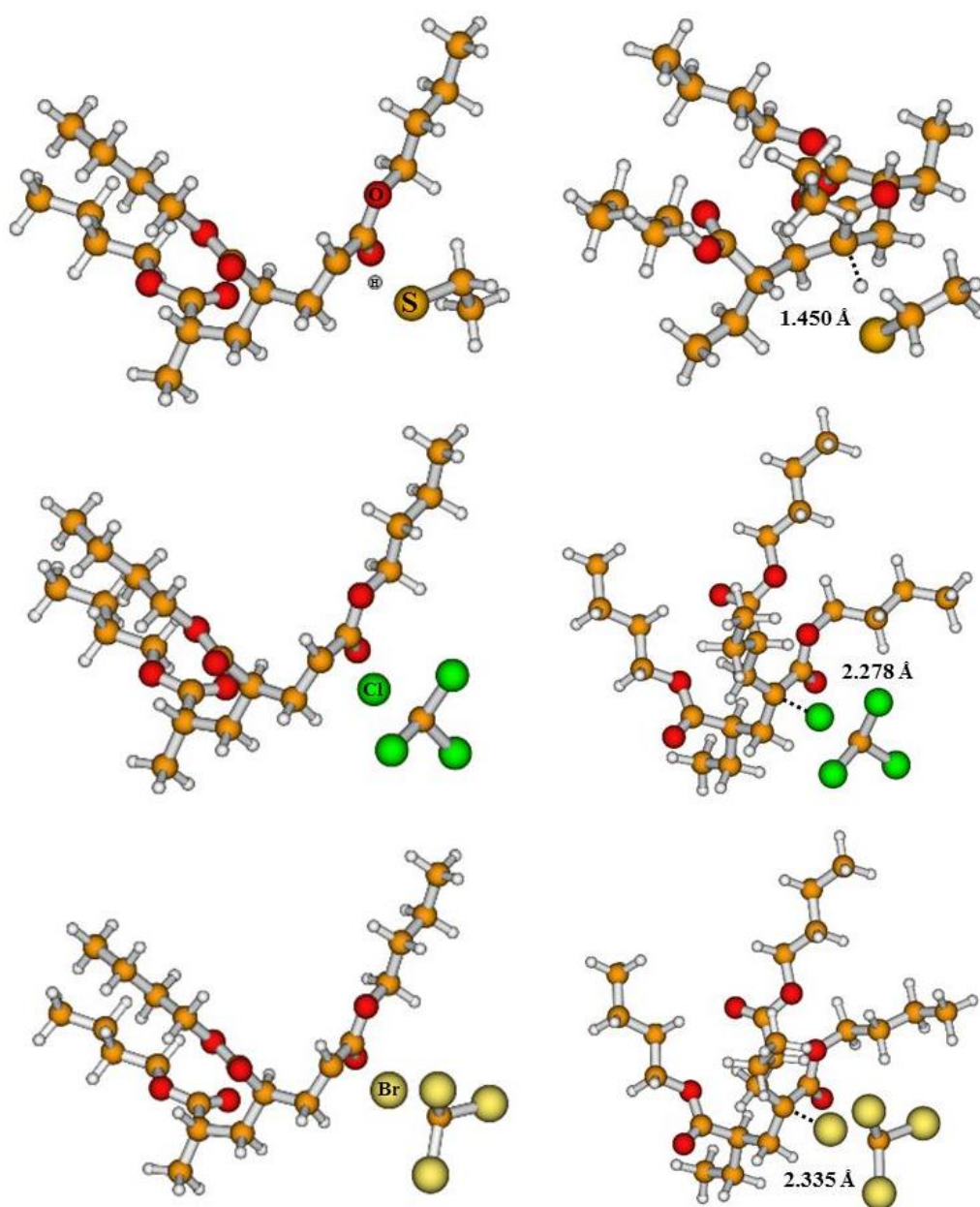
Figure 27. *Optimized geometries of the transition state structures relative to the investigated reactions of chain transfer to agent involving a trimer chain-end radical (left) and a mid-chain radical (right) of butyl acrylate. From top to bottom: chain transfer to ethanethiol, tetrachloromethane, and tetrabromomethane*.

128

Table 24. *Calculated values of tunneling factor, reaction enthalpy, activation energy, pre-exponential factor, rate coefficient, and forward-to-backward rate constant ratio for the chain transfer to agent reactions involving a trimer radical of butyl acrylate. Rate coefficients and kinetic parameters are evaluated at 323 K.*

CTA	Radical	Q_{tun}	E_a	A	k	K_{eq}
			$kJ\ mol^{-1}$	$L\ mol^{-1}\ s^{-1}$	$L\ mol^{-1}\ s^{-1}$	
$EtSH$	*Chain-end*	2.78	17.7	8.48E+05	3.25E+03	3.46E+05
	Mid-chain	4.51	27.0	2.83E+05	5.55E+01	5.88E+02
CCl_4	*Chain-end*	-	63.9	1.42E+07	6.65E-04	1.78E+07
	Mid-chain	-	73.3	3.12E+06	4.35E-06	2.97E+02
CBr_4	*Chain-end*	-	34.0	1.16E+07	3.67E+01	2.20E+08
	Mid-chain	-	51.5	5.10E+05	2.43E-03	1.64E+02

Focusing on the rate constant ratios, the behavior of EtSH and halocarbons is different when moving from the monomer to the trimer radical model. The former CTA does not appear to modify its reactivity in relation to the radical chain length. On the other hand, in the case of CCl_4 and, more dramatically, of CBr_4 the difference in K_{eq} values between the chain transfer reaction of chain-end and mid-chain radical is increased considering trimer chains (i.e., gaps are in the order of 10^5-10^6 for the trimer model). Moreover, the rate constant ratios related to trimer MCRs exhibit relatively small and quite comparable values in the order of one hundred for all of the three CTAs considered. These results suggest that the greater stability of an MCR of BA strongly reduces the efficacy of the radical patching in comparison with the chain transfer kinetics from a chain-end radical, and that this effect is quite homogeneous disregarding the selected CTA.

5.3.3. Chain Transfer to Agent and Degree of Branching

The predicted reaction rate coefficients along with the additional information of equilibrium between forward and backward reaction rates can be useful in the improving of polymerization models, providing a useful first-source of kinetic parameters that are still not experimentally determined. Moreover, the knowledge of side-reaction kinetics in the context of FRP can be helpful in the understanding of hardly observable mechanisms that are connected with some macroscopic

experimental evidences. In this regard, the proven influence of chain transfer to agent kinetics on the degree of branching in acrylate polymerization, depending on polymerization conditions and amount of CTA, takes place in a manner that is not yet clearly defined.

Recent studies on BA have shown that if a relatively large amount of CTA is added in the system (i.e., up to 0.4 mol L^{-1} in a bulk system), the degree of branching of the final polymer is considerably reduced. Particularly, it has been proposed a mechanism of MCR patching by the transferred atom of the CTA, identical to what happens commonly on chain-end radicals, which substantially prevents the MCR from further reactions. This phenomenon is in agreement with the experimental results obtained for BA polymerization in presence of 1-octanethiol, in terms of a decrease in the measured degree of branching and amount of β-scission products.[20]

Experimental investigations carried out by Aguirre et al. on a similar polymerization system but using CBr$_4$ have determined a reduced level of branching, due to the addition of CTA, which is qualitatively and in part quantitatively comparable to the result obtained in the former study. However, no C-Br structures involving tertiary carbons (i.e., as the result of chain transfer to agent from MCRs) were detected, thus in disagreement with the proposed mechanism of radical patching as the relevant contribution to the decrease in branching density. This conclusion is supported by the results shown in **Table 24**. Although MCRs may represent up to four times the amount of chain-end radicals, the reactivity of the former ones with regard to chain transfer to CBr$_4$ reaction is substantially smaller than that of the latter ones (four orders of magnitude in terms of reaction rate coefficients). Therefore, it is likely to suppose that the majority of the interaction with CBr$_4$ concerns terminal radicals rather than MCRs. Moreover, focusing on the rate coefficient values, the competition between MCR patching by bromine atoms and their propagation is strongly in favor of the latter mechanism.[14]

Moving back to the mercaptan, the evaluated kinetics of chain transfer to EtSH reported in **Table 24** is globally faster than that of CBr$_4$, with a radical patching by hydrogen atoms that is kinetically comparable with MCR propagation, though the reactivity difference between chain-end and mid-chain radicals is still conspicuous (two orders of magnitude in terms of reaction rate coefficients). Despite the

uncertainty in the estimation of absolute rate coefficients by quantum chemistry, the obtained results suggest that, concerning the mercaptan, a contribution of MCR patching to the decrease of the branching density is plausible.

However, the effectiveness of this phenomenon when using CBr_4 has contested by both experimental and computational evidences, whereas the two CTAs exhibit a very similar behavior in decreasing the branching density. Therefore, a further mechanism correlating chain transfer to agent kinetics and origination of branching ought to be considered. This effect should be investigated in the reactivity of the CTA radical fragments originated after chain transfer events, which could affect the distribution of radicals and their average kinetic behavior. Moreover, the role of the backward step of abstraction from the patched MCR and the chain transfer equilibrium in the overall kinetic scheme is to be investigated. Eventually, the dynamics of the origination of branches along with the polymerization time, with respect to the presence or absence of a CTA in the system, should be examined.

5.3.4. Conclusion

Reaction kinetics of chain transfer to agent from BA radical chains has been investigated using quantum chemistry, taking into account EtSH, CCl_4, and CBr_4 as representative CTAs of the common categories of thiols and halocarbons. First, the computational study has been focused on the selection of the best appropriate method to characterize the reactivity of the polymer chains as well as the different CTAs. For this purpose, simple reactions of chain transfer from a methyl radical have been modeled, while experimental data have been used to validate the computational approach. A good agreement has been obtained using the consolidated B3LYP/6-31G(d,p)//MPWB1K/6-31G(d,p) method for EtSH and CCl_4, while the MPWB1K/6-311G(d,p) method was required to perform sufficiently accurate single point calculations for CBr_4.

Afterwards, chain transfer reactions involving PBA radicals have been simulated discriminating the radical nature (mid-chain versus chain-end ones) as well as the polymer chain length (monomer versus trimer radicals). The results have shown that a difference in reactivity between the two types of radical is slightly perceptible

on monomer radicals and becomes significant as long as trimer chains are considered. Such difference is quite homogeneous for the different CTAs, and reveals that the radical patching is less effective on MCRs. Focusing the attention on the CTAs examined, their estimated kinetics with respect to BA radicals are quite different considering the absolute chain transfer rate coefficients but rather comparable in terms of rate constant ratios, especially as long as the reactivity of the MCRs is concerned.

The estimated kinetics of chain transfer to agent reactions have been used to shed light on the phenomenon of decrease in branching density subsequent to the addition of CTA in a bulk polymerization systems. The computational results support the experimental evidences regarding the mechanism of radical patching, which appears to have a greater relevance on thiols than on halocarbons. However, the correlation between chain transfer to agent kinetics and branching needs to be further investigated.

CHAPTER 6

Exploring the Limits

6.1. Summary

The quantum chemistry approach has proved its capability of providing satisfactorily accurate estimations of reaction rate coefficients and, with greater reliability, of kinetic constant ratios. Precisely, polymerization kinetics has been widely studied adopting simplified molecular systems, whereas an extension of the boundary of the computational study is set against the computation feasibility within the use of quantum chemistry. Nevertheless, it is possible to push the investigation up to a sort of borderline systems, in order to explore the limits of application of the DFT but still maintaining the cost-effectiveness performances of the method.

In this regard, the attention has been focused on two challenging problems. Firstly, the capability of the method in predicting the solvent effect as well as the kinetics of copolymer systems characterized by functional monomers has been tested. The quantum chemistry tool improved with the implementation of an implicit solvent model has proven to be useful in determining the qualitative behavior of copolymerization involving functional acrylic monomers in presence of polar solvents. Secondly, the research of optimized geometries of reactants, products, and transition states has been addressed, with focus on the discrimination between global and local minima structures. Torsion motions of side-chain groups have been performed on monomers and radicals involved in the propagation of an acrylic compound, in order to elucidate the impact of the different conformation energies on the rate coefficient estimations.

6.2. Functional Copolymers and Solvent Effect

Copolymerization of MMA with the functional monomers HEMA and MAA is investigated by both experimental and theoretical approaches. The effect of the reaction medium on the copolymerization behavior is studied taking into account various solvents characterized by different interaction with the functional groups of monomer and polymer molecules. The experimental results in terms of copolymer composition carried out through PLP experiments are compared with the computational data obtained using a DFT method, which is improved by the use of the IEFPCM model in order to account for an implicit solvent effect. The quantum chemistry approach reveals to be adequate for a semi-quantitative prediction of the copolymerization behavior in the presence of BuOH and DMF as well as in bulk, while it is not properly suited to describe accurately the kinetics of the process at high concentration of the functional monomer.

6.2.1. Introduction

The influence of functional groups of acrylic compounds on the kinetics of FRP has been recently highlighted in the context of propagation and backbiting reactions.[17-19, 55, 56] The presence of a polar or particularly interactive solvent can modify the kinetic behavior of the reacting moieties close to such functional groups. In principle, all acrylic compounds are sensible to intermolecular interactions that may involve their ester moieties, especially in presence of strongly polar or polarizable solvent molecules such as water. Hydrogen bonding interactions are particularly effective, and they are originated in presence of hydroxyl moieties. Nevertheless, the reactivity of acrylic monomers with strong functionality (i.e. characterized by hydroxyalkyl and carboxyl groups) can be subjected to slvation effect even in the presence of organic solvents. The critical reaction medium that may be represented by the functional monomer itself in the case of bulk polymerization belongs in this context.

With regard to copolymerization, the presence of at least one functional comonomer can be a source of uncertainty in the determination of the kinetic behavior of the system. Not only is the homopolymerization of the functional monomer likely to be affected, but also cross-propagation reactions are interested, thus the estimation of the corresponding reactivity ratios for the system at issue may result to be challenging. From the experimental point of view, a large set of trials is needed in order to characterize the kinetics of a functional copolymer system with respect to the selected reaction medium, while every additional solvent choice would require additional experimentations.

On the other hand, a computational approach can be adopted with the aim of reducing the onerousness of the experimental analysis by focusing on those reactions that primarily determine the overall polymerization kinetics, along with the definition of appropriate copolymerization models. Once proved the potentiality of quantum chemistry in the prediction of rate coefficients and reactivity ratios in the field of FRP, the computational approach based on the DFT can be a useful tool in the investigation of functional copolymerization kinetics, providing that the solvent effect is dealt with properly. In this regard, implicit solvent models represent a good compromise between computation feasibility and capability of treating the general aspects of the solvent effect.

In this work, the reactivity of two copolymer systems including functional monomers is studied. Specifically, MMA-co-HEMA and MMA-co-MAA copolymerization processes are investigated, focusing on the definition of composition plots and monomer reactivity ratios under the assumption of a terminal model. The kinetic behavior of the selected copolymer systems is studied taking into account the following configurations of the reaction medium: a bulk process, the polymerization in a polar and hydrogen bond-enhancing solvent (BuOH), and in a hydrogen bond-disrupting solvent (DMF). The problem is addressed by both experimental and computational approaches. A comparison between the obtained results is aimed at emphasizing the peculiar behavior of the functional copolymer systems in presence of representative classes of interacting solvents as well as at shedding light on the capability of the improved quantum chemistry method in predicting the solvent effect.

6.2.2. Materials and Methods

The experimental analysis has been carried out through PLP experiments. A Spectra-Physic Quanta-Ray 100 Hz Nd:YAG instrument has been used to initiate copolymerization in monomer solutions with $5\ 10^{-3}$ mol L^{-1} of 2,2-dimethoxy-2-phenylacetophenone (DMPA). Monomer conversions have been kept below 5% in order to avoid significant composition drifts. After the monomer removal by drying, polymers produced by PLP have been analyzed by ^{1}H NMR, while copolymer composition has been estimated rationing the areas of specific peaks detected in the NMR spectrum. The HEMA molar fraction in the MMA-co-HEMA copolymer has been evaluated considering the peak areas from: the hydroxyl protons of HEMA (A_H), the total protons of the methyl groups attached to the backbone (A_C) and the protons attached to the double bond of the residual HEMA monomer (A_M), as detailed in **Equation 6.1**, with reference to the ^{1}H NMR spectrum reported in **Figure 28**.

$$F_{HEMA} = \frac{A_H - A_M}{\dfrac{A_C}{3}} \tag{6.1}$$

Figure 28. *Proton-nuclear magnetic resonance spectrum of methyl methacrylate-co-2-hydroxyethyl methacrylate copolymer. Detail of the relevant peak assignment.*

The MAA molar fraction in the MMA-co-MAA copolymer has been evaluated considering the peak areas from: the methyl protons of the ester groups in the MMA copolymer units (A_A), the total methylene protons of the backbone plus the methyl protons of the residual MAA monomer plus the total protons of the methyl groups attached to the backbone (A_{B+C}), and the protons attached to the double bond of the residual MAA monomer (A_M), as detailed in **Equations 6.2-6.3**, with reference to the ^{1}H NMR spectrum reported in **Figure 29**.

$$U_{tot} = \frac{(A_{B+C} - 3A_M)}{5} \tag{6.2}$$

$$F_{MAA} = \frac{U_{tot} - \frac{A_A}{3}}{U_{tot}} \tag{6.3}$$

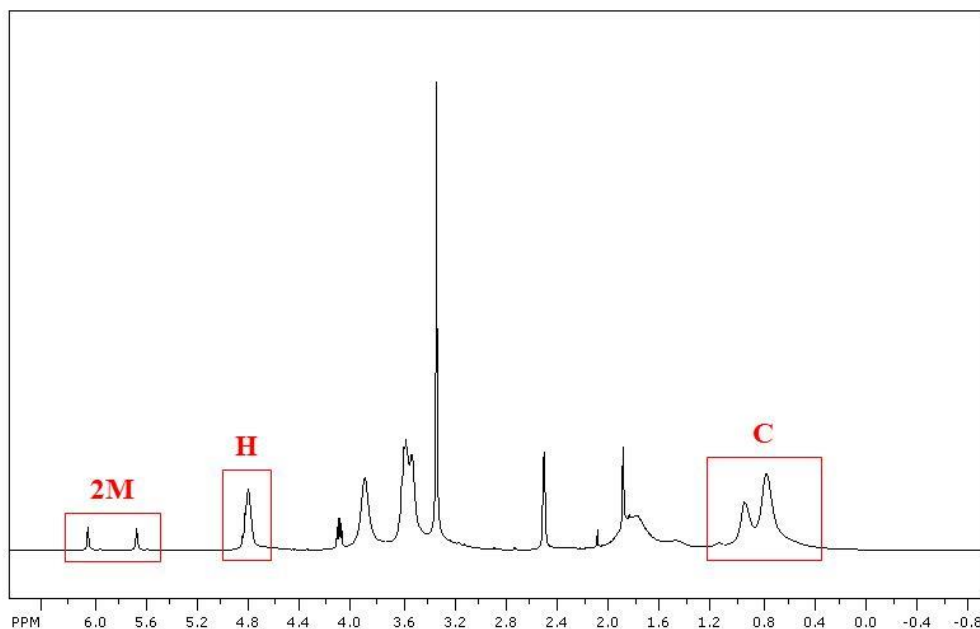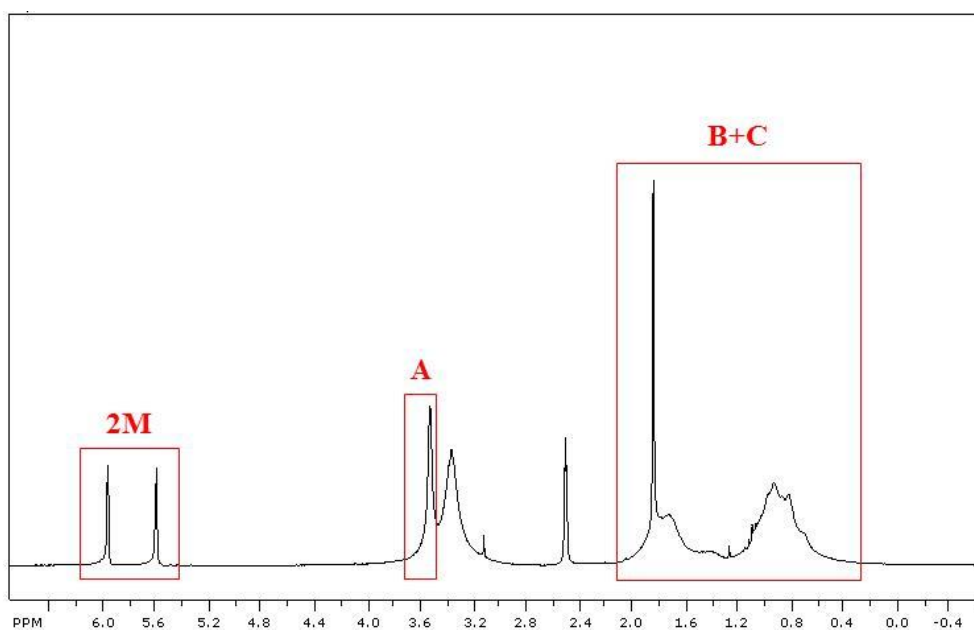**Figure 29**. *Proton-nuclear magnetic resonance spectrum of methyl methacrylate-co-methacrylic acid copolymer. Detail of the relevant peak assignment.*

In both systems, A_M has been defined under the assumption that the contribution of MMA to the residual monomer is negligible with respect to HEMA and MAA, due to the higher volatility of MMA in the sample drying step.

The computational study has consisted of DFT calculations in order to evaluate the reaction rate coefficients of homo- and cross-propagation within the selected copolymer systems. A combined B3LYP/6-31G(d,p)//MPWB1K/6-31G(d,p) approach has been adopted to estimate energy and kinetic parameters, with reference to the details provided in Chapter 3. The computational method has been improved by the use of the IEFPCM model in order to describe the implicit solvent effect.[58] Specifically, parameters of the selected solvents were defined by the use of the corresponding keywords taken from the Gaussian database, which identify the dielectric constant of each reaction medium along with a set of other internal parameters defining the solvent accessible surface, such as the solvent molecule radius.

Monomer reactivity ratios r_A and r_B have been evaluated for the investigated binary systems in agreement with the terminal model, as detailed in **Equations 6.4-6.5**. Reactivity ratios are functions of homo (k_{pii})- and cross (k_{pij})-propagation rate coefficients, where k_{pij} is referred to the addition of monomer j to a radical with terminal unit i. The computational composition plot of instantaneous copolymer fraction of monomer A (F_A) as a function of the fraction of monomer A in the $A+B$ comonomer mixture (f_A) has been obtained as detailed in **Equation 6.6**.[176]

$$r_A = \frac{k_{pAA}}{k_{pAB}} \tag{6.4}$$

$$r_B = \frac{k_{pBB}}{k_{pBA}} \tag{6.5}$$

$$F_A = \frac{r_A f_A^2 + f_A f_B}{r_A f_A^2 + 2 f_A f_B + r_B f_B^2} \tag{6.6}$$

With regard to each specific copolymer system and reaction medium, experimental data of composition have been collected and diagrammed, along with the computational composition plots obtained through **Equation 6.6**. The results concerning the two copolymer systems examined are discussed hereinafter.

6.2.3. **Methyl Methacrylate-co-2-Hydroxyethyl Methacrylate**

The copolymerization of MMA and HEMA has been studied experimentally considering a bulk reaction as well as the polymerization in a $50\%_{vol}$ DMF solution. Experimental data have been collected at 323 K from PLP reactions at 20, 33, and 50 Hz. Propagation reactions have been computationally modeled in vacuum as well as in presence of DMF and BuOH as implicit solvents at 323 K. All of the results are reported in **Figure 30**, while the estimated reactivity ratios are shown in **Table 25**.
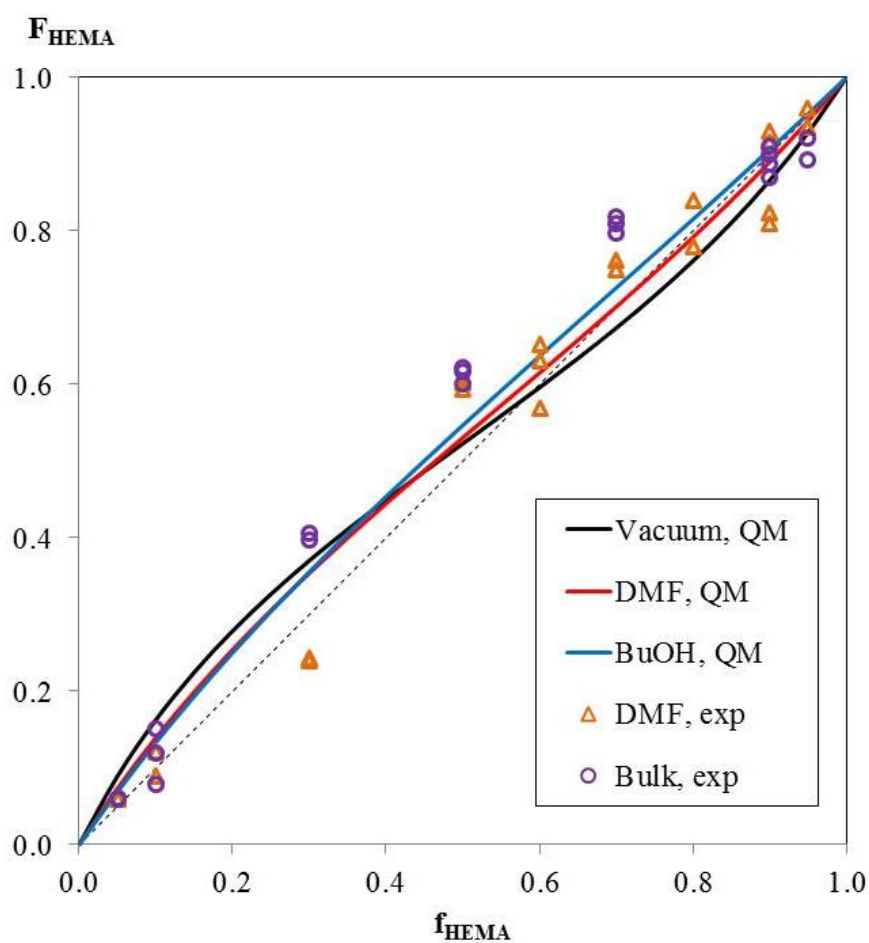

Figure 30. *Composition plots of methyl methacrylate-co-2-hydroxyethyl methacrylate copolymerization. Molar fraction of 2-hydroxyethyl methacrylate in the copolymer (F_{HEMA}) as a function of its molar fraction in the monomer mixture (f_{HEMA}). Comparison between experimental data (exp) and computational curves (QM) in various solvents.*

Focusing on the plots in **Figure 30**, the computational curve in vacuum follows the experimental data in bulk only at low HEMA monomer fraction. This result agrees with the fact that the solvent effect is likely to become relevant at higher concentration of the functional monomer in the mixture composing the reaction medium. Otherwise, at high concentration of HEMA, the computational curve in BuOH approaches qualitatively the behavior of the bulk system. The alcohol is supposed to approximate the effect of a largely polar and hydroxylated medium such as a high fraction of HEMA monomer in the bulk system. The computational curve in DMF reproduces the bulk behavior at low HEMA fraction, while for higher values it approaches the diagonal, in agreement with the experimental data that are scattered around that line. In this case, the strong interactions involving the hydroxyalkyl groups are reduced, thus the kinetic behavior of the two methacrylates is supposed to be more similar than in bulk as well as in a polar solvent.

Table 25. *Reactivity ratios of methyl methacrylate-co-2-hydroxyethyl methacrylate copolymerization. Comparison between experimental and computational parameters in various solvents*.

Reactivity Ratios	Computational			Experimental	
	Vacuum	*DMF*	*BuOH*	*Bulk*	*DMF*
r_{HEMA}	0.65	0.85	1.04	1.81 ± 0.06	0.93 ± 0.34
r_{MMA}	0.50	0.64	0.69	0.79 ± 0.08	0.97 ± 0.17

Turning the attention on the reactivity ratios, the accuracy of the computational results is not satisfactory. However, it should be noted that r_{HEMA} appears to be more sensitive to the variation of the solvent than r_{MMA}. Although the computational method is not suited to reproduce accurately the hydrogen bonding effect that is associated with the presence of hydroxyalkyl groups, the implicit solvent model proves to be able to enhance the prediction performances of the DFT method with respect to the use of simulations in vacuum.

6.2.4. **Methyl Methacrylate-co-Methacrylic Acid**

The copolymerization of MMA and MAA has been studied experimentally considering a bulk reaction as well as the polymerization in toluene and isopropyl alcohol (IPA). Experimental data in bulk have been collected at 323 K from PLP reactions at 33 Hz, while literature data were adopted for polymerization at 343 K in $10\%_{wt}$ comonomer solutions of toluene and IPA.[177] Propagation reactions have been computationally modeled in vacuum as well as in the presence of DMF and BuOH as implicit solvents at 323 K. All of the results are reported in **Figure 31**, while the estimated reactivity ratios are shown in **Table 26**.
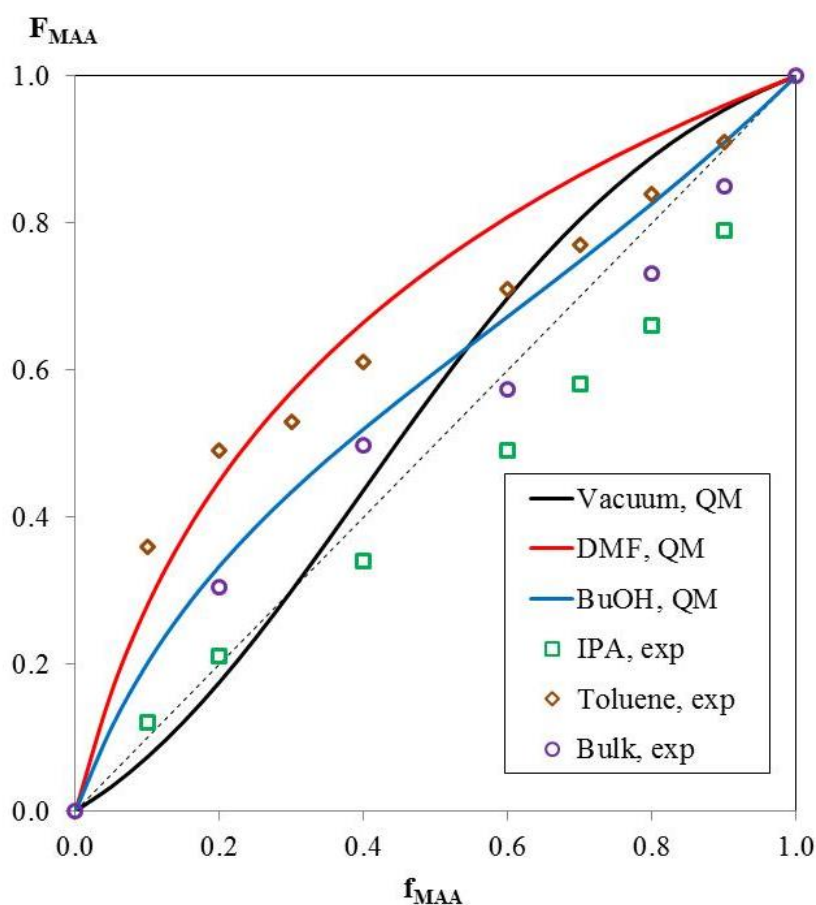

Figure 31. *Composition plots of methyl methacrylate-co-methacrylic acid copolymerization. Molar fraction of methacrylic acid in the copolymer (F_{MAA}) as a function of its molar fraction in the monomer mixture (f_{MAA}). Comparison between experimental data (exp) and computational curves (QM) in various solvents.*

First, it should be noted that in the system at issue the solvent effect on copolymerization kinetics appears to be larger than in the previous one, since both experimental and computational trends are quite different from each other when the reaction medium changes. Focusing on the experimental data, those collected in bulk exhibit an intermediate behavior between the trends of composition points in toluene and IPA. Moreover, at high monomer fraction of MAA, the bulk kinetics seems to approach that of the copolymerization in IPA rather than that of the less-interactive toluene. Turning the attention on the computational results, the curve obtained in vacuum appears to be unable to describe the kinetic behavior of the system, while the use of the implicit solvent model modifies significantly the computational predictions. Particularly, the computational curve in BuOH approximates the data in bulk, while the one in DMF seems to follow the experimental data collected in toluene, though these correspondences are effective mostly at low MAA fraction.

Table 26. *Reactivity ratios of methyl methacrylate-co-methacrylic acid copolymerization. Comparison between experimental and computational parameters in various solvents.*

Reactivity Ratios	Computational			Experimental		
	Vacuum	*DMF*	*BuOH*	*Bulk*	*Toluene*	*IPA*
r_{MAA}	2.62	2.63	1.05	0.51	1.06 ± 0.02	0.33 ± 0.02
r_{MMA}	1.70	0.26	0.38	0.35	0.10 ± 0.01	0.78 ± 0.03

The first comment about these results is to be made regarding the behavior of the system at low MAA fraction. A remarkable solvent effect is observed in this area of the plot, where the bulk behavior agrees with the results obtained with a polar and interactive solvent (BuOH), as noted above. The presence of a very interactive reaction medium in the bulk system, even at low fraction of the functional monomer, is reflected also by the fact that the copolymerization behavior is strongly modified by the dilution of the reacting mixture in DMF and toluene. The former solvent acts as hydrogen bond disrupting agent, while the latter simply dilutes the functional moieties and softens their interactions. Moreover, in these conditions, the MAA monomer is incorporated in the copolymer at a larger extent than in bulk, due to the reduced

hindrance of the interactions that involve the carboxyl moieties. As the monomer fraction of MAA increases, the computational curves at issue lose the trend of the corresponding experimental values. This feature can be ascribed to the poor capability of the implicit solvent model in the characterization of a very interactive system, which is likely to modify significantly its kinetic properties as the functional monomer fraction changes.

6.2.5. Conclusion

A combined experimental and computational investigation of the copolymerization behavior of systems involving functional monomers has been carried out. Specifically, MMA-co-HEMA and MMA-co-MAA have been examined, with focus on the solvent effect on the reaction kinetics. PLP has been adopted to produce polymer samples that were analyzed by ^{1}H NMR to obtain polymer-to-monomer composition data and reactivity ratios according to the terminal model of copolymerization. The reaction medium has been considered computationally by the use of an implicit solvent model, in addition to the standard DFT procedure in vacuum.

The first system examined exhibits a solvent effect that is mostly localized at high fraction of HEMA monomer. The implicit solvent model has revealed to be useful in increasing the performances of the quantum chemistry method in the qualitative prediction of the copolymerization kinetics in presence of solvents enhancing and disrupting strong intermolecular interactions. However, the use of the implicit solvent model does not provide accurate estimations of the reactivity ratios, especially when the parameter referred to the functional monomer is considered. Regarding the copolymerization between MMA and MAA, the latter monomer is responsible of a very strong solvent effect, which affects the behavior of the system even at low fraction of the functional monomer. Although this system is also characterized by a better description of the copolymerization kinetics with the use of an implicit solvent model, this approach reveals to be inadequate to predict the kinetic behavior as long as the MAA fraction increases.

With the aim of achieving a more accurate definition of the solvent effect, the computational description of the interactions between the functional reacting moieties and the solvent molecules needs to be improved by a better accurate and explicit modeling of the reaction medium. This goal is to be sought using a lower level of theory that allows extending the size of the molecular system under investigation. On the other hand, the quantum chemistry method can be used as a preliminary tool to verify whether the solvent effect is likely to be significant or not in the system at issue. In this context, the implicit solvent model is undoubtedly a relevant improvement to the DFT calculations.

6.3. Conformation Effects on Propagation Kinetics

Functionalized carboxylic groups in acrylic compounds are characterized by many rotational degrees of freedom, which originate a wide range of rotamers. In this work, a quantum chemistry investigation is carried out to study the relative stability of acrylate conformers. Internal rotations around peculiar dihedral angles are performed on monomer as well as radical molecules of MMA with the aim of evaluating conformation energies and rotational energy barriers. The obtained parameters are used to identify the most relevant conformers and to differentiate global energy minima from the local ones. Afterwards, these molecular structures are adopted to investigate propagation reaction kinetics and elucidate how the choice among different conformations of reactants, products, and transition states can affect the rate coefficient value.

6.3.1. Introduction

In the last decades, the computational investigation of FRP systems, and in particular acrylate polymers, has been notably improved. Thanks to the strong development of the computing power, it has been possible to use very demanding methods based on quantum mechanics to predict the reaction rate coefficients in such systems. The accuracy and reliability of these computational techniques have been tested on various polymer systems and on a large set of reactions, making this a powerful tool to investigate polymerization kinetics. In several cases, a good agreement has been found between the computational results and the data obtained from experiments, within the experimental uncertainty, as detailed in the previous chapters.[43-45, 105, 122, 123]

Although appreciable results have been obtained so far mostly in the determination of reactivity ratios, the computational approach can be improved to obtain even better predictions of absolute rate coefficients. With the aim of modeling properly a given reaction in order to get an accurate description of its kinetic behavior, several issues should be taken into account. Among them, a prominent role ought to be given to the solvent effect, the chain length effect, and the stereochemistry of the

adjacent units in chain. Such effects need to be modeled under certain hypothesis and approximations, and sometimes they are even neglected, due to the relatively small and limited chain model that can be considered under the use of quantum chemistry methods.

In this work, the attention is focused on another aspect that may influence the estimation of the rate coefficients in certain FRP systems, at the level of the geometry optimization of the molecules involved in the reactions. It is well known that a conventional gradient-based optimization returns a molecular geometry that is sensitive to the input structure. In the eventuality of the existence of different conformations of the molecules under investigations, as in the case of acrylate moieties, the optimized geometry is strictly related to the given initial structure. When dealing with large molecules characterized by several degrees of freedom, which allow rotations around some dihedral angles, local energy minima can be identified instead of the global ones. Based on which conformer is taken into account for each molecule involved in a given reaction, differences in the estimation of the corresponding rate coefficient are expected.

The aim of this work is thus to investigate the conformations of monomers and radical chains of MMA using quantum chemistry. Focusing on the degrees of freedom related to the ester side groups, torsion scans around the dihedral angles of interest are simulated to identify the most relevant conformers and compare their conformation energies. Energy barriers are estimated in order to compare the probability of interconversion between the conformers with propagation kinetics. All of the identified conformations of the reactants, products, and transition states are used to define a set of propagation pathways referred to the addition of MMA to its monomer radical. A comparison between the evaluated rate coefficients is aimed at elucidating the correlation between the choice of the input structures for geometry optimizations and the propagation rate coefficient. This way, the use of quantum chemistry in the estimation of specific rate coefficients is critically examined.

6.3.2. Methyl Methacrylate Monomer and Monomer Radical

Torsion energy scans around relevant bonds of the ester moiety of MMA monomer have been performed first. Specifically, the dihedral angles φ_1 and φ_2 have been considered, with reference to the structure and atom numeration reported in **Figure 32**. The B3LYP/6-31G(d,p) method was used to carry out the energy scans in order to obtain the relative energy plots, which are shown in **Figure 32**, while energy barriers (E_B) and conformation energies (ΔE) were estimated also at the MPWB1K/6-31G(d,p) level. The calculated parameters are reported in **Table 27**. The conformer c_1, which exhibits a *trans* configuration between the two double bonds of the monomer, is found to be the most stable conformer corresponding to the global energy minima with respect to the torsion motions examined, though the energy difference between c_1 and c_2 is very small.

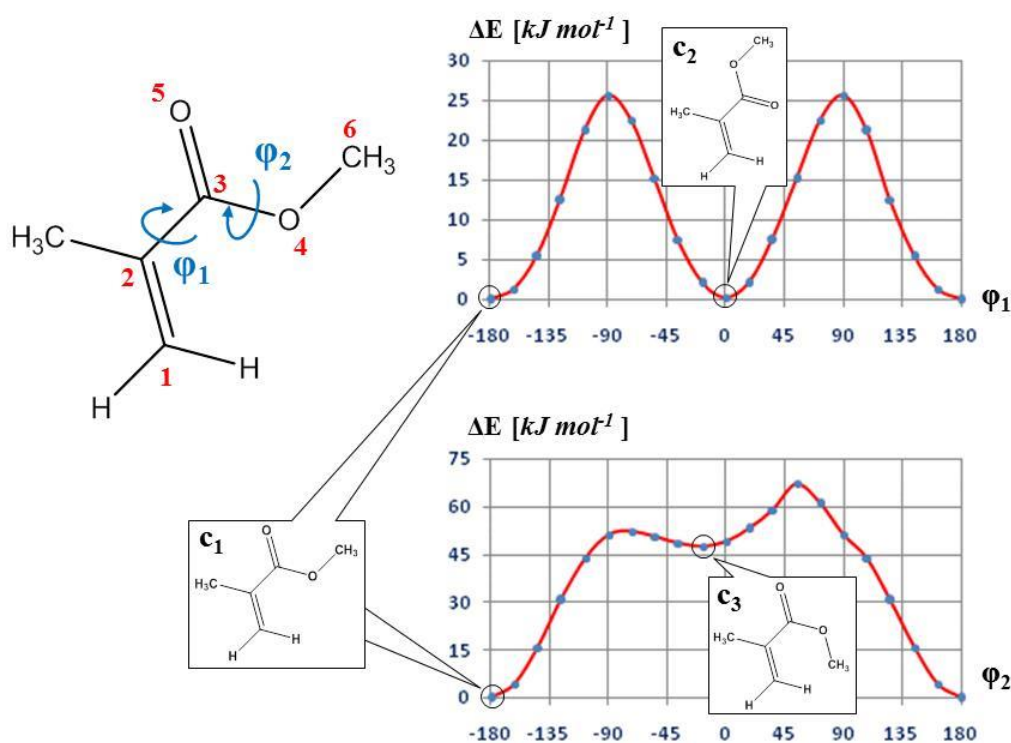**Figure 32**. *Torsion energy scans around the dihedral angles φ_1 and φ_2 of the methyl methacrylate monomer, and detail of the atom numeration. Molecular energies (ΔE) are referred to the value of the minimum energy structure c_1.*

There are no significant differences between the estimated parameters between the two computational methods. While the configurations c_1 and c_2 are interchangeable with an energy barrier in the order of the activation energy of MMA propagation,[178] the conformer c_3 is not likely to be obtained. Therefore, only the rotation of the ester group has been considered in the following study.

Table 27. *Calculated values of conformation energy difference between the minimum energy structures (ΔE) and minimum energy barrier referred to the global minimum structure (E_B) of the conformers of methyl methacrylate monomer.*

Dihedral	Atoms	Method	Conformers	ΔE $kJ\ mol^{-1}$	E_B $kJ\ mol^{-1}$
φ_1	*1, 2, 3, 5*	*B3LYP/6-31G(d,p)*	c_1, c_2	0.3	25.8
		MPWB1K/6-31G(d,p)		0.3	21.1
φ_2	*2, 3, 4, 6*	*B3LYP/6-31G(d,p)*	c_1, c_3	47.8	52.3
		MPWB1K/6-31G(d,p)		49.3	51.7

Torsion energy scan of the ester moiety of MMA monomer radical has confirmed that the rotation around the dihedral angle φ_1, with reference to the corresponding monomer shown in **Figure 32**, gives two identical conformers as long as the methylene group of the monomer is replaced by a methyl group. The monomer radical is thus identified with only one minimum energy structure.

6.3.3. Methyl Methacrylate Dimer Radical

Torsion energy scans about the ester moieties of MMA dimer radical have been performed focusing on the dihedral angles φ_{1A} and φ_{1B}, with reference to the structure and atom numeration of the racemo diad reported in **Figure 33**. The calculated energy parameters are reported in **Table 28**. The radical unit of the dimer shows a thermodynamically favored configuration of the ester group with the carbonyl oriented toward the outside of the backbone, while the ester group involved in the torsion around φ_{1B} prefers the carbonyl facing inwards (i.e., oriented toward the methyl side group).
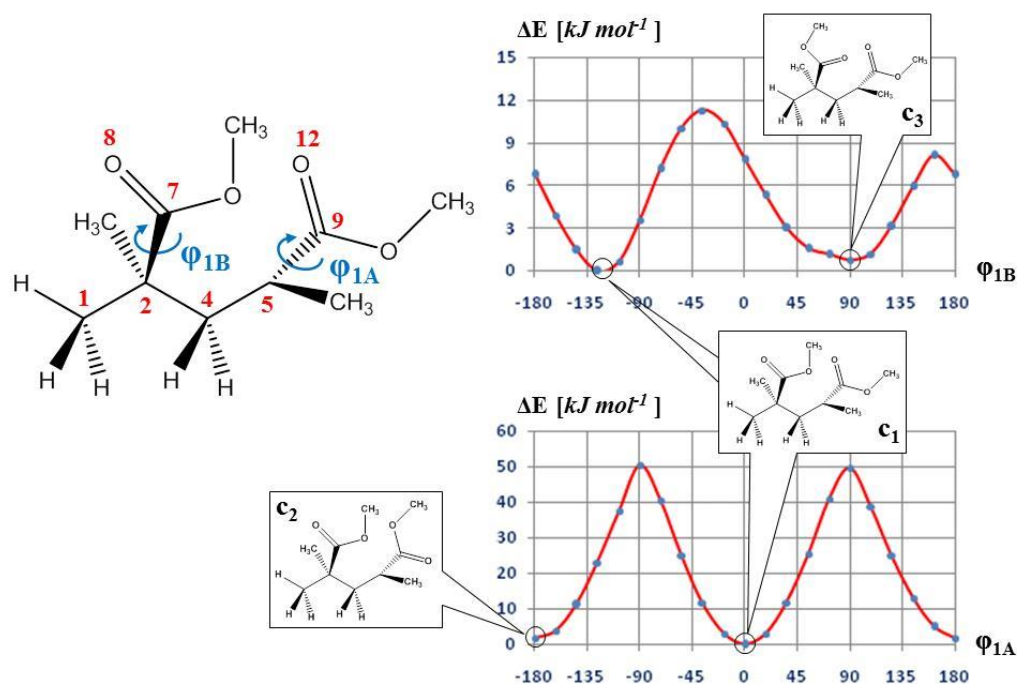
Figure 33. *Torsion energy scans around the dihedral angles φ_{1A} and φ_{1B} of the methyl methacrylate dimer radical, and detail of the atom numeration. Molecular energies (ΔE) are referred to the value of the minimum energy structure c_1.*

The energy differences between local and global energy minima are in the order of 1-2 kJ mol^{-1}. Focusing on the rotational energy barriers, the torsion around the dihedral φ_{1A} is by far more hindered than φ_{1B} as well as the corresponding motion of the ester group in the monomer (defined previously by φ_1).

Table 28. *Calculated values of conformation energy difference between the minimum energy structures (ΔE) and minimum energy barrier referred to the global minimum structure (E_B) of the conformers of methyl methacrylate dimer radical.*

Dihedral	Atoms	Method	Conformers	ΔE	E_B
				kJ mol^{-1}	kJ mol^{-1}
φ_{1A}	4, 5, 9, 12	*B3LYP/6-31G(d,p)*	c_1, c_2	1.8	49.6
		MPWB1K/6-31G(d,p)		1.6	52.6
φ_{1B}	1, 2, 7, 8	*B3LYP/6-31G(d,p)*	c_1, c_3	0.8	7.3
		MPWB1K/6-31G(d,p)		1.9	8.8

6.3.4. Propagation Rate Coefficient

The previous analysis has led to the definition of conformation structures of monomer, radical monomer, and radical dimer of MMA, distinguishing local and global energy minima, which are summarized in **Figure 34**. In the context of a propagation reaction occurring on the monomer radical, these structures can be adopted to calculate the corresponding reaction rate coefficient. For this purpose, the combination of the obtained conformers produce different propagation pathways, which are characterized by different rate constant values as long as different conformation energies are used in the calculations. An overview of the propagation reactions examined is shown in **Figure 34**. It should be noted that the different configurations of the product of the propagation reaction examined determine also different configurations of the transition state structure.
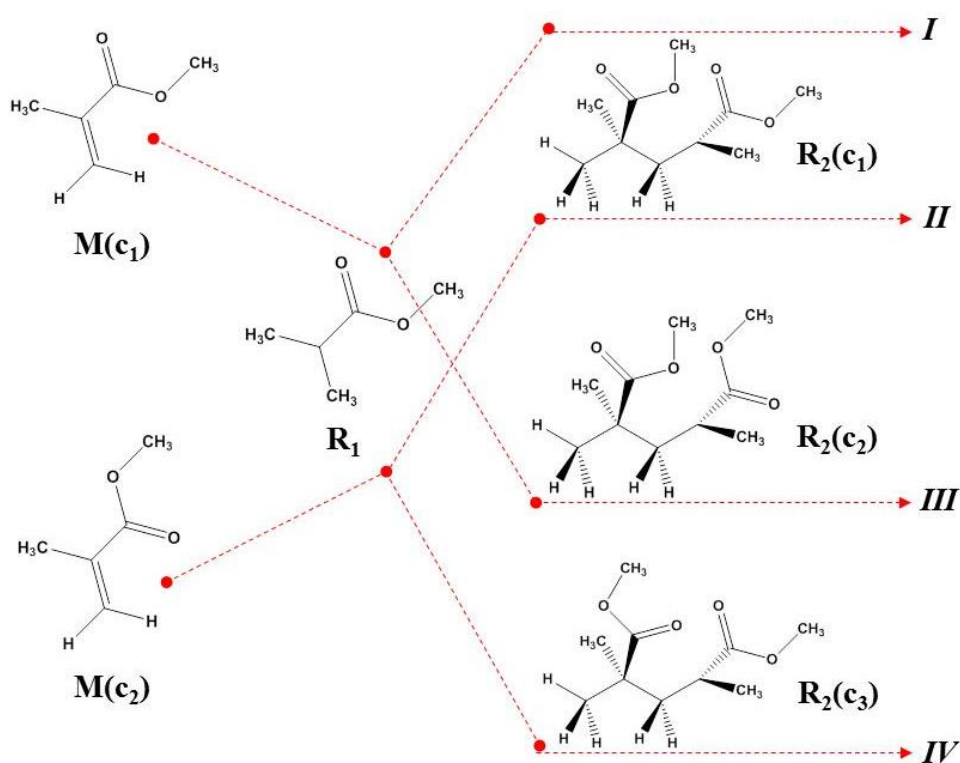

Figure 34.*Propagation pathways involving different conformers of reactants and products, with reference to the torsion energy scans performed on monomer (M), monomer radical (R_1), and dimer radical (R_2) of methyl methacrylate.*

The rate coefficient values corresponding to the selected combinations of conformers are reported in **Table 29**. A first discrimination is to be made between reactions *II-IV*, which are defined considering conformations of the ester moieties that remain consistent between the structures adopted to evaluate the rare coefficients, and reaction *I*, which considers the global minimum structures of reactants, products, and transition states. The sensitivity of the rate constant value to the choice of the input geometries for the molecular optimization is demonstrated. The calculated rate parameters show that the selection of the minimum energy conformers does not guarantee the detection of the minimum energy pathway (i.e., reaction *I* is characterized neither by the smallest activation energy nor by the largest rate coefficient). Moreover, this choice does not assure that the side-group orientation of the minimum energy product of propagation is consistent with those of the minimum energy reactants. Therefore, the detection of minimum energy structures for reactants and products to determine absolute rate coefficients with quantum chemistry cannot be considered as the most reliable approach. A detailed analysis of the conformation effect on reaction kinetics should be performed exploring all of the possible conformers of the molecules involved. Once detected, their relative thermodynamic stability and the probability of interconversion between the various rotamers should be determined, in order to identify the most probable pathways. However, this procedure is too much onerous to be carried out at the quantum chemistry level, while the use of molecular dynamics simulations is better suited for this purpose.

Table 29. *Calculated values of activation energy, pre-exponential factor, and rate coefficient for the propagation reactions involving different conformers of monomer and dimer radical of methyl methacrylate. Rate constants and parameters are evaluated at 323 K.*

Reaction	Conformers		E_a	A	k_p
	Monomer	*Dimer Radical*	*kJ mol^{-1}*	*L mol^{-1} s^{-1}*	*L mol^{-1} s^{-1}*
I	c_1	c_1	13.8	2.42×10^4	142
II	c_2	c_1	13.5	2.84×10^4	185
III	c_1	c_2	16.6	2.89×10^4	60
IV	c_2	c_3	11.1	2.10×10^4	333

6.3.5. Conclusion

The quantum chemistry tool has been used to investigate the conformations of monomer and radicals of MMA, with focus on the torsion motions of the ester moieties. This study has led to the definition of conformers corresponding to global and local minima energy structures, and to the estimation of their energy differences as well as the energy barriers of the rotations around relevant dihedral angles. The obtained conformers have been adopted to calculate the propagation rate coefficient with reference to a set of reaction pathways, obtained by the combination of the different conformers of reactants and products.

The conventional approach of considering only minimum energy structures in order to evaluate accurately the rate coefficients has been discussed with regard to the definition of the minimum energy pathway. Emphasis is given to the consistence between the side-group orientations of the molecules that are used to calculate the reaction rate constant, which requires a detailed analysis of the internal torsion motions. The screening of the many conformers that may arise if large polymer systems are considered has been found as the critical aspect of the conformation study at the quantum chemistry level. A support to this study may come from a molecular dynamics approach, which is better suited to explore the internal degrees of freedom related to the internal rotations of polymer chains and to detect the most probable conformers. Moreover, coupled torsion scans are feasible with this approach, while they are indispensable for a comprehensive examination of all the possible conformation structures. Therefore, the quantum chemistry investigation could be matched with molecular dynamics in order to increase the accuracy in the estimation of absolute rate coefficients.

——————————————— ——————————— ————————— ————— ——— —— ——

——————————————— ——————————— ————————— ————— ——— —— ——

Conclusion

——————————————— ——————————— ————————— ————— ——— —— ——

T
he PhD research has been focused on the computational investigation of reaction kinetics in the context of FRP, with particular emphasis on secondary reactions and pathways that are not easy to be studied at the experimental level. To this end, a consolidated quantum chemistry approach based on the DFT has been adopted and improved. Its capability in the theoretical prediction of reaction rate coefficients and kinetic parameters has been tested, shifting the attention from well-known homopolymer systems to challenging acrylate copolymers. The computational tool has proved to be a valid alternative to the experimental analysis for a detailed investigation of specific reactions of interest. Promising results have been obtained regarding backbiting reactions and pathways involving MCRs as well as other sort of radicals. The kinetics of these steps, along with that of secondary reactions in the context of copolymerization, has been determined. Wherever possible, the computational results have been validated through a comparison with experimental data, thus emphasizing the predictive power of the tool as well as its limits of application in FRP.

Concerning the emerged potentiality of the computational approach, the possibility of examining and characterizing intriguing reactions within complex kinetic schemes of radical polymerization belongs in this context. Moreover, quantum chemistry methods have reached a level of development that is a good compromise between prediction accuracy and opportunity to explore relatively large polymer systems. Therefore, the attention could be moved to the polymerization of interesting

acrylic monomers, which are known to host a large variety of side reactions inside their kinetic schemes. In this context, the support of quantum chemistry to the recent experimental achievements about acrylates has led to a deeper elucidation of the mechanisms that correlate secondary reaction kinetics to the definition of the polymer microstructure, particularly concerning the formation of branches.

Studies of borderline systems have helped to shed light on the limits of application of the computational tool in the investigation of FRP. The capability of the method in the description of the solvent effect on copolymerization kinetics of functional acrylates has revealed to be feasible using an implicit solvent model, which is however not enough accurate to predict reactivity ratios that agree quantitatively with the experimental data. A better description of the intermolecular interactions of the solvent molecules with the reacting moieties and is achievable only by treating them explicitly. Furthermore, the limits of the tool in performing geometry optimization have been discussed, focusing on the conformation effect on the absolute rate coefficient estimation. The computational tool is capable of discriminating between local and global energy minima structures in order to identify the most probable pathways, though a comprehensive examination of all the possible conformations of large polymer structures is not affordable at the quantum chemistry level.

This critical analysis of the potentiality and limitations of the quantum chemistry tool leads to the following conclusive remarks. The capability of the tool in predicting reactivity ratios with satisfying accuracy and investigating scarcely observable reactions places it as a considerable resource in the analysis of FRP mechanisms. Moreover, the continuous improvement of the performances of computational methods and kinetic models is promising for an increasing accuracy also in the estimation of absolute rate coefficients. This is also a challenge for the improvement of the experimental techniques for the determination of reaction kinetics, which are undergoing a rapid development in parallel with the computational tools. Eventually, the setup of quantum chemistry methods coupled with molecular dynamics represents the forthcoming step of the approach to FRP, which is supposed to make feasible the study of phenomena at larger scale without losing too much level of detail.

Bibliography

[1] G. Odian, *Principles of Polymerization (4th Edition)*, Wiley, **2004**.

[2] T. Junkers, C. Barner-Kowollik, *J. Polym. Sci. Pol. Chem.,* **2008**, *46*, 7585.

[3] M. Soroush, M. C. Grady, G. A. Kalfas, *Comp. Chem. Eng.,* **2008**, *32*, 2155.

[4] P. J. Flory, *J. Am. Chem. Soc.,* **1937**, *59*, 241.

[5] M. J. Roedel, *J. Am. Chem. Soc.,* **1953**, *75*, 6110.

[6] R. S. Lehrle, C. S. Pattenden, *Polym. Degrad. Stabil.,* **1999**, *63*, 153.

[7] D. Moscatelli, C. Cavallotti, M. Morbidelli, *Macromolecules,* **2006**, *39*, 9641.

[8] C. Plessis, G. Arzamendi, J. M. Alberdi, A. M. v. Herk, J. R. Leiza, J. M. Asua, *Macromol. Rapid Comm.,* **2003**, *24*, 173.

[9] A. N. Nikitin, R. A. Hutchinson, *Macromolecules,* **2005**, *38*, 1581.

[10] W. Wang, A. N. Nikitin, R. A. Hutchinson, *Macromol. Rapid Comm.,* **2009**, *30*, 2022.

[11] A. N. F. Peck, R. A. Hutchinson, *Macromolecules,* **2004**, *37*, 5944.

[12] S. E. Levine, L. J. Broadbelt, *Polym. Degrad. Stabil.,* **2008**, *93*, 941.

[13] A. N. Nikitin, R. A. Hutchinson, M. Buback, P. Hesse, *Macromolecules,* **2007**, *40*, 8631.

[14] J. Barth, M. Buback, P. Hesse, T. Sergeeva, *Macromolecules,* **2010**, *43*, 4023.

[15] C. Plessis, J. R. Leiza, H. A. S. Schoonbrood, D. Charmot, J. M. Asua, *Macromolecules,* **2000**, *33*, 5041.

[16] D. Schmaljohann, *Adv. Drug Deliv. Rev.* **2006**, *58*, 1655.

[17] K. Liang, R. A. Hutchinson, *Macromolecules,* **2010**, *43*, 6311.

[18] K. Liang, R. A. Hutchinson, *Macromol. Rapid Commun.,* **2011**, *32*, 1090.

[19] K. Liang, R. A. Hutchinson, J. Barth, S. Samrock, M. Buback, *Macromolecules,* **2011**, *44*, 5843.

[20] M. Gaborieau, S. P. S. Koo, P. Castignolles, T. Junkers, C. Barner-Kowollik, *Macromolecules,* **2010**, *43*, 5492.

[21] G. Arzamendi, J. R. Leiza, *Ind. Eng. Chem. Res.,* **2008**, *47*, 5934.

[22] A. N. Nikitin, R. A. Hutchinson, *Macromol. Rapid Comm.,* **2009**, *30*, 1981.

[23] W. Wang, R. A. Hutchinson, *Chem. Eng. Technol.,* **2010**, *33*, 1745.

[24] M. Buback, *Macromol. Symp.,* **2009**, *275-276*, 90.

[25] O. F. Olaj, I. Bitai, F. Hinkelmann, *Macromol. Chem.,* **1987**, *188*, 1689.

[26] C. Barner-Kowollik, F. Günzler, T. Junkers, *Macromolecules,* **2008**, *41*, 8971.

[27]   S. Beuermann, M. Buback, *Prog. Polym. Sci.,* **2002**, *27*, 191.

[28]   J. M. Asua, S. Beuermann, M. Buback, P. Castignolles, B. Charleux, R. G. Gilbert, R. A. Hutchinson, J. R. Leiza, A. N. Nikitin, J. P. Vairon, A. M. v. Herk, *Macromol. Chem. Phys.,* **2004**, *205*, 2151.

[29]   G. Arzamendi, C. Plessis, J. R. Leiza, J. M. Asua, *Macromol. Theor. Simul.,* **2003**, *12*, 315.

[30]   Y. Reyes, G. Arzamendi, J. M. Asua, J. R. Leiza, *Macromolecules,* **2011**, *44*, 3674.

[31]   J. Barth, M. Buback, P. Hesse, T. Sergeeva, *Macromol. Rapid Commun.,* **2009**, *30*, 1969.

[32]   M. L. Coote, *Macromol. Theor. Simul.,* **2009**, *18*, 388.

[33]   H. Fischer, L. Radom, *Angew. Chem. Int. Ed.,* **2001**, *40*, 1340.

[34]   V. V. Speybroeck, D. V. Neck, M. Waroquier, S. Wauters, M. Saeys, G. B. Marin, *J. Phys. Chem. A,* **2000**, *104*, 10939.

[35]   M. Dossi, G. Storti, D. Moscatelli, *Macromol. Theor. Simul.,* **2010**, *19*, 170.

[36]   D. Moscatelli, M. Dossi, C. Cavallotti, G. Storti, *J. Phys. Chem. A,* **2011**, *115*, 52.

[37]   V. V. Speybroeck, K. V. Cauter, B. Coussens, M. Waroquier, *ChemPhysChem,* **2005**, *6*, 180.

[38]   K. V. Cauter, V. V. Speybroeck, P. Vansteenkiste, M. F. Reyniers, M. Waroquier, *ChemPhysChem,* **2006**, *7*, 131.

[39]   E. I. Izgorodina, M. L. Coote, *Chem. Phys.,* **2006**, *324*, 96.

[40]   K. V. Cauter, V. V. Speybroeck, M. Waroquier, *ChemPhysChem,* **2007**, *8*, 541.

[41]   D. Moscatelli, M. Dossi, C. Cavallotti, G. Storti, *Macromol. Symp.,* **2007**, *259*, 337.

[42]   X. Yu, J. Pfaendtner, L. J. Broadbelt, *J. Phys. Chem. A,* **2008**, *112*, 6772.

[43]   K. Liang, M. Dossi, D. Moscatelli, R. A. Hutchinson, *Macromolecules,* **2009**, *42*, 7736.

[44]   M. Dossi, K. Liang, R. A. Hutchinson, D. Moscatelli, *J. Phys. Chem. B,* **2010**, *114*, 4213.

[45]   E. Mavroudakis, K. Liang, D. Moscatelli, R. A. Hutchinson, *Macromol. Chem. Phys.,* **2012**, *213*, 1706.

[46]   M. Dossi, D. Moscatelli, *Macromol. React. Eng.,* **2012**, *6*, 74.

[47]   S. Bebe, X. Yu, R. A. Hutchinson, L. J. Broadbelt, *Macromol. Symp.,* **2006**, *243*, 179.

[48]   X. Yu, S. E. Levine, L. J. Broadbelt, *Macromolecules,* **2008**, *41*, 8242.

[49]   J. Purmova, K. F. D. Pauwels, W. V. Zoelen, E. J. Vorenkamp, A. J. Schouten, M. L. Coote, *Macromolecules,* **2005**, *38*, 6352.

[50]   J. Pfaendtner, X. Yu, L. J. Broadbelt, *J. Phys. Chem. A,* **2006**, *110*, 10863.

[51]   M. Dossi, G. Storti, D. Moscatelli, *Macromol. Symp.,* **2010**, *289*, 110.

[52]   K. V. Cauter, B. J. V. d. Bossche, V. V. Speybroeck, M. Waroquier, *Macromolecules,* **2007**, *40*, 1321.

[53]   J. Purmova, K. F. D. Pauwels, M. Agostini, M. Bruinsma, E. J. Vorenkamp, A. J. Schouten, M. L. Coote, *Macromolecules,* **2008**, *41*, 5527.

[54]   X. Yu, L. J. Broadbelt, *Macromol. Theor. Simul.,* **2012**, *21*, 461.

[55]   B. D. Sterck, R. Vaneerdeweg, F. D. Prez, M. Waroquier, V. V. Speybroeck, *Macromolecules,* **2010**, *43*, 827.

[56]   I. Degirmenci, S. Eren, V. Aviyente, B. D. Sterck, K. Hemelsoet, V. V. Speybroeck, M. Waroquier, *Macromolecules,* **2010**, *43*, 5602.

[57]   A. Klamt, G. Schueuermann, *J. Chem. Soc., Perkin Trans.,* **1993**, *2*, 799.

[58]   S. Miertus, E. Scrocco, J. Tomasi, *J. Chem. Phys.,* **1981**, *55*, 117.

[59]   C. Y. Lin, E. I. Izgorodina, M. L. Coote, *Macromolecules,* **2010**, *43*, 553.

[60]   S. C. Thickett, R. G. Gilbert, *Polymer,* **2004**, *45*, 6993.

[61]   F. Jensen, *Introduction to Computational Chemistry (2nd Edition)*, Wiley, **2007**.

[62]   W. Kolos, L.Wolniewicz, *J. Chem. Phys.,* **1964**, *41*, 3663.

[63]   B. T. Sutcliffe, *Adv. Quant. Chem.,* **1997**, *28* 65.

[64]   B. T. Sutcliffe, *Adv. Chem. Phys.,* **2000**, *114* 1.

[65]   A. Szabo, N. S. Ostlund, *Modern Quantum Chemistry*, McGraw-Hill, **1982**.

[66]   R. McWeeny, *Methods of Molecular Quantum Mechanics*, Academic Press, **1992**.

[67]   W. J. Hehre, L. Radom, J. A. Pople, P. v. R. Schleyer, *Ab Initio Molecular Orbital Theory*, Wiley, **1986**.

[68]   J. Simons, *J. Phys. Chem.,* **1991**, *95*, 1017.

[69]   J. Simons, J. Nichols, *Quantum Mechanics in Chemistry*, Oxford University Press, **1997**.

[70]   T. Helgaker, P. Jørgensen, J. Olsen, *Molecular Electronic Structure Theory*, Wiley, **2000**.

[71]   R. J. Bartlett, J. F. Stanton, *Rev. Comp. Chem.,* **1994**, *5* 65.

[72]   C. D. Sherrill, H. F. Schaefer, *Adv. Quant. Chem.,* **1999**, *34* 143.

[73]   R. J. Bartlett, *J. Phys. Chem.,* **1989**, *93* 1697.

[74]   C. Møller, M. S. Plesset, *Phys. Rev.,* **1934**, *46*, 618.

[75]   D. Feller, E. R. Davidson, *Rev. Comp. Chem.,* **1990**, *1*, 1.

[76]   J. C. Slater, *Phys. Rev.,* **1930**, *36* 57.

[77]   S. F. Boys, *Proc. R. Soc. (London) A,* **1950**, *200* 542.

[78]   F. Jensen, *J. Chem. Phys.,* **2005**, *122* 074111.

[79]   M. J. Frisch, J. A. Pople, J. S. Binkley, *J. Chem. Phys.,* **1984**, *809* 3265.

[80]   M. M. Francl, W. J. Pietro, W. J. Hehre, J. S. Binkley, M. S. Gordon, D. J. DeFrees, J. A. Pople, *J. Chem. Phys.,* **1982**, *77* 3654.

[81]   J. W. Ochterski, G. A. Petersson, J. A. Montgomery, *J. Chem. Phys.,* **1996**, *104*, 2598.

[82]   W. Koch, M. C. Holthausen, *A Chemist's Guide to Density Functional Theory*, Wiley-VCH, **2000**.

[83]   L. H. Thomas, *Proc. Cambridge Philos. Soc.,* **1927**, *23*, 542.

[84]   E. Fermi, *Rend. Accad. Naz. Lincei,* **1927**, *6*, 602.

[85]   P. Hohenberg, W. Kohn, *Phys. Rev.,* **1964**, *136* B864.

[86]   W. Kohn, L. J. Sham, *Phys. Rev.,* **1965**, *140* A1133.

[87]   J. C. Slater, *Phys. Rev.,* **1951**, *81* 385.

[88]   A. D. Becke, *Phys. Rev. A,* **1988**, *38* 3098.

[89]   C. Lee, W. Yang, R. G. Parr, *Phys. Rev. B,* **1988**, *37* 785.

[90]   J. P. Perdew, Y.Wang, *Phys. Rev. B,* **1986**, *33* 8800.

[91]   J. P. Perdew, J. A. Chevary, S. H. Vosko, K. A. Jackson, M. R. Pederson, D. J. Singh, C. Fiolhais, *Phys. Rev. B,* **1992**, *46* 6671.

[92]   J. P. Perdew, K. Burke, M. Ernzerhof, *Phys. Rev. Lett.,* **1996**, *77* 3865.

[93]   A. D. Becke, *J. Chem. Phys.,* **1993**, *98*, 5648.

[94]   P. J. Stephens, F. J. Devlin, C. F. Chabalowski, M. J. Frisch, *J. Phys. Chem.,* **1994**, *98*, 11623.

[95]   H. Eyring, *J. Chem. Phys.,* **1935**, *3*, 107.

[96]   M. G. Evans, M. Polanyi, *Trans. Faraday Soc.,* **1935**, *31*, 875.

[97]   E. Wigner, *Trans. Faraday Soc.,* **1938**, *34*, 29.

[98]   J. Steinfeld, J. Francisco, W. Hase, *Chemical Kinetics and Dynamics (2nd Edition)*, Prentice Hall, **1999**.

[99]   A. L. L. East, L. Radom, *J. Chem. Phys.,* **1997**, *106*, 6655.

[100] J. Pfaendtner, X. Yu, L. J. Broadbelt, *Theor. Chem. Acc.,* **2007**, *118*, 881.

[101] J. P. A. Heuts, R. G. Gilbert, L. Radom, *Macromolecules,* **1995**, *28*, 8771.

[102] P. Vansteenkiste, V. V. Neck, V. V. Speybroeck, M. Waroquier, *J. Chem. Phys.,* **2006**, *124*, 044314.

[103] P. Vansteenkiste, V. V. Speybroeck, G. B. Marin, M. Waroquier, *J. Phys. Chem. A,* **2003**, *107*, 3139.

[104] M. K. Sabbe, M. F. Reyniers, V. V. Speybroeck, M. Waroquier, G. B. Marin, *ChemPhysChem,* **2008**, *9*, 124.

[105] D. Cuccato, M. Dossi, D. Polino, C. Cavallotti, D. Moscatelli, *Macromol. React. Eng.,* **2012**, *6*, 496.

[106] E. Wigner, *J. Chem. Phys.,* **1937**, *5*, 720.

[107] I. Shavitt, *J. Chem. Phys.,* **1959**, *31*, 1359.

[108] R. P. Bell, *The tunnel effect in chemistry*, Chapman and Hall, **1980**.

[109] C. Eckart, *Phys. Rev.,* **1930**, *35*, 1303.

[110] R. A. Marcus, M. E. Coltrin, *J. Chem. Phys.,* **1977**, *67*, 2609.

[111] W. H. Miller, N. C. Handy, J. E. Adams, *J. Chem. Phys.,* **1980**, *72*, 99.

[112] R. T. Skodje, D. G. Truhlar, B. C. Garrett, *J. Phys. Chem.,* **1981**, *85*, 3019.

[113] T. Wu, H.-J. Werner, U. Manthe, *Science,* **2004**, *306*, 2227.

[114] M. J. Frisch, G. W. Trucks, H. B. Schlegel, G. E. Scuseria, M. A. Robb, J. R. Cheeseman, G. Scalmani, V. Barone, B. Mennucci, G. A. Petersson, H. Nakatsuji, M. Caricato, X. Li, H. P. Hratchian, A. F. Izmaylov, J. Bloino, G. Zheng, J. L. Sonnenberg, M. Hada, M. Ehara, K. Toyota, R. Fukuda, J. Hasegawa, M. Ishida, T. Nakajima, Y. Honda, O. Kitao, H. Nakai, T. Vreven, J. A. Montgomery, J. E. Peralta, F. Ogliaro, M. Bearpark, J. J. Heyd, E. Brothers, K. N. Kudin, V. N. Staroverov, R. Kobayashi, J. Normand, K. Raghavachari, A. Rendell, J. C. Burant, S. S. Iyengar, J. Tomasi, M. Cossi, N. Rega, J. M. Millam, M. Klene, J. E. Knox, J. B. Cross, V. Bakken, C. Adamo, J. Jaramillo, R. Gomperts, R. E. Stratmann, O. Yazyev, A. J. Austin, R. Cammi, C. Pomelli, J. W. Ochterski, R. L. Martin, K. Morokuma, V. G. Zakrzewski, G. A. Voth, P. Salvador, J. J. Dannenberg, S. Dapprich, A. D. Daniels, Ö. Farkas, J. B. Foresman, J. V. Ortiz, J. Cioslowski, D. J. Fox, *Gaussian 09, Revision A.1*, Gaussian, Inc., Wallingford CT, **2009**.

[115] Y. Zhao, D. G. Truhlar, *J. Phys. Chem. A,* **2004**, *108*, 6908.

[116] W. J. Hehre, R. Ditchfield, J. A. Pople, *J. Chem. Phys.,* **1972**, *56*, 2257.

[117] R. Ditchfield, W. J. Hehre, J. A. Pople, *J. Chem. Phys.,* **1971**, *54*, 724.

[118] R. Krishnan, J. S. Binkley, R. Seeger, J. A. Pople, *J. Chem. Phys.,* **1980**, *72*, 650.

[119] T. Clark, J. Chandrasekhar, G. W. Spitznagel, P. v. R. Schleyer, *J. Comput. Chem.,* **1983**, *4*, 294.

[120] J. A. Montgomery, M. J. Frisch, J. W. Ochterski, G. A. Petersson, *J. Chem. Phys.,* **1999**, *110*, 2822.

[121] D. Cuccato, M. Dossi, D. Moscatelli, G. Storti, *Macromol. Symp.,* **2011**, *302*, 100.

[122] D. Cuccato, M. Dossi, D. Moscatelli, G. Storti, *Macromol. React. Eng.,* **2012**, *6*, 330.

[123] D. Cuccato, E. Mavroudakis, M. Dossi, D. Moscatelli, *Macromol. Theor. Simul.,* **2013**, *22*, 127.

[124] D. Braun, *J. Polym. Sci. Pol. Chem.,* **2004**, *2*, 578.

[125] R. Bacaloglu, M. Fisch, *Polym. Degrad. Stabil.,* **1994**, *45*, 301.

[126] W. H. Starnes, *Prog. Polym. Sci.,* **2002**, *27*, 2133.

[127] F. D. Vleeschouwer, A. Toro-Labbe, S. Gutierrez-Oliva, V. V. Speybroeck, M. Waroquier, P. Geerlings, F. D. Proft, *J. Phys. Chem. A,* **2009**, *113*, 7899.

[128] T. D. Roo, J. Wieme, G. J. Heynderickx, G. B. Marin, *Polymer,* **2005**, *46*, 8340.

[129] C. Kiparissides, G. Daskalakis, D. S. Achilias, E. Sidiropoulou, *Ind. Eng. Chem. Res.,* **1997**, *36*, 1253.

[130] A. E. Hamielec, R. Gomez-Vaillard, F. L. Marten, *J. Macromol. Sci.-Chem.,* **1982**, *A17*, 1005.

[131] E. Sidiropoulou, C. Kiparissides, *J. Macromol. Sci.-Chem.,* **1990**, *A27*, 257.

[132] T. Y. Xie, A. E. Hamielec, P. E. Wood, D. R. Woods, *Polymer,* **1991**, *32*, 537.

[133] J. Wieme, D. R. D'hooge, M.-F.Reyniers, G. B. Marin, *Macromol. React. Eng.,* **2009**, *3*, 16.

[134] T. Y. Xie, A. E. Hamielec, P. E. Wood, D. R. Woods, *Polymer,* **1991**, *32*, 1098.

[135] J. Wieme, T. D. Roo, G. B. Marin, G. J. Heynderickx, *Ind. Eng. Chem. Res.,* **2007**, *46*, 1179.

[136] J. Brandrup, E. H. Immergut, *Polymer Handbook*, Wiley, **1989**.

[137] M. Rogestedt, T. Hjertberg, *Macromolecules,* **1993**, *26*, 60.

[138] S. W. Benson, *Thermochemical Kinetics*, Wiley, **1976**.

[139] J. A. Miller, R. Knee, C. K. Westbrook, *Annu. Rev. Phys. Chem.,* **1990**, *41*, 317.

[140] H. J. Curran, P. Gaffuri, W. J. Pitz, C. K. Westbrook, *Combust. Flame,* **1998**, *114*, 149.

[141] H. J. Curran, P. Gaffuri, W. J. Pitz, C. K. Westbrook, *Combust. Flame,* **2002**, *129*, 253.

[142] C. J. Hayes, D. R. Burgess, *J. Phys. Chem. A,* **2009**, *113*, 2473.

[143] H. Richter, J. B. Howard, *Prog. Energy Combust. Sci.,* **2000**, *26*, 565.

[144] M. Buback, P. Hesse, T. Junkers, T. Sergeeva, T. Theis, *Macromolecules,* **2008**, *41*, 288.

[145] W. Tsang, J. A. Walker, J. A. Manion, *Proc. Combust. Inst.,* **2007**, *31*, 141.

[146] W. Tsang, W. S. McGivern, J. A. Manion, *Proc. Combust. Inst.,* **2009**, *32*, 131.

[147] W. Chan, I. Hamilton, H. Pritchard, *J. Chem. Soc., Faraday Trans.,* **1998**, *94*, 2303.

[148] T. G. Denisova, E. T. Denisov, *Kinet. Catal.,* **2001**, *42*, 620.

[149] W. Tsang, J. A. Walker, J. A. Manion, *Int. Symp. Combust.,* **1998**, *1*, 135.

[150] B. Sirjean, E. Dames, H. Wang, W. Tsang, *J. Phys. Chem. A,* **2012**, *116*, 319.

[151] L. C. Jitariu, L. D. Jones, S. H. Robertson, M. J. Pilling, I. H. Hillier, *J. Phys. Chem. A,* **2003**, *107*, 8607.

[152] B. Bankiewicz, L. K. Huynh, A. Ratkiewicz, T. N. Truong, *J. Phys. Chem. A,* **2009**, *113*, 1564.

[153] J. Zheng, D. G. Truhlar, *J. Phys. Chem. A,* **2009**, *113*, 11919.

[154] A. Ratkiewicz, B. Bankiewicz, T. N. Truong, *Phys. Chem. Chem. Phys.,* **2010**, *12*, 10988.

[155] S. E. Levine, L. J. Broadbelt, *Polym. Degrad. Stabil.,* **2009**, *94*, 810.

[156] A. Ratkiewicz, B. Bankiewicz, *J. Phys. Chem. A,* **2012**, *116*, 242.

[157] A. N. Nikitin, R. A. Hutchinson, *Macromol. Theor. Simul.,* **2006**, *15*, 128.

[158] T. W. G. Solomons, C. B. Fryhle, *Organic Chemistry (8th Edition)*, Wiley, **2004**.

[159] K. P. C. Vollhardt, N. E. Schore, *Organic Chemistry (3rd Edition)*, Freeman, **1999**.

[160] W. Wang, R. A. Hutchinson, *Macromol. React. Eng.,* **2008**, *2*, 199.

[161] W. Wang, R. A. Hutchinson, *Macromol. Symp.,* **2010**, *289*, 33.

[162] M. Dubé, A. Penlidis, K. F. O'Driscoll, *Chem. Eng. Sci.,* **1990**, *45*, 2785.

[163] M. Dubé, A. Penlidis, K. F. O'Driscoll, *Canadian J. Chem. Eng.,* **1990**, *68*, 974.

[164] C. Plessis, G. Arzamendi, J. R. Leiza, H. A. S. Schoonbrood, D. Charmot, J. M. Asua, *Macromolecules,* **2001**, *34*, 5147.

[165] W. Wang, R. A. Hutchinson, *AIChE J.,* **2011**, *57*, 227.

[166] D. Li, R. A. Hutchinson, *Macromol. Rapid Commun.,* **2007**, *28*, 1213.

[167] S. Hamzehlou, Y. Reyes, J. R. Leiza, *Macromol. React. Eng.,* **2012**, *6*, 319.

[168] T. Junkers, M. Schneider-Baumann, S. S. P. Koo, P. Castignolles, C. Barner-Kowollik, *Macromolecules,* **2010**, *43*, 10427.

[169] M. Buback, R. G. Gilbert, R. A. Hutchinson, B. Klumperman, F.-D. Kuchta, B. G. Manders, K. F. O'Driscoll, G. T. Russell, J. Schweer, *Macrom. Chem. Phys.,* **1995**, *196*, 3267.

[170] C. Plessis, G. Arzamendi, J. R. Leiza, J. M. Alberdi, H. A. S. Schoonbrood, D. Charmot, J. M. Asua, *J. Polym. Sci. A,* **2001**, *39*, 1106.

[171] A. Echevarria, J. R. Leiza, J. C. d. l. Cal, J. M. Asua, *AIChE J.,* **1998**, *44*, 1667.

[172] W. A. Brauneckerunecker, K. Matyjaszewski, *Prog. Polym. Sci.,* **2007**, *32*, 93.

[173] G. Lendvay, T. Bérces, *J. Photochem. Photobiol. A,* **1987**, *40*, 31.

[174] I. Matheson, J. Tedder, *Int. J. Chem. Kinet.,* **1982**, *14*, 1033.

[175] D. M. Tomkinson, H. O. Pritchard, *J. Phys. Chem.,* **1966**, *70*, 1579.

[176] F. R. Mayo, F. M. Lewis, *J. Am. Chem. Soc.,* **1944**, *66*, 1594.

[177] G. S. Georgiev, I. G. Dakova, *Macromol. Chem. Phys.,* **1994**, *195*, 1695.

[178] S. Beuermann, M. Buback, T. P. Davis, R. G. Gilbert, R. A. Hutchinson, O. F. Olaj, G. T. Russell, J. Schweer, A. M. v. Herk, *Macromol. Chem. Phys.,* **1997**, *198*, 1545